RICE UNIVERSITY

Delivery of molecular-specific optical contrast agents for cancer biomarker detection in live cells and tissues

by

Anne Louise van de Ven

A THESIS SUBMITTED
IN PARTIAL FULFILLMENT OF THE
REQUIREMENTS FOR THE DEGREE

Doctor of Philosophy

APPROVED, THESIS COMMITTEE:

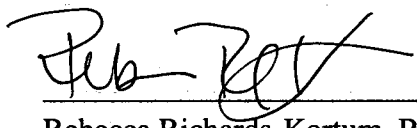

Rebecca Richards-Kortum, Professor
Bioengineering, Rice University

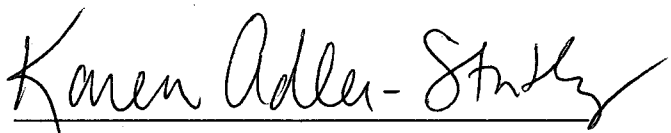

Karen Adler-Storthz, Assoc. Dean, Professor
Diagnostic Sciences,
University of Texas,
Health Science Center at Houston – Dental Branch

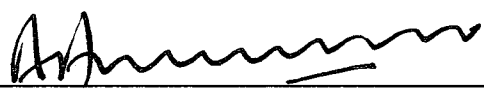

Ananth Annapragada, Professor
School of Health Information Sciences,
University of Texas,
Health Science Center at Houston

HOUSTON, TEXAS
SEPTEMBER 2008

ABSTRACT

Delivery of molecular-specific optical contrast agents

for cancer biomarker detection in live cells and tissues

by

Anne Louise van de Ven

Molecular-specific optical contrast agents have shown promise as potential non-invasive probes for the detection of cancer and its precursors. The topical use of optical contrast agents *in vivo* has been hindered, however, by the difficulty of delivering macromolecules through mucosal tissue. My goal was to develop a robust strategy for the delivery of molecular-specific optical contrast agents into live cells and tissues. Specifically, I sought to: 1) develop an efficient and reproducible strategy for intracellular delivery of optical contrast agents into live cells, 2) evaluate the feasibility of targeting human telomerase reverse transcriptase (hTERT) in live cells and fresh tissues, and 3) translate intracellular delivery strategies for the topical permeation of multi-layer mucosal tissue.

This dissertation describes the development of a surfactant-based strategy to effectively and reproducibly label cancer biomarkers in live cells and tissues. Triton-X100 was evaluated for its ability to deliver targeted and untargeted optical contrast agents to different cell compartments. My findings indicate that Triton-X100, when used at the

appropriate concentration, can permeabilize a variety of live cells in a reproducible and reversible manner. To assess the usefulness of Triton-X100 for the delivery molecular-specific contrast agents, antibodies specific to hTERT were delivered into live permeabilized cells. The sensitivity of this approach was validated using cell lines that differentially express hTERT and paired clinically normal and abnormal human biopsies. The feasibility of enhancing tissue permeation with Triton-X100 was assessed in freshly excised mucosal specimens. The depth and rate of tissue permeation following topical Triton-X100 treatment was evaluated as function of optical probe size. Delivery of molecular-specific optical contrast agents was tested in xenograft tumor specimens co-treated with Triton-X100. These experiments revealed that Triton-X100 can facilitate simultaneous labeling of clinically relevant intracellular and extracellular biomarkers in a controlled, uniform manner. Together, these findings provide evidence that cell- and tissue-impermeant contrast agents can be delivered into mucosal tissue in a sufficiently controlled and uniform manner to allow for cancer biomarker detection. Further studies are proposed to establish the safety of Triton-X100 for topical use *in vivo*.

ACKNOWLEDGEMENTS

This thesis is dedicated to my family, fiancée, and dogs for their love and support.

I would like to express my thanks to the following people

whose support made this work possible:

Dr. Rebecca Richards-Kortum

Vivian Mack

Dr. Karen-Adler Storthz

Laura Dillon

THE UNIVERSITY OF TEXAS
MD ANDERSON
CANCER CENTER

Dr. Ann Gillenwater

Dr. Sharmila Ananda

Dr. Lezlee Coghlan

This work was funded by an NIH BRP grant (CA103830) and a training fellowship from the Keck Center Nanobiology Training Program of the Gulf Coast Consortia (NIH grant 5 T90 DK071054-03).

TABLE OF CONTENTS

Chapter 1. Introduction..... 1-2

Chapter 2. Background and Rationale..... 3-10

2.1 Clinical motivation 3

2.2 Detection of dysplasia and cancer in the oral cavity 4

2.3 Targeting cancer biomarkers with molecular-specific agents 5

2.4 The challenge of intracellular delivery 7

2.5 Surfactants as chemical permeation enhancers 8

2.6 Measuring the success of topical delivery strategies 9

Chapter 3. Reversible Permeabilization of Live Cells for Intracellular Delivery of Optical Contrast Agents..... 11-38

3.1 Introduction 12

3.2 Materials and methods 13

Cell Culture *13*

Dose Dependency of Cell Permeabilization *14*

Permeabilization Detection Using Macromolecules *15*

Tracking the Time-Course of Macromolecule Entry *16*

Cell Metabolic Assay *16*

Population Doubling Assay *17*

Membrane Integrity Assay *17*

TABLE OF CONTENTS, CON'T

Chapter 3, Continued..... 11-38

Immunocytochemistry of Live Cells 18

Confocal Image Acquisition 19

3.3 Results 20

Dose-Dependent Permeabilization of Live Cells 20

Macromolecule Penetration Following Permeabilization 22

Cell Recovery After Treatment 29

Delivery of Targeted Optical Contrast Agents 32

3.4 Discussion 34

Chapter 4. Molecular Imaging of Telomerase in Live Cells and Fresh Tissues... 39-59

4.1 Introduction 40

4.2 Materials and methods 42

Cell Culture 42

Antibodies 42

Immunocytochemical Detection of hTERT 43

Competitive Binding Assay 43

Population Doubling Assay 43

Cell Viability Assessment 44

Animal Tumor Models 44

Fresh Human Tissues 45

TABLE OF CONTENTS, CON'T

Chapter 4, Continued..... 39-59

Image Acquisition and Analysis 45

4.3 Results 46

Detection of hTERT in Live Cell Monolayers 46

Quantitation of hTERT Labeling in Cells 49

Evaluation of Cell Viability 49

Detection of hTERT in Fresh Mouse Tumor Slices 52

Detection of hTERT in Human Oral Biopsies 53

4.4 Discussion 54

Chapter 5. Enhanced Mucosal Delivery of Topical Contrast Agents for Cancer Biomarker Detection..... 60-85

5.1 Introduction 61

5.2 Materials and methods 63

Cell Lines 63

Tissue Models 64

Permeation of Fresh Tissues 64

Permeabilization Detection Using Macromolecules 65

Tracking the Time Course of Tissue Permeation 65

Determination of the Depth of Penetration 66

Comparison of Macromolecule Penetration in Normal and Cancer Tissue 67

TABLE OF CONTENTS, CON'T

Chapter 5, Continued..... 60-85

Synthesis and Validation of Molecular-Specific Contrast Agents 67

Comparison of anti-EGFR Delivery Strategies in Tumors. 68

Demonstration of Multi-Target Labeling in Tumors. 68

Confocal Image Acquisition and Analysis. 69

5.3 Results 70

Permeabilization of Fresh Guinea Pig Bladder. 70

Depth of Mucosal Permeation. 72

Comparison of Macromolecule Penetration in Normal and Cancer Tissue 75

EGFR Targeting in Cancer 77

Multi-Target Labeling in Tumors. 77

5.4 Discussion 79

Chapter 6. Discussion and Future Directions..... 86-92

Chapter 7. Conclusions..... 93

References..... 94-109

LIST OF TABLES

1. Sensitivity of different cell lines to Triton-X100 permeabilization 22

LIST OF FIGURES

1.	Permeabilization of 1483 cell monolayers treated with different concentrations of Triton-X100, as measured by MTT reduction and 3kDa rhodamine-dextran uptake	21
2.	Macromolecule penetration into the cytoplasm and nucleus as a function of Triton-X100 concentration.	23
3.	Time-course of IgG accumulation in the cytoplasm and nucleus of Triton-X100 treated cells.	25
4.	Confocal images of AlexaFluor IgG influx and accumulation in a monolayer of 1483 cells	26
5.	Cumulative macromolecule penetration as a function of time following the administration of 0.55pmol/cell Triton-X100	28
6.	Cell recovery after treatment with Triton-X100	30-31
7.	Detection of intra-nuclear markers by immunofluorescence following Triton-X100 treatment	33
8.	Determination of hTERT antibody specificity in different cell lines	48
9.	Quantitation of hTERT labeling in HT1080 cells subjected to differing levels of serum	50
10.	The metabolic activity of 1483 cells 24 hours after treatment as assessed by MTT assay	51
11.	Optical detection of hTERT in freshly excised slices of 1483 cell tumors generated subcutaneously in mice.	54
12.	False-colored confocal images of hTERT labeling in transverse slices of oral biopsies.	55
13.	Macromolecule penetration of guinea pig bladder epithelium following permeation treatment.	71

LIST OF FIGURES, CON'T

14	The time course of tissue permeation following treatment with 0.5% Triton-X100.	73
15.	Permeation of normal oral mucosa as a function of time and Triton-X100 concentration	74
16.	Comparison of macromolecule penetration in normal oral mucosa and squamous cell carcinoma	76
17.	EGFR targeting in the presence of topical permeation enhancers.	78
18.	Simultaneous labeling of clinically relevant cancer biomarkers with 1.0% Triton-X100 co-treatment	80

CHAPTER 1

INTRODUCTION

Cancer results from an accumulation of key mutations at the molecular level. A technology facilitating the early identification of these molecular changes *in vivo* would have important clinical benefits. Molecular-specific optical contrast agents have received attention for their ability to selectively label cells expressing markers of interest. Efforts to design optical probes for detection of cancer and its precursors have focused on targeting biomarkers over-expressed on the surface of abnormal cells. Strategies to label intracellular targets in live cells and tissues have met limited success due to the challenge of delivering contrast agents with high specificity while maintaining cell viability. The goal of this project was to develop a robust strategy for the delivery of molecular-specific optical contrast agents into live cells and tissues. The following aims were designed to achieve this goal:

(1) To develop an efficient and reproducible strategy for intracellular delivery of optical contrast agents into live cells.

(2) To evaluate the feasibility of targeting human telomerase reverse transcriptase (hTERT) in live cells and fresh tissues.

(3) To translate intracellular delivery strategies for the topical permeation of mucosal tissue.

The collection of work contained in this thesis describes the development of a surfactant-based strategy to effectively and reproducibly label cancer biomarkers in live cells and tissues. Chapter 2 provides the background and rationale for this project. Chapter 3 introduces the use of Triton-X100 as a topical permeation agent. We demonstrate that Triton-X100, when used at the appropriate concentration, can deliver molecules of up to 150kDa into the nucleus of a variety of cells. Chapter 4 shows that Triton-X100 can be used in conjunction with molecular-specific optical contrast agents to investigate the expression of cancer biomarkers in cells and tissues. The clinical potential of this approach is demonstrated by labeling for hTERT in paired biopsies of human oral tissue. Chapter 5 describes the use of Triton-X100 to deliver contrast agents of variable sizes through multiple layers of normal and cancer tissue. Chapter 6 discusses the potential of Triton-X100 for topical use *in vivo* and proposes further experiments. The last chapter provides the conclusions that can be drawn from this work.

CHAPTER 2

BACKGROUND AND RATIONALE

In this chapter, I describe the motivation for developing a robust strategy to deliver molecular-specific contrast agents into live cells and tissues. Diagnostic approaches to the detection of dysplasia and cancer of the oral cavity are discussed to exemplify the weaknesses of current detection strategies. Molecular-specific optical contrast agents are presented as a non-invasive strategy to assess the molecular changes associated with tumorigenesis. Epidermal growth factor receptor (EGFR) and human telomerase reverse transcriptase (hTERT) are introduced as promising targets for the optical detection of cancer and its precursors. The challenge of delivering macromolecules into live cells and tissues is discussed within the context of topical delivery strategies. The chapter concludes with a discussion on the need for new methodologies to measure the success of the topical delivery strategies.

2.1 Clinical Motivation

Cancer is the second leading cause of death in developed countries and is widely acknowledged as one of the biggest public health problems worldwide. In the last decade, our understanding of the molecular changes that accompany carcinogenesis has

greatly advanced. The identification of unique cancer biomarkers has led to the successful development of molecular-specific therapies such as chemoprevention, chemo-radiation, and immunotherapeutics. Further molecular characterization of cancer and its precursors would provide important clinical benefits, including 1) earlier detection of precancerous cellular changes, 2) easier identification of high-risk lesions, 3) enhanced delineation of tumor margins, 4) smarter selection of molecular therapies, and 5) faster assessment of therapy success.

Over 85% of human cancers originate in epithelial tissues [1]. It is believed that a vast majority of epithelial cancers start as pre-invasive lesions, usually decades before a tumor is palpable [2, 3]. Precancerous changes of the epithelium originate near the basement membrane and are typically less than 500 microns below the tissue surface, making them amenable to examination with optical imaging technologies [4-7]. It has been demonstrated that bulk changes in tissue properties, including tissue fluorescence [8-10] and reflectance [11-14], are useful for distinguishing between normal and precancerous tissue *in vivo*. Molecular-specific contrast agents promise to increase the sensitivity of optical imaging modalities, facilitating the detection of small intra-epithelial lesions before bulk tissue changes occur.

2.2 Detection of Dysplasia and Cancer in the Oral Cavity

In the United States, it is predicted that nearly 30,000 new cases of oral cancer are diagnosed each year, with approximately 7,200 deaths due to oral cancer in 2003 [15]. Despite the fact that the oral cavity is an easily accessible area for screening, oral cancer

still accounts for 1.7% of all cancer-related deaths [16]. Overall, the five-year-survival rates for patients with advanced stage disease remain at 23% or less [15, 17]. This five-year survival rate is among the lowest of major cancers worldwide [18].

The diagnosis of oral cancer is achieved through visual identification and recognition, which relies on the experience of the treating clinician. Thus oral cancer is generally not diagnosed until it has reached advanced stages when treatment is more difficult and debilitating. Early diagnosis could potentially improve the five-year survival rate from 9% (stage IV at diagnosis) to nearly 100% (premalignant at diagnosis) [16, 19]. Early diagnosis can also improve patient quality of life since less radical and debilitating treatments are needed for earlier lesions [19]. At present, there is no mechanism to adequately screen and detect pre-malignant changes of the oral mucosa. Thus there is great interest in the development of optical techniques to facilitate a non-invasive assessment of the molecular changes preceding cancer.

2.3 Targeting Cancer Biomarkers with Molecular-Specific Contrast Agents

Molecular-specific optical contrast agents have been investigated as potential non-invasive probes for the detection of cancer and its precursors. These contrast agents are preferentially targeted to molecules that are differentially expressed with disease. Targeting agents which have been successfully used for optical detection of cancer in animal models include antibodies [20-25], growth factors [26-30], peptide analogs of extracellular ligands [31-34], and enzymatically activatable polymers [35-39]. The coupling of optically active tags to these targeting agents allows molecular events to be monitored

non-invasively *in vivo* [40]. These molecular-specific optical contrast agents have the potential to provide dynamic, real-time information without the need for biopsy and associated patient discomfort

Most optical contrast agents developed for cancer detection have been targeted towards biomarkers over-expressed on the surface of dysplastic and/or neoplastic cells. For example, human epidermal growth factor receptor (EGFR) is thought to be a promising target for optical contrast agents because its expression is elevated in a variety of cancers including that of the brain, bladder, colon, lung, ovary, and prostate [41-43]. EGFR has been implicated to play a role in both the pathogenesis and progression of multiple carcinomas [44]. Over-expression of EGFR is associated with increased metastatic potential and poor prognosis in patients with cancer of the breast [45] and oral cavity [46, 47]. Recognition of the widespread over-expression of EGFR has led to the development of four EGFR antagonists for anti-tumor therapy [48, 49]. Optically active EGFR-targeted contrast agents have been shown to effectively target cells over-expressing EGFR in pre-clinical studies [26-29].

The development of contrast agents targeted to intracellular biomarkers has been hindered by a lack of robust delivery strategies. The detection of human telomerase reverse transcriptase (hTERT) protein, the most widely expressed cancer biomarker identified to-date [50, 51], has traditionally been limited to immunohistochemistry studies in fixed cells and tissues. Like EGFR, hTERT appears to be a promising target for optical contrast agents due to its diagnostic and prognostic potential (described further in chapter

4). The successful labeling of hTERT, however, requires the development of an effective and reproducible intracellular delivery strategy.

2.4 The Challenge of Intracellular Delivery

The delivery of macromolecules into live cells has proven to be a major challenge. Important metabolic ions and molecules that are taken up by cells depend on specific transport mechanisms present at the plasma membrane. Molecules which do not bind surface receptors with high specificity and affinity are not internalized by cells [52]. Well-established procedures for *in vitro* delivery of macromolecules, including pressure, microinjection, lipofection, and electroporation, are not amenable to clinical application. Strategies that take advantage of natural cell uptake mechanisms, such as conjugating contrast agents to proteins or peptides to facilitate receptor-mediated endocytosis, have met limited success. This strategy requires a contrast agent to bind the cell surface, initiate endosomal uptake, escape from the resulting lysosome, and reach the target in sufficient quantity to allow optical detection. Nuclear penetration adds an additional level of complexity since molecules larger than 9 nm require transport by specific cargo-receptor interactions [53, 54]. The engineering of highly specific, optically active probes with the appropriate physiochemical properties for cell-mediated internalization is not always practical or feasible.

There has recently been a surge of interest in the use of chemical permeation enhancers for the topical delivery of contrast agents into cells and tissues. Polar aprotic solvents, terpenes, bile salts, pyrroliodones, and surfactants have been all investigated for their

ability to enhance the transport of small molecules. For example, dimethyl sulfoxide (DMSO) is readily permeable through biological membranes, including human skin. The dipolar structure of DMSO allows it interact with the hydrophilic region of membrane lipids to modify cell membrane permeability [55]. When co-administered with low molecular weight solutes of hydrophilic or lipophilic nature, it increases the ability of solutes to penetrate cell and tissue barriers [56]. Thus DMSO is commonly used as a drug adjuvant to enhance delivery [55, 56].

2.5 Surfactants as Chemical Permeation Enhancers

Surfactants are frequently used in oral pharmaceutical preparations to improve the wetting and solubilization of insoluble drugs. Surfactants have come under investigation as potential permeation enhancers for the topical delivery of cell- and tissue-impermeant molecules. The goal of these topical formulations is to reversibly enhance tissue permeability with minimal side-effects. Since surfactants increase molecule flux by damaging cell membranes, the feasibility of this approach remains to be determined

Triton-X100™ ($C_{14}H_{22}O(C_2H_4O)_{9.5}$) is a non-ionic surfactant comprised of hydrophilic polyethylene oxide and lipophilic hydrocarbon moieties. It is distinguished from the other members of the Triton-X family by the number of ethylene oxide units per molecule (9-10 units). Triton-X100 is well-known for its ability to solubilize a number of integral membrane proteins without compromising their biological activities [57]. At lower concentrations, Triton-X100 can act as a membrane preturbant [57]. Triton-X100 has been used at low concentrations to study intracellular protein activity and release [58-62].

The mechanism by which Triton-X100 facilitates cell permeabilization is not yet fully known. Surfactant monomers, when mixed with phospholipid bilayers, have the ability to intercalate into bilayers. When a critical insertion concentration is reached, the lipid and detergent molecules reorganize into mixed micelles and a variety of intermediate structures [63]. For biological membranes, containing both protein and lipid components, it is still debated whether changes in cell membrane permeability are caused by increased fluidity of the lipid phase or by a direct interaction of the surfactant with membrane proteins [64-66]. The existence of insoluble lipid rafts following treatment with Triton-X100 monomers suggests that Triton-X100 preferentially partitions into specific lipid domains [67, 68]. Recent optical studies of cells treated with Triton-X100 demonstrated selective solubilization of the non-raft, liquid-disordered phase of the cell membrane [69]. In all studies contained in this thesis, Triton-X100 is used at concentrations below the critical micelle concentration. Thus, Triton-X100 is expected to behave similarly as described here.

2.6 Measuring the Success of Topical Delivery Strategies

The use of chemical permeation enhancers in live cells presents many challenges. A successful strategy for the delivery of optical contrast agents must be nondestructive, efficient, and reproducible. With the use of chemical permeation enhancers, it will be important to show that both the contrast agent and the target itself are stable in the presence and absence of the permeation treatment. General measures of cell health, such as metabolic activity, proliferative capacity, and membrane integrity should recover following treatment. In an ideal case, all cells would be permeabilized rapidly and simultaneously so that each cell would be subjected to the same labeling conditions.

Reproducibility will play an important role in the quantitation of labeling from experiment to experiment.

In translating intracellular labeling strategies from cells to tissues, it is important to recognize that contrast agent delivery presents different challenges than drug delivery. Traditional measures of tissue permeability, such as the tissue flux and blood serum concentration following topical application, have little relevance. The end goal of topical contrast agent administration is to deliver the molecules uniformly to all cells within a region of interest. A non-uniform distribution of contrast agent will result in incomplete labeling, which in turn will affect the conclusion drawn about the relative intensity and localization of labeling. New methodologies are needed for studying the distribution of contrast agent delivery within tissue.

CHAPTER 3

REVERSIBLE PERMEABILIZATION OF LIVE CELLS FOR INTRACELLULAR DELIVERY OF OPTICAL CONTRAST AGENTS

Effective delivery of optical contrast agents into live cells remains a significant challenge. I sought to determine whether Triton-X100, a surfactant commonly used for membrane isolation and protein purification, could be used to effectively and reversibly permeabilize live cells for delivery of targeted optical contrast agents. Although Triton-X100 is widely recognized as a good cell permeabilization agent, no systematic study has evaluated the efficiency, reproducibility, and reversibility of Triton-X100 mediated permeabilization in live mammalian cells. In this chapter, I report a series of studies to characterize macromolecule delivery in cells following Triton-X100 treatment. Using this approach, I demonstrate that molecules ranging from 1kDa to 150kDa in molecular weight can be reproducibly delivered into live cells by controlling the moles of Triton-X100 relative to the number of cells to be treated. When Triton-X100 is administered at or near the minimum effective concentration, cell permeabilization is generally reversed within 24 hours, and treated cells continue to proliferate and show metabolic activity during the restoration of membrane integrity. I conclude that Triton-X100 is a promising permeabilization agent for efficient and reproducible delivery of optical contrast agents into live mammalian cells.

3.1 INTRODUCTION

The identification of unique molecular markers of cancer and its precursors has stimulated the development of new cancer screening tools. A technology facilitating the non-invasive identification of precancerous lesions at high risk for progression would have important clinical benefits. Molecular-specific optical contrast agents have garnered attention for their ability to selectively label cells expressing markers of interest. Optical probes targeting extracellular biomarkers have advanced to preclinical animal models and pilot clinical trials. The development of contrast agents targeted to intracellular biomarkers has proved to be more challenging. Multi-functional contrast agents designed to utilize cell uptake mechanisms have been reported; however, the engineering of highly specific, optical probes with the appropriate physiochemical properties for cell internalization is difficult and not always feasible. There is need for a strategy to facilitate the intracellular delivery of existing contrast agents into live cells.

Chemical surfactants have traditionally been used as solubilizing agents for the study of biological membranes [70]. At sub-solubilizing concentrations, surfactants can be used to perturb membrane structure and increase cell permeability [57, 63, 71-74]. Chemical surfactants have achieved widespread use as permeabilization agents for immunohistochemistry. In live cells, surfactants have shown limited success as permeabilization agents due to the challenge of retaining cell viability following permeabilization. Of the surfactants tested to date, Triton-X100 has shown the most promise as a cell permeabilization agent. Triton-X100 has been used to non-destructively release secondary metabolites in plant cells [58-60] and to study *in situ* enzymatic assays in

yeast [61, 62]. No systematic study has been performed in mammalian cells to determine how universally efficient, reproducible, and reversible this process is.

I sought to determine whether Triton-X100 can be used to effectively and reversibly permeabilize live mammalian cells for contrast agent delivery. Here I describe the use of macromolecule uptake assays to evaluate the efficiency of cell permeabilization. I find that there is a minimum effective Triton-X100 concentration, in which cell permeabilization efficiency is balanced with cell loss after treatment. Cell recovery after treatment is evaluated using cell viability, population doubling, and membrane integrity assays. Together the findings indicate that Triton-X100, when used at or near the minimum effective concentration, can permeabilize a variety of live cells in a reproducible and reversible manner.

3.2 MATERIALS AND METHODS

Cell Culture. The ability of Triton-X100 to permeabilize human cell lines was evaluated using carcinoma cells (1483, HeLa), SV-40 transformed cells (GM847), and primary cells (HDF, MCF-10A). The 1483 cell line [75] was obtained from Dr. Reuben Lotan at the M.D. Anderson Cancer Center (Houston, TX). HeLa and MCF-10A cells were purchased from American Type Culture Collection (ATCC, Manassas, VA). GM847 cells were obtained from Coriell Cell Repositories (Camden, NJ). HDF cells were purchased from Lonza (Walkersville, MD). 1483 cells were cultured in Dulbecco's Modified Eagle Medium:Nutrient Mix F-12® medium supplemented with L-glutamine (Invitrogen, Carlsbad, CA) and 10% fetal bovine serum (FBS; Hyclone, Logan, UT).

HeLa and GM847 cells were cultured in Minimum Essential Medium® supplemented with L-glutamine, non-essential amino acids, sodium pyruvate, vitamins (Invitrogen) and 10% FBS. HDF cells were cultured in Fibroblast Growth Medium-2® (Lonza). MCF-10A cells were cultured in Mammary Epithelium Growth Medium® (Lonza).

Dose Dependency of Cell Permeabilization. To determine the minimum effective Triton-X100 concentration required to permeabilize live cells, 1483, Hela, GM847, HDF, and MCF-10A cells were assayed for membrane integrity and cell viability following treatment with different concentrations of Triton-X100. Briefly, subconfluent monolayers of cells (plated 24 hours in advance at 5×10^4 cells/cm^2) were washed once with cold phosphate buffered saline (PBS; Sigma-Aldrich, St. Louis, MO) and treated with Triton-X100 (Sigma-Aldrich) for 10 minutes at 4°C. Triton-X100 concentrations ranged from 0 to 5.5 pmol/cell, normalized relative to the cell count at the time of plating. After permeabilization, the cells were washed once in media and returned to the incubator. Four hours later, pre-warmed 3-(4,5-dimethylthiazol-2-yl)-2,5-diphenyl tetrazolium bromide (MTT; Sigma-Aldrich) was added for 20 minutes at a concentration of 0.5mg/ml. Thereafter, the cells were washed, labeled with 1μM 3kDa rhodamine-dextran (Invitrogen), and imaged using confocal microscopy (described below). Viable cells were identified by the reduction of MTT in using light microscopy and permeabilized cells by the intracellullar uptake of fluorescence. The minimum effective Triton-X100 concentration was defined as the concentration at which ≥ 95% of cells were permeabilized. 300-500 cells were evaluated from representative fields of view for each treatment condition in 5 independent experiments. Differences between cell lines were

assessed using a two-tailed, unpaired Student's t-test, with p-values of < 0.05 considered statistically significant.

Permeabilization Detection Using Macromolecules. To determine whether Triton-X100 treated cells are permeable to macromolecules of different sizes, monolayers of treated cells were probed with 3kDa, 40kDa, 150kDa fluorescent macromolecules. Briefly, subconfluent monolayers of 1483 cells were permeabilized with 0 to 1.1 pmol/cell Triton-X100 for 10 minutes at 4°C, cells were washed once in media, and covered with a 1:1:1 mixture of rhodamine-dextran (3kDa, Invitrogen), fluorescein-dextran (40kDa, Invitrogen), and AlexaFluor647 IgG (150kDa, Invitrogen), each diluted to a concentration of 1μM in PBS. Cells were incubated with this solution for 20 minutes at 4°C and then imaged using fluorescence confocal microscopy at three different excitation wavelengths. The optical imaging plane was focused to yield a cross-section of the cytoplasm and nucleus for each cell in the field of view. Using NIH ImageJ v1.34 software (http://rsbweb.nih.gov/ij/), the mean fluorescence intensity was determined for selected regions of interest. The mean fluorescence intensity of the cytoplasm and nucleus was compared to that of the extracellular solution on a cell to cell basis. Cells were defined as permeable if the mean cytoplasmic and/or nuclear fluorescence intensity was equal or greater than ½ of the mean extracellular fluorescence intensity. This threshold parameter was selected based on the observation that not all cells reach 100% of the extracellular mean fluorescence intensity. 100-300 cells were evaluated from representative fields of view in 3 separate experiments.

Tracking the Time-Course of Macromolecule Entry. Macromolecule entry was tracked in real-time to evaluate macromolecule penetration as a function of time. Rhodamine-dextran (3kDa), fluorescein-dextran (40kDa, 70kDa), and AlexaFluor647 IgG were individually diluted to a concentration of 1μM in 0.05% Triton-X100. These solutions were topically applied to subconfluent 1483 cell monolayers grown on glass coverslips. Based on the cell count at the time of plating, an appropriate volume was selected to yield a final concentration of 0.55 pmol/cell Triton-X100. This concentration was selected to facilitate both cytoplasmic and nuclear penetration of the larger macromolecules. The movement of macromolecules into the cells was monitored using time-lapse fluorescence confocal microscopy. Again, the optical imaging plane was focused to yield a cross-section of the cytoplasm and nucleus for each cell in the field of view. Images were acquired every 15 seconds. The mean fluorescence intensities of the cytoplasm and nucleus were compared to that of the extracellular solution by selecting regions of interest within a time stack and normalizing relative to the mean fluorescence intensity of the extracellular solution in each image. No other background corrections were made. Ten cells were evaluated from a representative field of view in 5 separate experiments. All fluorescence quantitation was performed using ImageJ software. The mean fluorescence intensity of each cell compartment one hour after macromolecule addition and the time required to achieve > 98% fluorescence accumulation was determined from time versus intensity plots for each macromolecule.

Cell Metabolic Assay. Cells were assayed for metabolic activity 24 hours following Triton-X100 treatment by monitoring the reduction of MTT as described in [76].

Subconfluent monolayers of 1483 cells were permeabilized with 0 to 5.5 pmol/cell Triton-X100 for 10 minutes at 4°C, washed once, and then returned to pre-warmed complete medium for 24 hours. Cellular metabolic activity was evaluated in triplicate in five separate experiments using the ATCC MTT assay. The absorbance measurement from each well was divided by the number of cells per well remaining after treatment to determine the mean absorbance per cell.

Population Doubling Assay. Population doubling experiments were performed with subconfluent monolayers of 1483 and MCF-10A cells to determine the effect of Triton-X100 treatment on cell proliferation. Cells were plated at an appropriate concentration to allow log-linear growth for 5 days. Twenty-four hours after plating, cells were washed with PBS, treated with 0.55 pmol/cell Triton-X100 or PBS for 10 minutes at 4°C, and then returned to pre-warmed complete media. The number of cells remaining after treatment and the rate of population doubling was assessed in duplicate at 4 different timepoints in three separate experiments. Differences in rate of population doubling between each treatment group were assessed using a two-tailed, unpaired Student's t-test, with p-values of < 0.05 being considered statistically significant.

Membrane Integrity Assay. To determine whether cells recover their membrane integrity after Triton-X100 treatment, cells were tested for their ability exclude macromolecules 8-24 hours after permeabilization. Subconfluent monolayers of 1483 cells cultured on glass coverslips were permeabilized for 10 minutes at 4°C with 0.55 pmol/cell Triton-X100, washed once, and then returned to pre-warmed complete media.

At regular intervals after permeabilization, cells were treated with 0.5mg/ml MTT for 20 minutes at 37°C, washed, and covered with a 1:1:1 mixture of rhodamine-dextran, fluorescein-dextran, and AlexaFluor647 IgG (each diluted to 1μM in PBS). Viable cells were identified by color deposition under brightfield imaging. Macromolecule exclusion was monitored using fluorescence confocal microscopy. Cells were considered to have an intact membrane if the mean fluorescence intensity of the cytoplasm and/or nucleus was less than 1% of the extracellular intensity. 100-300 cells were evaluated from representative fields of view in 3 separate experiments.

Immunocytochemistry of Live Cells. Cells were labeled with nuclear-specific antibodies to validate the use of Triton-X100 for delivery of targeted contrast agents. Polyclonal rabbit anti-human PC563-hTERT antibody was purchased from EMD Biosciences (San Diego, CA). Monoclonal mouse anti-human NCL-hTERT antibody was purchased from Novocastra (Newcastle upon Tyne, United Kingdom). Goat anti-rabbit AlexaFluor 647 IgG, goat anti-mouse AlexaFluor 488 IgG, purified polyclonal rabbit IgG, and monoclonal mouse IgG_{2aK} were purchased from Invitrogen. Subconfluent monolayers of live 1483 cells (5×10^4 cells/cm^2) cultured on coverslips were labeled with antibodies as follows: 24 hours after plating, the cells were washed with PBS, treated with 0.55 pmol/cell Triton-X100 for 10 minutes, blocked for 10 minutes with a saline buffer containing 1% BSA/2% goat serum, and then labeled for 1 hour with PC563-hTERT (1:80 dilution) and NCL-hTERT (1:800 dilution) antibodies. Following 3 washes, cells were probed with a 1:500 dilution of AlexaFluor 647 and 488 IgG antibodies for 1 hour, washed, and imaged live using confocal microscopy. As a control,

live cells were labeled in parallel with primary IgG antibodies and secondary AlexaFluor antibodies. For comparison with established immunocytochemistry protocols, cells were fixed for 30 minutes with 10% formalin immediately before or after Triton-X100 treatment. Fixed cells were immuno-labeled as described above. Cell labeling was evaluated in triplicate in three separate experiments. All cells were imaged in the same optical plane. All stock solutions were diluted in PBS; all labeling was performed at 4°C.

Confocal Image Acquisition. All images were obtained using a Carl Zeiss LSM 510 confocal microscope (Thornwood, New York) equipped with 488 nm (30mW), 543 nm (1mW), and 633 nm (5mW) lasers. Images were collected using PMT detectors and Zeiss LSM 5 image examiner software. Samples were sequentially excited with each laser line, with power settings of 50%, 100%, 100% respectively. Fluorescence emission was collected using 505-550 nm, 565-615 nm, and 650-710 nm band-pass filters respectively. Images were acquired at 0.5 frames per second using a 63X oil objective with a pinhole of 2.56 Airy units. For macromolecule uptake and exclusion studies, the gain was held constant below the saturation level of the extracellular solution. For the immunocytochemistry studies, the gain was held constant at 535 (488 nm excitation) and 440 (633nm excitation). Fluorescence recovery after photobleaching tests were performed using these imaging parameters to ensure that no photobleaching of the macromolecules occurred.

3.3 RESULTS

Dose-Dependent Permeabilization of Live Cells. To determine the relationship between cell permeabilization and short-term viability, monolayers of 1483 squamous carcinoma cells were treated for 10 minutes with different concentrations of Triton-X100 and then assayed for MTT reduction and 3kDa rhodamine-dextran uptake. The Triton-X100 concentration was normalized relative to the number of cells being treated. Figure 1 shows the dose-dependent response to Triton-X100 treatment, in terms of pmol Triton-X100 added per cell. The solid triangles indicate the percentage of cells permeabilized; the hollow diamonds indicate the percentage of viable cells remaining after treatment. Cells treated with 0.18 pmol/cell or less showed little to no uptake of dextran following treatment. Cells treated with 0.28 pmol/cell or above showed dextran uptake in >95% of the cells. Cell loss was dependent on Triton-X100 dose, with the percentage of viable cells decreasing as the concentration of Triton-X100 was increased. After treatment with 0.28 pmol/cell Triton-X100, 98 ± 3% of the cells were viable, compared to 99 ± 1 % of PBS-treated controls.

Different cell lines were evaluated for their sensitivity to Triton-X100 treatment. Table 1 shows the minimum Triton-X100 concentration required to permeabilize ≥ 95% of each cell population for the delivery of 3kDa molecules. No significant differences were observed between squamous carcinoma cells, SV-40 transformed cells, and primary cells. The minimum effective Triton-X100 concentration was 0.27 pmol/cell for all cell lines evaluated. Cell viability after treatment was greater than 90% for all cell lines at the minimum effective Triton-X100 concentration.

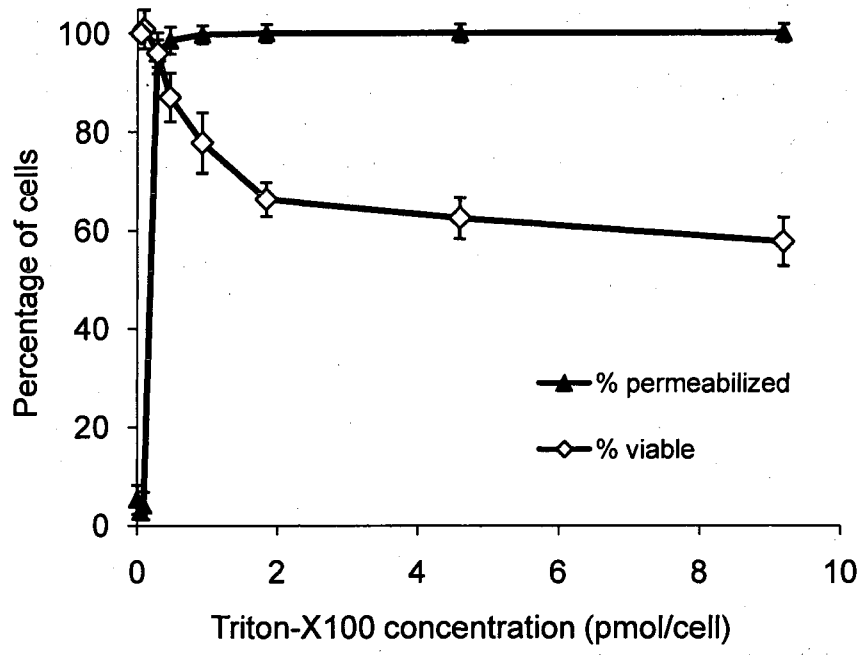

Figure 1. Permeabilization of 1483 cell monolayers treated with different concentrations of Triton-X100, as measured by MTT reduction and 3kDa rhodamine-dextran uptake. Cells were treated with Triton-X100 for 10 minutes, incubated in media for 4 hours, and then assayed for cell viability and membrane integrity. The percentage of cells permeabilized (▲) appears to have a threshold concentration above which nearly all cells admit 3kDa rhodamine-dextran. Little to no dextran uptake occurs at lower Triton-X100 concentrations. The viability of cells after treatment (◊) is dependent on the amount of Triton-X100 used. The error bars represent 1 standard deviation.

Table 1. Sensitivity of different cell lines to Triton-X100 permeabilization

Cell Line	Derivation	Min. Triton Concentration to Permeabilize ≥ 95% of cells (pmol/cell)	Cells Remaining at Min. Concentration (%)
1483	oral squamous cell carcinoma	0.27 ± 0.07	97 ± 4
HeLa	cervical squamous cell carcinoma	0.27 ± 0.06	92 ± 8
GM847	SV-40 transformed fibroblast	0.27 ± 0.06	93 ± 6
HDF	primary fibroblast	0.26 ± 0.06	98 ± 3
MCF-10A	primary epithelial cell	0.27 ± 0.04	94 ± 7

Macromolecule Penetration Following Permeabilization. To determine whether cells are selectively permeable to macromolecules of different sizes, monolayers of Triton-X100 treated cells were topically labeled with a 1:1:1 mixture of 3kDa rhodamine-dextran, 40kDa fluorescein-dextran, and 150kDa AlexaFluor647 IgG. Dextrans were selected for their neutral charge and IgG was selected for its size and structural similarity to targeted antibodies. The fraction of cells permeable to each macromolecule is shown in Figure 2. Figure 2A shows the dose-dependent permeabilization of the cytoplasm; Figure 2B shows that of the nucleus. The 3kDa dextran successfully penetrated both cell compartments in over 95% of cells treated with 0.22 pmol/cell Triton-X100 and above. The penetration of larger molecules varied by cell compartment. At 0.22 pmol/cell Triton-X100, 83% of the cells that were permeable to 3kDa dextran also contained 40kDa dextran and 150kDa IgG in the nucleus. Concentrations upwards of 1.1 pmol/cell were required to permeabilize the nucleus of ≥ 95% of cells. Thus, for Triton-X100 concentrations ranging from 0.18 to 0.55 pmol/cell, we observed that some nuclei were permeable to 3kDa molecules but not 40kDa and 150kDa molecules.

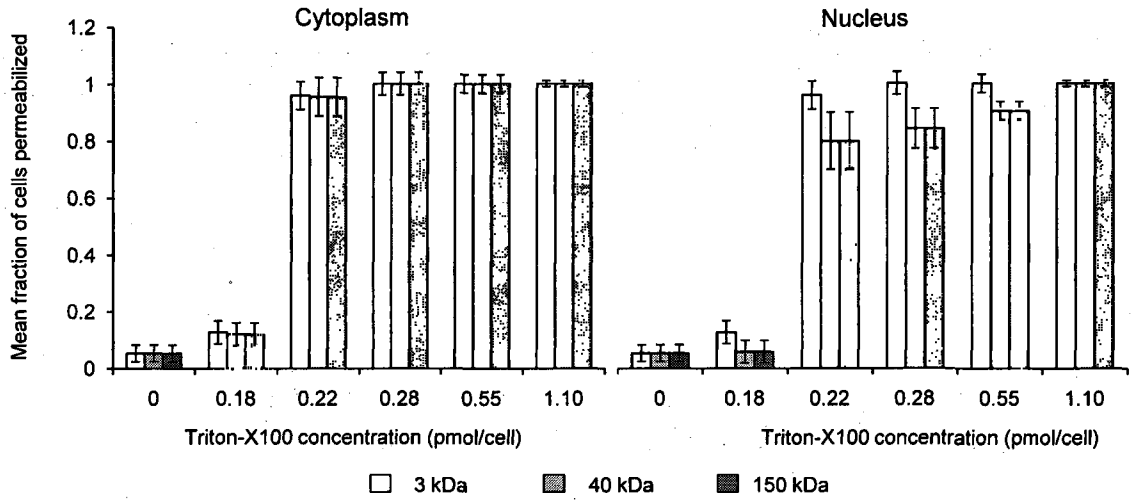

Figure 2. Macromolecule penetration into the cytoplasm and nucleus as a function of Triton-X100 concentration. Subconfluent monolayers of 1483 cells were pre-treated with different concentrations of Triton-X100 for 10 minutes, and then probed with a 1:1:1 mixture of 3kDa rhodamine-dextran, 40kDa fluorescein-dextran, and AlexaFluor647 IgG. Macromolecule penetration of the cytoplasm appears to independent of size, with no significant difference observed within each treatment group. Macromolecule penetration of the nucleus shows a stronger dependence on Triton-X100 concentration. Cells required a higher concentration of Triton-X100 permit nuclear entry of 40kDa and 150kDa molecules. At 1.10 pmol/cell, all macromolecules successfully penetrated both the cytoplasm and nucleus of treated cells. The error bars represent 1 standard deviation.

Interestingly, there was no exclusion of 150kDa molecules from nuclei which were permeable to 40kDa molecules. The mean fraction of cells permeabilized was independently validated by treating cells with one macromolecule at a time (data not shown) to exclude any interacting effects.

Macromolecule penetration was tracked as a function of time using time-lapse confocal microscopy. Molecules of all sizes could be observed in the cytoplasm and nucleus of cells as early as 15 seconds after the administration of Triton-X100. Figure 3 shows the cumulative uptake of fluorescent IgG (normalized relative to the fluorescence intensity of the extracellular solution) following the administration of 0.55pmol/cell Triton-X100. The solid triangles represent the mean fluorescence intensity of the cytoplasm and the hollow squares represent that of the nucleus. The circles represent IgG influx in the absence of Triton-X100. After the addition Triton-X100, fluorescent IgG rapidly enters both the cytoplasm and nucleus of cells. At approximately five minutes, both cell compartments reached a mean fluorescence intensity equal to that of the extracellular IgG. Continued influx of IgG slowly raised the mean fluorescence intensity of both cell compartments for an additional 10 minutes. Once the maximal intensity was reached at approximately 16 minutes, no further changes were observed over the course of an hour. The accumulation of IgG occurred in both the presence and absence of serum (data not shown). IgG uptake in the absence of Triton-X100 was negligible. Representative confocal time-lapse images of intracellular IgG accumulation are shown in Figure 4.

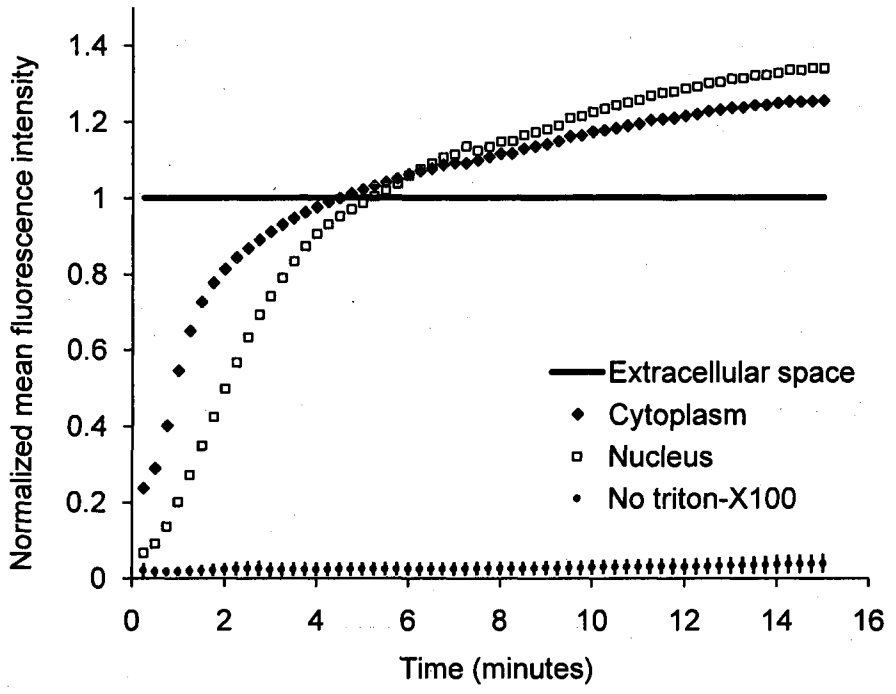

Figure 3. Time-course of IgG accumulation in the cytoplasm and nucleus of live 1483 cells treated with Triton-X100, averaged over 5 trials. Cells are permeabilized rapidly, with both the cytoplasm (◊) and nucleus (■) achieving a mean fluorescence intensity equal to that of the extracellular space at approximately 5 minutes. Cells treated with IgG in the absence of Triton-X100 showed no significant uptake of fluorescence. All samples were normalized relative to the extracellular fluorescence. Error bars were removed for clarity; the error ranged from ± 0.01 to 0.10 AU for one standard deviation.

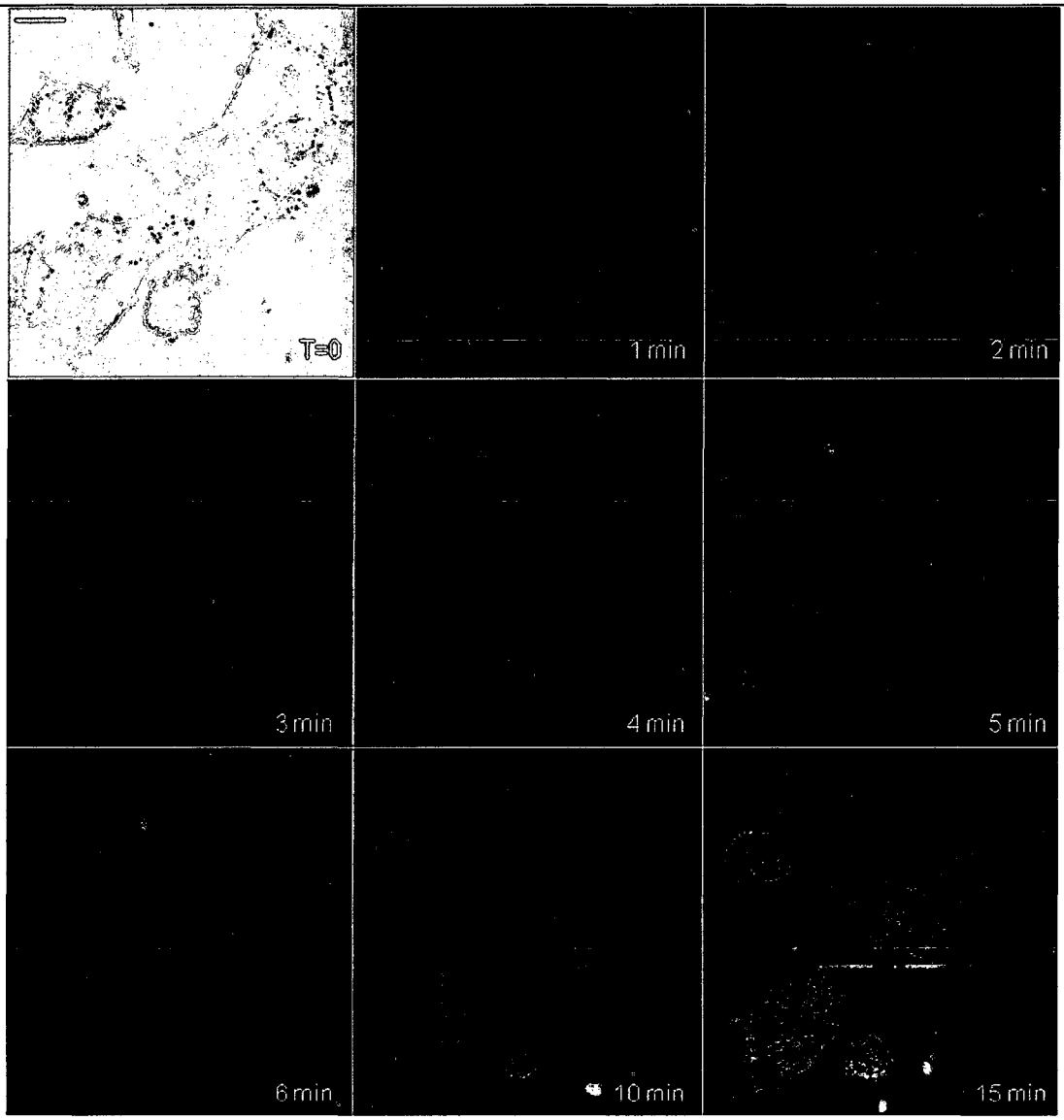

Figure 4. Confocal images of AlexaFluor IgG influx and accumulation in a monolayer of 1483 cells. The DIC image at time zero is shown at the top left. With the topical application of IgG in 0.55pmol/cell Triton-X100, selective permeabilization of the cell membrane, followed by that of the nuclear membrane, is observed. At 5 minutes, all cell compartments exhibit some fluorescence. Continued IgG influx causes mean fluorescence of cells to rise above that of the extracellular solution. The scale bar represents 20 μm

The cumulative macromolecule uptake following treatment with 0.55pmol Triton-X100 was measured for macromolecules of 4 sizes. As shown in Figure 5, the mean fluorescence intensity of cell cytoplasm and nucleus was measured relative to that of the extracellular space 1 hour after Triton-X100 addition. The total penetration varied by molecule size as well as the target cell compartment. The 3kDa dextran uniformly penetrated both the cytoplasm and nucleus of treated cells. The 40kDa and 70kDa dextrans penetrated to a lesser degree and preferentially localized to the cytoplasm. The 150kDa IgG preferentially accumulated in both cell compartments and raised the mean fluorescence intensity of both cell compartments above that of the extracellular space.

The time required for macromolecule accumulation was measured using time-lapse confocal microscopy. Figure 5B shows the time required to achieve > 98% macromolecule accumulation after Triton-X100 addition, as determined from the mean intracellular fluorescence accumulation over time. The time required for macromolecule uptake appeared dependent on macromolecule size, with the larger molecules requiring more time to accumulate inside treated cells. The macromolecule accumulation time ranged from 4.0 ± 0.8 to 9.1 ± 1.5 minutes for 3kDA and 40kDa molecules, and from 11.8 ± 1.3 to 16.0 ± 1.3 minutes for the 70kDa and 150kDa molecules. No significant differences were observed between cell compartments for any given macromolecule. These trends were independent of macromolecule concentration (data not shown).

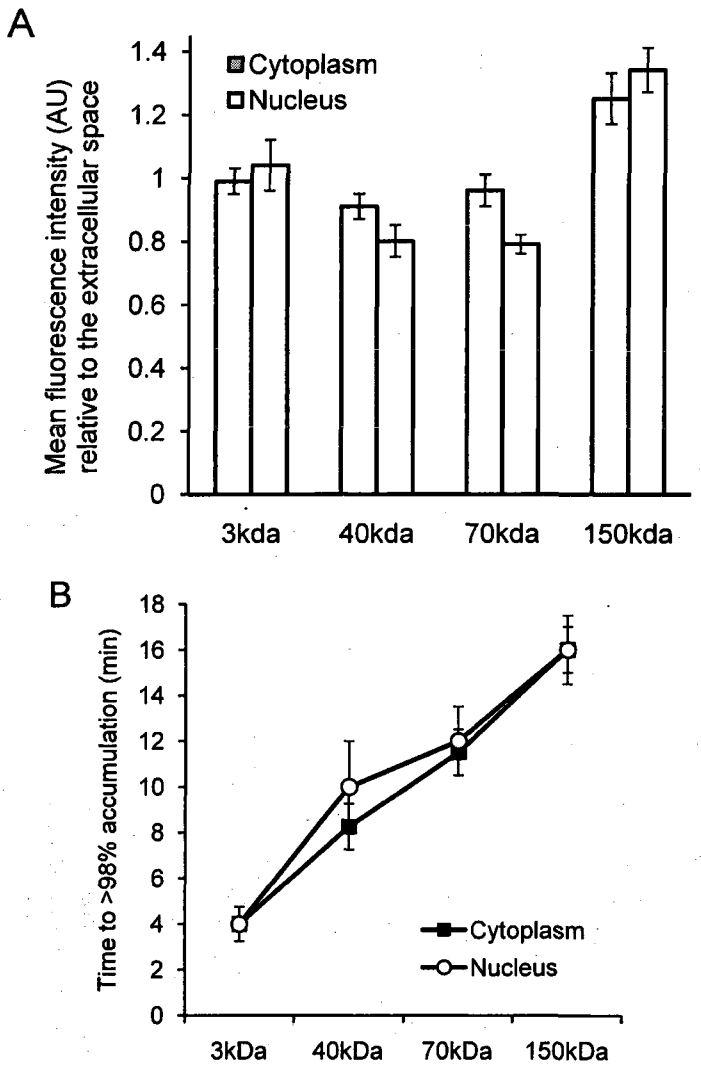

Figure 5. Cumulative macromolecule penetration as a function of time following the administration of 0.55pmol/cell Triton-X100. A) The mean fluorescence intensity of each cell compartment relative to that of the extracellular space one hour after Triton-X100 addition. B) The time required for greater than 98% macromolecule accumulation in the cytoplasm (■) and nucleus (○) of Triton-X100 treated cells. The time required for macromolecule uptake appears to be dependent on macromolecule size. No significant differences are observed between the cell compartments. Error bars represent 1 standard deviation.

Cell Recovery after Treatment. Monolayers of 1483 cells were assayed for metabolic activity 24 hours after treatment with different concentrations of Triton-X100. Figure 6A shows the mean absorbance measured at 570 nm following MTT reduction by viable cells. Absorbance measurements of the total cell population at each Triton-X100 concentration yielded a dose-dependent decrease in absorbance. When the population data was adjusted for the number of cells remaining after 24 hours after treatment, it was found that cells treated with 1.1 pmol/cell Triton-X100 or less retained full metabolic activity. Treatment with higher concentrations of Triton-X100 resulted in cell death and/or loss of metabolic activity, leading to a reduction in the mean absorbance per cell.

The proliferative capacity of 1483 cells following Triton-X100 treatment was determined using a population doubling assay. Figure 6B shows the cumulative cell number for 3 days following treatment with 0.55pmol/cell Triton-X100 or PBS. Approximately 87 ± 1% of the adherent cells remained immediately after Triton-X100 treatment. Both treatment groups continued to proliferate with time. We observed a slight difference in the rate of population doubling for each treatment group; however, the differences observed were not statistically significant (0.037 ± 0.012 cells/hr for Triton-X100 treatment versus 0.041 ± 0.008 cells/hr for PBS treatment). Similarly, no significant differences in population doubling were observed between Triton-X100 and PBS-treated primary MCF-10A cells (data not shown).

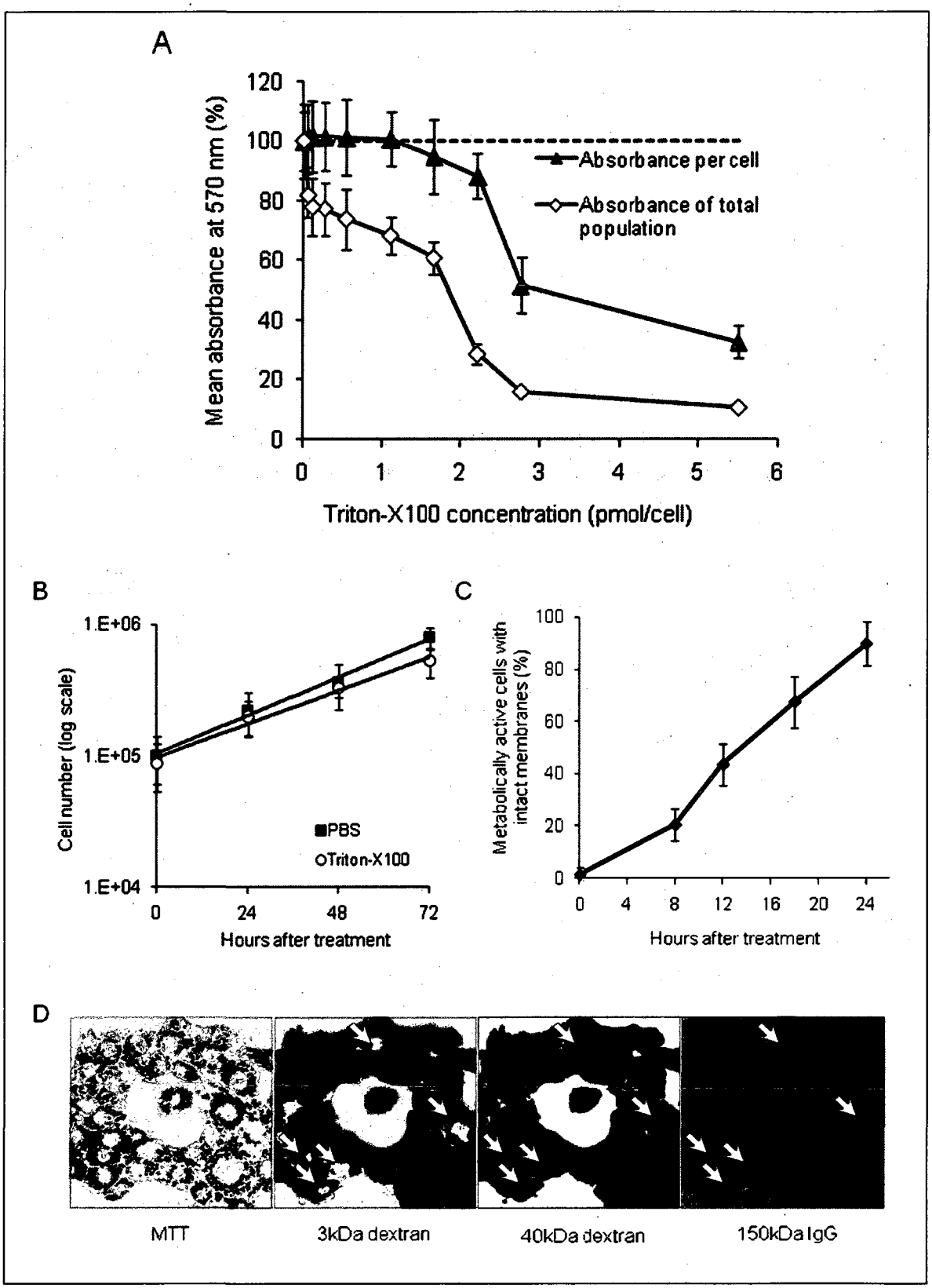
A
Mean absorbance at 570 nm (%)
120
100
80
60
40
20
0
0
1
2
3
4
5
6
Absorbance per cell
Absorbance of total population
Triton-X100 concentration (pmol/cell)
B
Cell number (log scale)
1.E+06
1.E+05
1.E+04
0
24
48
72
PBS
Triton-X100
Hours after treatment
C
Metabolically active cells with intact membranes (%)
100
80
60
40
20
0
0
4
8
12
16
20
24
Hours after treatment
D
MTT
3kDa dextran
40kDa dextran
150kDa IgG

Figure 6. Cell recovery after treatment with Triton-X100. A) Metabolic activity of 1483 cells 24 hours after treatment with different concentrations of Triton-X100, as measured by the MTT assay. A dose-dependent decrease in the metabolic activity (◊) was observed for each treatment group. When corrected for the number of cells remaining after treatment, changes in the mean metabolic activity per cell (▲) were only observed at Triton-X100 concentrations above 1.1 pmol/cell. B) Cell proliferation after treatment with 0.55 pmol/cell Triton-X100. Approximately 80% of the cells remained after Triton-X100 treatment (○) compared to the PBS control (■). Both cell populations continued to proliferate after treatment. C) Recovery of membrane integrity in metabolically active cells. The percentage of cells with intact membranes (♦) increases progressively with time. Membrane recovery was mostly restored at 24 hours. D) Confocal images of cells probed with MTT and fluorescent macromolecules 24 hours after treatment with 0.55 pmol/cell Triton-X100. Of the cells that show metabolic activity, less than 10% of cells exhibit permeability to 3kDA rhodamine-dextran (orange), 40kDa fluorescein-dextran (green), or 150kDa AlexaFluor 647 IgG (red). The arrows indicate cells which are permeable to macromolecules. The error bars represent 1 standard deviation.

To determine whether cells recover their membrane integrity, cell monolayers were tested for their ability to exclude macromolecules 8-24 hours after Triton-X100 treatment. Figure 6C shows the cumulative recovery of membrane integrity in metabolically active cells, as measured by MTT reduction and macromolecule uptake. The percentage of metabolically active cells exhibiting intact cell membranes increased progressively with time. At the 24 hour time-point, approximately 10% were still permeable to macromolecules. Figure 6D shows representative confocal microscopy images of cells assayed for membrane integrity 24 hours after Triton-X100 treatment. Metabolically active cells were identified by color deposition using light microscopy. Cells which remained permeable after 24 hours (arrows) admitted entry of all three molecule sizes.

Delivery of Targeted Optical Contrast Agents. Live and fixed cells were labeled with antibodies before or after treatment with 0.55pmol/cell Triton-X100. Figure 7 shows representative confocal fluorescence images of 1483 cells probed for two different nuclear targets. The PC563-hTERT labeling is shown in red and the NCL-hTERT labeling is shown in green. In cells fixed with 10% formalin, both targets were available for immuno-labeling. Pre-treatment with Triton-X100 before fixation enhanced the availability of the PC563 target. Treatment of live cells with Triton-X100 allowed both targets to be successfully labeled and imaged without fixation. Positive dual labeling was observed in all live permeabilized cells and varied in intensity less than ± 5% from cell to cell (data not shown). A slight decrease in NCL-hTERT labeling intensity was observed when comparing live to fixed cells, likely due to repeated washing of the non-crosslinked proteins. No antibody cross-reactivity or non-specific labeling was observed.

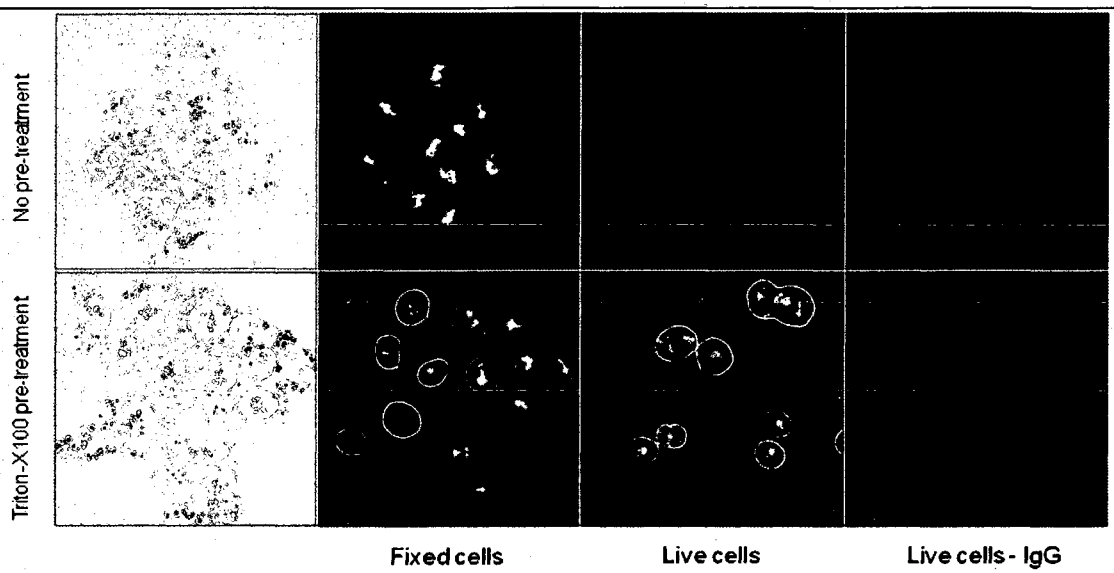

Figure 7. Detection of intra-nuclear markers by immunofluorescence following Triton-X100 treatment. DIC and confocal fluorescence images of 1483 cells labeled with the PC563-hTERT antibody (red) and NCL-hTERT antibody (green) or IgG control antibodies (left panels). We observe enhanced availability of the PC563 target for labeling following treatment with 0.55 pmol/cell Triton-X100 in both fixed and live cells. In contrast, there is a slight decrease in the availability of the NCL target after treatment in live cells, possibly due to washing effects. No labeling is observed in live cells which are not treated with Triton-X100 or cells labeled with IgG antibodies.

3.4 DISCUSSION

The results of this study demonstrate that Triton-X100 can be used at sub-solubilizing concentrations to permeabilize the membrane and nucleus of live cells. Both targeted and untargeted optical contrast agents can be reproducibly delivered into live cells by using the appropriate concentration of Triton-X100. In membrane-bound protein solubilization studies, it is generally recognized that the Triton-X100 concentration should be adjusted relative to the amount of protein to be extracted [77]; similarly, we observed that the Triton-X100 concentration used for live cell permeabilization should be normalized relative to the number of cells to be treated. Using this approach, I found that the Triton-X100 concentration could be readily optimized and scaled for treating different numbers of cells.

The cell permeabilization efficiency was evaluated as a function of Triton-X100 concentration. Studies of fluorescent dextran uptake suggest that cell permeabilization has a threshold, since as little as a 1.5-fold change in Triton-X100 concentration increases the percentage of permeabilized cells by 88 ± 4%. The percentage of viable cells remaining after treatment is directly related to Triton-X100 concentration, with increasing doses of Triton-X100 leading decreased cell viability. These results demonstrate the importance of determining the minimum effective Triton-X100 concentration for a given application. By using the lowest Triton-X100 concentration that provides sufficient permeabilization efficiency, one can minimize cell loss following treatment.

To determine what variables are important for the optimization of Triton-X100 concentration, confocal microscopy was used to track the entry of untargeted contrast agents into live permeabilized cells. Interestingly, permeabilization of the cytoplasm permits the entry of all macromolecules up to 150kDa in size. Nuclear permeabilization, however, is more dose-dependent, requiring increasing doses of Triton-X100 to permit the entry of larger macromolecules into all cells. Macromolecule size also appears to play a role in the rate of contrast agent accumulation, with larger molecules requiring more time to accumulate after Triton-X100 addition. The total accumulation following cell permeabilization varies by molecule, with different molecules preferentially accumulating in different cell compartments to different degrees. Thus, the minimum effective Triton-X100 concentration required for nuclear permeabilization is dependent on the specific molecule to be delivered and is generally higher than that required for efficient permeabilization of the cytoplasm. The amount of macromolecule delivered and the time required is dependent on the specific macromolecule used.

The cell recovery studies suggest that permeabilization can be a reversible process when the appropriate concentration of Triton-X100 is used. The results of the MTT assay further highlight the importance of optimizing Triton-X100 addition, since concentrations above 1.1 pmol/cell lead to a decrease in the mean metabolic activity per cell. The findings show that minimizing the use of Triton-X100 will reduce both immediate and long-term cell loss. A ten-minute treatment with 0.55 pmol/cell Triton-X100, a concentration that facilitates intranuclear labeling with antibodies, allows cells to retain both metabolic and proliferative capacities. Surprisingly, the immediate restoration of

membrane integrity does not appear to be a prerequisite for cell function. No lag in the rate of proliferation is observed in the first 24 hours after treatment, despite that fact that only 90 ± 8 % of metabolically active cells recover full membrane integrity in this time.

All cell lines evaluated here exhibited similar sensitivities to Triton-X100 treatment. The minimum effective concentration required for 3kDa dextran uptake did not significantly vary between cell lines. All cells showed a dose-dependent response, with the percentage of viable cells remaining after treatment decreasing as the concentration of Triton-X100 was increased. No significant differences were observed in cell viability between cell lines. When the rate of population doubling was evaluated in both squamous cell carcinoma and primary epithelial cell lines, Triton-X100 treatment was found to have no significant effect on either population. Based on these results, I believe that Triton-X100 treatment may useful in a range of mammalian cells.

In thinking about potential applications of Triton-X100 mediated permeabilization, it is important to recognize the limitations of this approach. Triton-X100 treatment, even at the low concentrations used here, may have deleterious effects on cells. Antibody labeling of permeabilized cells was observed to be is specific and reproducible, suggesting that unbound antibodies are removed during cell washing steps. Triton-X100 has been reported to release intracellular proteins [62, 78], modulate the activity of intracellular enzymes [74], and reorganize membrane domains [68]. These effects, however, do not appear to affect the ability of cells to recover membrane integrity, MTT reduction capacity, or proliferative activity. Triton-X100 cannot be used to target specific cell

populations, since all topically treated cells are permeabilized. Thus, Triton-X100 mediated permeabilization will be most useful for applications requiring delivery of contrast agents to large populations of live cells.

Triton-X100 permeabilization holds several advantages over existing intracellular contrast agent delivery techniques. Unlike microinjection, which is only useful for studying small numbers of cells, Triton-X100 can simultaneously deliver both targeted and untargeted contrast agents to any number of cells. Cell loading is more uniform than can be achieved with electroporation, thus no secondary purification step is required to isolate populations of uniformly loaded cells. Triton-X100 can be used as a pre-treatment or co-administered with the macromolecules to be delivered. Contrast agent delivery is not dependent on natural cell uptake mechanisms, allowing cells to be labeled quickly and reproducibly. Triton-X100, when combined with molecular specific contrast agents, will provide a useful tool for *in situ* optical studies.

In summary, Triton-X100 can be used at sub-solubilizing concentrations to permeabilize the cytoplasm and nucleus in a variety of mammalian cells. Targeted and untargeted molecules ranging from 1kDa to 150kDa in weight can be reproducibly delivered into adherent cells by controlling the concentration of Triton-X100 relative to the number of cells to be treated. Permeabilization of the cell cytoplasm appears to be a threshold event, whereas nuclear permeabilization is dependent on both macromolecule size and Triton-X100 concentration. When Triton-X100 as used at or near the minimum effective concentration, cell permeabilization is generally reversed in 24 hours. Treated cells continue to proliferate and show metabolic activity during the restoration of membrane

integrity. Increasing Triton-X100 beyond the minimum effective concentration reduces both short-term and long-term cell survival. Different cell lines exhibit similar sensitivities to Triton-X100 treatment, suggesting that Triton-X100 mediated permeabilization will be widely useful. We conclude that Triton-X100 is a promising permeabilization agent for efficient, reproducible, and scalable delivery of optical contrast agents into live mammalian cells.

CHAPTER 4

MOLECULAR IMAGING OF TELOMERASE IN LIVE CELLS AND FRESH TISSUES

The ability to monitor *in vivo* molecular markers that are differentially activated during tumorigenesis is critical to the development of new detection and treatment strategies. Human telomerase reverse transcriptase (hTERT) was selected as a potential target for the optical detection of cancer. The purpose of this study was to develop an effective strategy to optically label hTERT in live cells and fresh tissues. To facilitate intra-nuclear labeling, a fast, non-toxic cell permeabilization strategy was developed. Using antibody-based optical contrast agents, it was found that hTERT was available for labeling in live cells. The observed labeling was specific, reproducible, and consistent across different cancer cell lines. The intensity of labeling, as assessed by confocal microscopy, was highest in rapidly proliferating cells. To evaluate the feasibility of targeting hTERT *in situ*, fresh unfixed tissues were probed for hTERT. Topically labeled, subcutaneous tumors generated in mice showed a pattern of labeling similar to that observed in cell culture. Fresh biopsies of normal and cancerous human oral mucosa, sliced transversely and labeled topically, demonstrated differential labeling as a function of disease state. In summary, this study provides evidence supporting the potential for targeting hTERT with optical contrast agents for *in vivo* molecular-specific imaging.

4.0 INTRODUCTION

Telomerase is a specialized cellular enzyme that catalyzes the synthesis and extension of telomeric DNA with its own RNA template [79, 80]. Telomerase activity has been found in almost all human cancer tissues and cancer cell lines examined to date [81, 82]. In somatic cells, telomerase activity is limited to actively dividing stem cells, peripheral lymphocytes, and proliferating cells in renewable tissues [83, 84]. Since tumor growth is dependent on cell proliferation, it is thought that telomerase activation may be a critical and rate limiting step for carcinogenesis [85, 86].

The development of the PCR-based Telomere Repeat Amplification Protocol (TRAP) assay has demonstrated that telomerase activity is useful as both a diagnostic and prognostic indicator. In a survey of over 1500 tissue samples, the TRAP assay was estimated to yield a specificity of 91% and sensitivity of 85% for the detection of telomerase activity in malignant tissues [86, 87]. High telomerase activity correlates with a poor prognosis for patients with cancer of the stomach [88, 89], colon [90], breast [91, 92], lung [93, 94], and oral cavity [95]. In adenocarcinomas derived from the stomach and colon, telomerase activity increases with cancer stage [89, 90, 96, 97]. Conversely, the absence of telomerase activity in patients with metastatic neuroblastoma has been shown to lead to spontaneous tumor regression [98, 99]. Together, these data suggest that telomerase activity may be a useful biomarker for cancer characterization.

The catalytic activity of telomerase is modulated by a reverse transcriptase called hTERT. Expression of this protein has been found in over 85% of human cancers [50, 51].

The presence of hTERT is predictive of poor survival for patients with cancer of the lung [100] and liver [101, 102]. Increasing evidence suggests that changes in hTERT expression during carcinogenesis can predict clinical outcome [51, 103-105]. hTERT expression may also be a useful marker for grading pre-cancerous lesions. In patients with cervical intraepithelial neoplasia (CIN), the number of hTERT positive cells increases nearly linearly with the transition from CIN1 to CIN3 [106, 107]. In patients with Barrett's esophagus, hTERT expression increases with transition from metaplasia to dysplasia to adenocarcinoma [108]. Progressive up-regulation of hTERT expression is also observed in neoplasia of the oral cavity [109], stomach [110] and bronchioles [111]. In normal tissues, increased hTERT expression has been observed in liver injury [112], carcinogenic insult to the oral cavity [113], and in clinically normal squamous epithelium of patients presenting both metaplasia and cancer of the esophagus [108].

Although hTERT expression and activity can be assessed *in vitro* using complex, time-consuming protocols, there is currently no method to detect hTERT *in vivo*. An hTERT-specific contrast agent could enable new approaches to non-invasive detection and characterization of cancer. Here we present work towards the development of a topical contrast agent capable of labeling hTERT *in vivo*. We show that antibody-based contrast agents can be rapidly and effectively delivered into the nucleus of live cells with the use of an appropriate permeation-enhancing formulation. The observed labeling is specific, reproducible, and selective for rapidly proliferating cells. At the tissue level, individual cells are defined by a characteristic nuclear labeling pattern. Labeling is limited to the basal and parabasal epithelium in normal oral mucosa, suggesting that differential

labeling can be used to distinguish between clinically normal and cancerous biopsies. I conclude that hTERT is a promising target for *in vivo* optical molecular imaging.

4.2 MATERIALS AND METHODS

Cell Culture. HT1080, SiHa, and MDA-MB-435S cell lines were purchased from American Type Culture Collection (Manassas, VA). The 1483 cell line, derived from a patient with head and neck squamous cell carcinoma, was obtained from Dr. Reuben Lotan at the M.D. Anderson Cancer Center (Houston, TX). The SV40-transformed GM847 cell line was obtained as a negative control from Coriell Cell Repositories (Camden, NJ). SiHa and 1483 cells were cultured in DMEM/F-I2 media supplemented with L-glutamine (GIBCO-BRL, Grand Island, NY). MDA-MB-435S and GM847 cells were cultured in Minimum Essential Medium supplemented with L-glutamine, non-essential amino acids, sodium pyruvate, and vitamins (GIBCO-BRL, Grand Island, NY). HT1080 cells were cultured in 4:1 ratio of MEM to M199 and supplemented as described above. All cell culture media were enhanced with 10% FBS (Hyclone, Logan, UT), with exception of the HT1080 cell media, in which the FBS concentration was varied from 0% to 10%. HT1080 cells were cultured for 7 days at each serum concentration for hTERT labeling studies.

Antibodies. Polyclonal rabbit anti-human PC563-hTERT antibody was purchased from EMD Biosciences (San Diego, CA). Highly cross-absorbed, goat anti-rabbit AlexaFluor 647 IgG and purified polyclonal rabbit IgG were purchased from Invitrogen (Carlsbad, CA).

Immunocytochemical Detection of hTERT. To determine the cellular localization of hTERT, sub-confluent monolayers of live cells (5 x 10^4 cells/cm^2) were labeled with antibodies as follows: 24 hours after seeding, the cells were washed with PBS, treated with 0.55pmol/cell Triton-X100 for 10 minutes, blocked with a 1% BSA/2% goat serum PBS solution for 10 minutes, and then labeled for 1 hour with a 1:80 dilution of PC563-hTERT antibody. Following 3 washes, cells were probed with a 1:500 dilution of AlexaFluor 647 IgG for 1 hour, washed, and imaged live. For controls, cells were labeled in parallel with a polyclonal IgG antibody and the Alexa Fluor 647 IgG, or with AlexaFluor 647 IgG only. All labeling was performed at 4°C.

Competitive Binding Assay. To determine the specificity of the PC563-hTERT antibody, competitive inhibition was performed using a PC563 immunizing epitope (hTERT amino acids 348-358, PSFLLSSLPPS) that was custom synthesized by the M.D. Anderson Peptide Synthesis Core (Houston, TX). A 5 to 500-fold excess of the peptide was pre-incubated with the antibody at room temperature for 30 minutes or added to the primary antibody solution at the time of cell labeling.

Population Doubling Assay. Population doubling experiments were performed with subconfluent HT1080 cells. Cells were plated at appropriate concentrations to allow log-linear growth for 7 days. Cells were cultured in 10%, 5%, 2.5%, 0.6%, or 0% FBS-supplemented media and assessed at days 0, 2, 3, 5, and 7. The rate of doubling was assessed in duplicate in three separate experiments.

Cell Viability Assessment. Cells were assayed for viability following Triton-X100 treatment by monitoring the reduction of 3-(4,5-dimethylthiazol-2-yl)-2,5-diphenyl tetrazolium bromide as described in [76]. Subconfluent monolayers of 1483 cells (5×10^4 cells/cm^2) were permeabilized for 10 minutes with 0.55pmol/cell Triton-X100, washed, and incubated with PC563-hTERT antibody, IgG antibody, or PBS for one hour on ice. Cells were subsequently washed 3 times, covered with media, and returned to a 37°C incubator for 24 hours. Cellular metabolic activity was evaluated in triplicate in five separate experiments using the American Type Culture Collection MTT assay. The absorbance measurement from each well was divided by the number of cells per well.

Animal Tumor Models. Subcutaneous tumors were generated in mice as a three-dimensional model for fresh tissue labeling. 1483 cells were implanted subcutaneously (10^6 viable cells in 100 µl PBS) in the right and left posterior mammary fat pads of female nu/nu mice (6–8 weeks old, Charles River Laboratories). The protocol was reviewed and approved by the IACUC at Rice University. Mice were cared for in accordance with institutional guidelines. When tumors reached 3-5mm in diameter, the tumors were excised and sliced into 200 µm thick transverse slices using a Krumdieck tissue slicer (Alabama Research & Development, Munford, AL). After slicing, the tissues were topically treated with 1.0 ml of 0.05% Triton-X100 and labeled as described above. The tissue slices were subsequently imaged, fixed in 10% formalin, and submitted for hematoxylin and eosin (H&E) staining. Slices from 5 pairs of tumors were evaluated for hTERT labeling.

Fresh Human Tissues. Paired clinically normal and abnormal biopsies of the oral mucosa were obtained from 4 consenting patients at the University of Texas M. D. Anderson Cancer Center (MDACC). Patients gave written informed consent. The clinical protocols were approved by the Institutional Review Boards at MDACC and Rice University. Biopsies were immediately placed and remained in chilled cell culture media until they were sliced transversely into 200 μm thick transverse slices using a Krumdieck tissue slicer. After slicing, the biopsies were topically treated with 1.0 ml of 0.05% Triton-X100 and labeled as described above. The tissue slices were subsequently imaged, fixed in 10% formalin, and submitted for hTERT immunohistochemistry and H&E staining.

Image Acquisition and Analysis. Confocal fluorescence images of the cells and tissues were obtained using a Carl Zeiss LSM 510 confocal microscope (Thornwood, New York) equipped with 488 nm (30mW) and 633 nm (5mW) lasers. Images were collected using PMT detectors and Zeiss LSM 5 image examiner software. For permeabilization time-course studies, samples were excited at 488 nm (48% laser power) and the fluorescence emission was collected using a 505-550 nm band-pass filter. Images were acquired every 15 seconds at 0.5 frames per second using a 63x oil objective with a detector gain of 570, a pinhole of 1.0 Airy Units, and no line averaging. The mean fluorescence intensity of the cytoplasm and nucleus were compared to that of the extracellular solution by selecting regions of interest within a time stack and normalizing the mean fluorescence intensity of each compartment relative to that of the extracellular solution on a frame-by-

frame basis. Ten cells were evaluated from a representative field of view in 5 separate experiments.

For cell and tissue labeling studies, samples were excited at 633 nm (100% laser power). Squamous cells were first identified using reflectance imaging and then fluorescence images were collected using a 650-710 nm band-pass filter. Images were acquired at 0.5 frames per second using 20x or 63x objectives with a detector gain of 440 (tissues) or 500 (cells), a pinhole of 2.56 Airy units, and no line averaging. These parameters remained constant for all images. Stacks of images were obtained with a z-step size of 2.5 to 6 μm to avoid oversampling. To quantitate the average fluorescence per cell, image stacks were summed, regions of interest were selected, and mean intensity per unit area determined. Ten cells were evaluated from a representative field of view in 5 separate experiments. Differences in mean labeling intensity between each serum concentration were assessed using a two-tailed, unpaired Students t-test, with p-values of < 0.01 being considered statistically significant.

4.3 RESULTS

Detection of hTERT in Live Cell Monolayers. We investigated Triton-X100, a non-ionic surfactant, for permeabilization of the outer membrane of living cells. We found that the concentration of Triton-X100 was critical for successful permeabilization. The ideal formulation was found to be approximately 0.55pmol of Triton-X100 per cell, normalized to the cell count at time of plating. Cell monolayers pre-treated with Triton-X100 were probed with antibodies targeted to hTERT. Figure 8 shows confocal

fluorescence images of four different cell lines labeled with PC563-hTERT and Alexa Fluor 647 IgG. Labeling was observed in cell lines derived from oral squamous cell carcinoma (1483), cervical squamous cell carcinoma (SiHa), and breast adenocarcinoma (MDA-MB-435S). No labeling was observed in GM847 cells, an SV-40 transformed cell line that expresses the telomerase RNA subunit (aka. hTERC, hTR) but not hTERT itself. In cell lines expressing hTERT, labeling was consistently observed throughout each cell, but appeared to localize most strongly in the nucleus. Nuclear labeling was characterized by a ring-like structure at the periphery of the nucleus, as well as diffuse and punctate labeling throughout the nucleus. DNA counter-stains were used to confirm that the ring-like labeling structure was situated in the nucleus (data not shown). In each experiment, all cells were labeled, although some cell-to-cell variation in labeling intensity was observed.

The labeling specificity was tested in a competitive binding assay (Fig. 8b) using the immunizing epitope for the PC563-hTERT antibody. Addition of the peptide to the antibody solution, either during or before labeling, resulted in a loss of PC563- hTERT labeling. The greatest decrease in labeling was obtained when the peptide was pre-incubated with the antibody for 30 minutes. It was not possible to fully block PC563-hTERT labeling; however, no labeling was observed in cells labeled with primary and secondary IgG antibodies. Using serial dilutions of peptide, the maximum decrease in labeling intensity was achieved with an peptide-to-antibody ratio of 100:1.

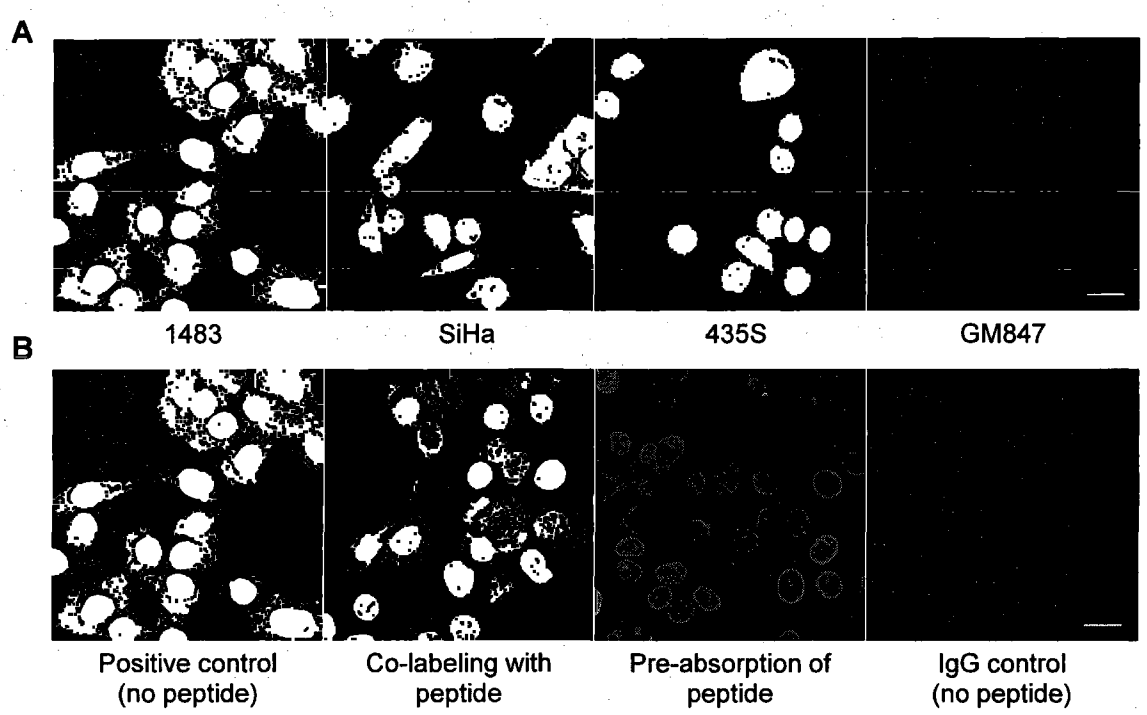

Figure 8. Determination of antibody specificity in different cell lines. A) Confocal fluorescence images of live, permeabilized cell lines labeled with PC563-hTERT and Alexa Fluor 647 antibodies. Strong nuclear labeling and diffuse cytoplasmic labeling appears in cells that express hTERT (1483, SiHa, and 435S). No labeling is observed in cells which do not express hTERT (GM847). B) Images of live 1483 cells labeled in a competitive binding assay. Antibody binding can be partially blocked by incubating excess immunizing peptide with the antibody during or before labeling. The strongest decrease in labeling appears in the nucleus. No labeling was observed in the IgG control. The scale bars represent 20 μm

Quantitation of hTERT Labeling in Cells. The HT1080 cell line, a fibrosarcoma derivative that shows variable telomerase activity as a function of serum starvation [114], was used to evaluate differential hTERT labeling *in vitro*. As shown in Figure 9, the hTERT labeling intensity varied relative to the amount of serum provided in culture. All cells supplemented with 10%, 5%, or 2.5% FBS labeled positive for hTERT (Fig. 9a). The mean fluorescence intensity per cell, as determined by quantitative confocal microscopy, decreased as serum levels were reduced (Fig. 9b). The measured fluorescence intensity was greatest in cells that proliferated rapidly (Fig. 9c). Cells supplemented with 0.6% or 0% serum continued to proliferate, but less than 1% of these cells labeled positive for hTERT. Statistically significant differences in the mean labeling intensity (two-tailed Student's t- test, $p < 0.01$) were observed between cells cultured in 10%, 5%, 2.5%, 0.6%, and 0% serum.

Evaluation of Cell Viability. Cells were evaluated for metabolic activity after Triton-X100 permeabilization treatment by monitoring the reduction of MTT. Figure 10 shows the measured average metabolic activity per cell, normalized by the activity of untreated cells. No significant differences in metabolic activity were observed between the treated and untreated cells.

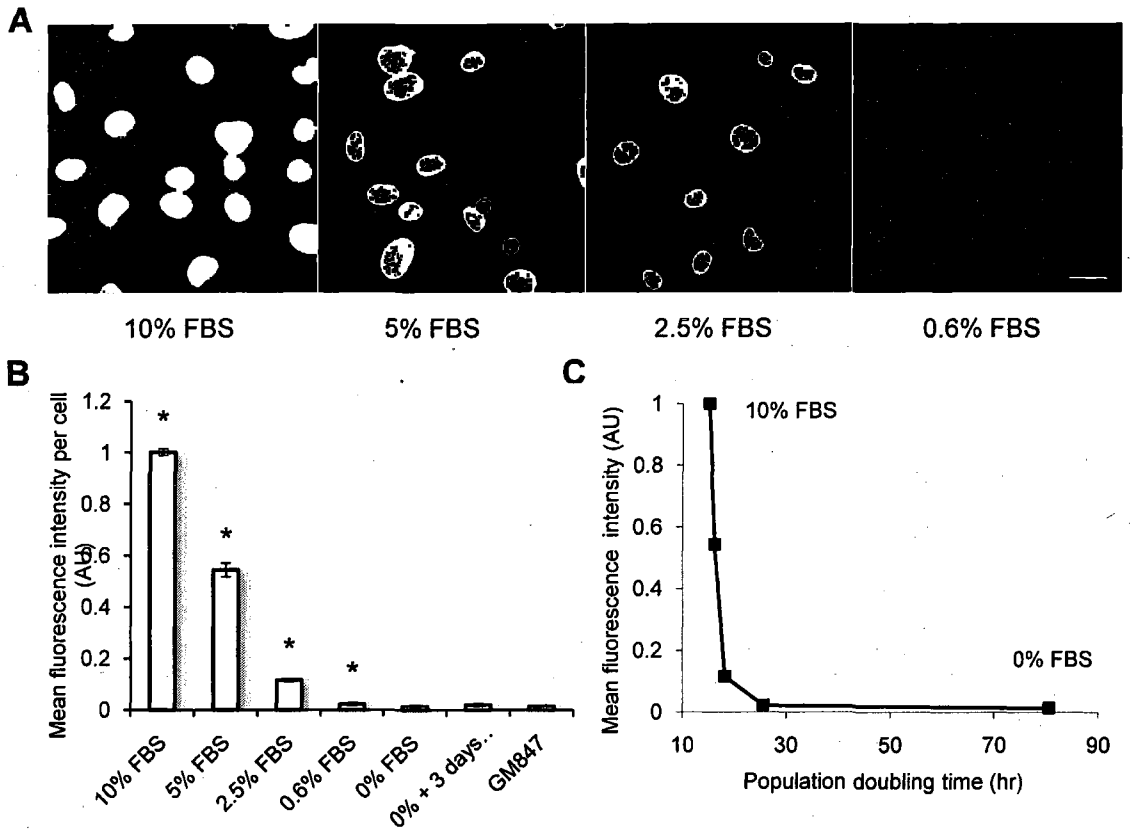

Figure 9. Quantitation of hTERT labeling in HT1080 cells subjected to differing levels of serum. A) False color confocal images of PC563-hTERT labeling in cell monolayers grown for 7 days in 10%, 5%, 2.5%, or 0.6% serum. The scale bar represents 20 μm. B) Using fluorescence quantitation microscopy, the mean fluorescence intensity of hTERT labeling per cell was determined. The labeling intensity decreased as serum levels were reduced. The asterisks indicate statistically significant differences in the mean labeling intensity between each serum group (two-tailed Students' T-test, $P < 0.01$). C) The mean fluorescence intensity as a function of population doubling time. The highest levels of hTERT labeling were observed in rapidly proliferating cells.

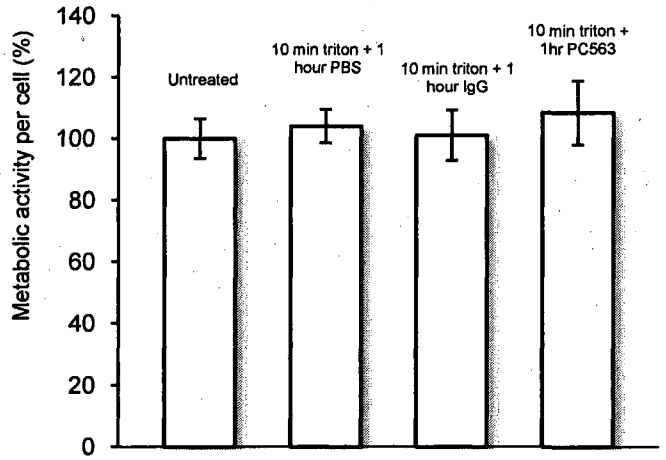

Figure 10. The metabolic activity of 1483 cells 24 hours after treatment as assessed by the MTT assay, averaged over 5 trials. Treated cells were permeabilized for 10 minutes with 0.05% Triton-X100 and then labeled for one hour with either PBS, IgG antibody, or the PC563-hTERT antibody. No significant differences in metabolic activity were observed between the different treatments. All treated cells made a complete recovery in the 24 hour time period. The error bars represent one standard deviation.

Detection of hTERT in Fresh Mouse Tumor Slices. To test hTERT labeling in tissue, subcutaneously generated 1483 cell tumors were labeled for hTERT (Fig. 11). Fresh, unfixed tumor slices demonstrated strong nuclear labeling. Both ring-like and diffuse nuclear labeling was consistently observed from sample to sample. A small amount of non-specific labeling appeared in slices with large amounts of connective tissue. No labeling was observed in regions of tissue comprised of infiltrating, non-squamous cells or slices labeled with only IgG antibodies. The observed size and orientation of the labeled nuclei was in agreement with the tissue morphology as assessed by H&E staining.

Detection of hTERT in Human Oral Biopsies. The human oral cavity was selected as promising site for hTERT detection because of its ease of access for topical labeling, optical imaging, and biopsy collection. Representative confocal fluorescence images from paired clinically normal and abnormal biopsies of the oral mucosa are shown in Figure 12. Transverse tissue slices were permeabilized and labeled with PC563-hTERT and Alexa Fluor 647 IgG. Histologic analysis of the normal sample (Fig. 12a) obtained from the left side of the tongue revealed normal squamous epithelium with hyperkeratosis. The abnormal sample (Fig 12b,d), obtained from the right tongue, was well-differentiated, invasive squamous cell carcinoma. A total of 4 biopsy pairs were obtained from the oral cavity of consenting patients.

In normal squamous epithelium, faint PC563-hTERT labeling was detected in the basal and parabasal layers of epithelium. Labeling at the basal layer was predominantly cytoplasmic. Occasional cells with weak ring-like nuclear labeling were observed in the

parabasal layers. In tissues diagnosed as squamous cell carcinoma, characteristic hTERT labeling was observed across the entire lesion. At 200X and 630X magnification, individual nuclei could be distinguished by their ring-like labeling. Diffuse cytoplasmic labeling (similar to that observed *in vitro*) appeared in some cell populations and was generally associated with strong nuclear labeling. The intensity of labeling varied from cell to cell. Increased heterogeneity was observed in cancer, with the peak labeling intensity ranging from 0.5 to 3 times greater than that of normal basal epithelium and 6 to 10 times greater than that of normal parabasal epithelium.

4.4 DISCUSSION

Studies of telomerase expression and activity in human tissues suggest that hTERT is a promising cancer biomarker. The hTERT detection methods developed to date are complex, time-consuming, and require biopsies. An hTERT-specific *in vivo* contrast agent could facilitate non-invasive detection and characterization of cancer. Targeting hTERT, however, presents a difficult challenge because the catalytically active protein is primarily localized in the nucleus. As a first step in designing an hTERT-specific contrast agent, we sought to determine the feasibility of targeting intra-nuclear hTERT. Presented here is the first evidence that hTERT can be labeled in live cells and fresh tissues.

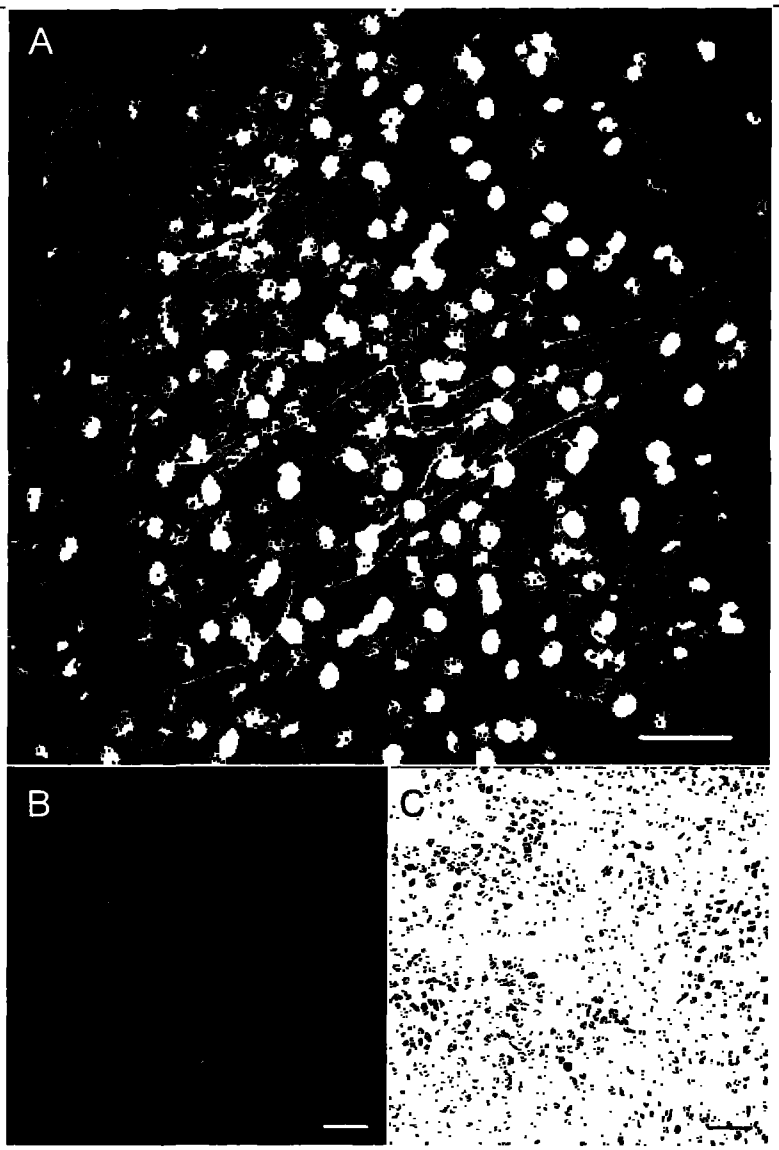

Figure 11. Optical detection of hTERT in freshly excised slices of 1483 cell tumors generated subcutaneously in mice. A) Confocal fluorescence image of a tumor slice labeled with PC563-hTERT and Alexa Fluor 647 IgG. The fluorescent labeling intensity and localization observed is similar to that of live 1483 cells labeled *in vitro.* B) Confocal fluorescence image of an adjacent tissue slice labeled with a non-specific IgG and Alexa Fluor 647 IgG. C) H&E image of the region of interest. The scale bars represent 50 μm.

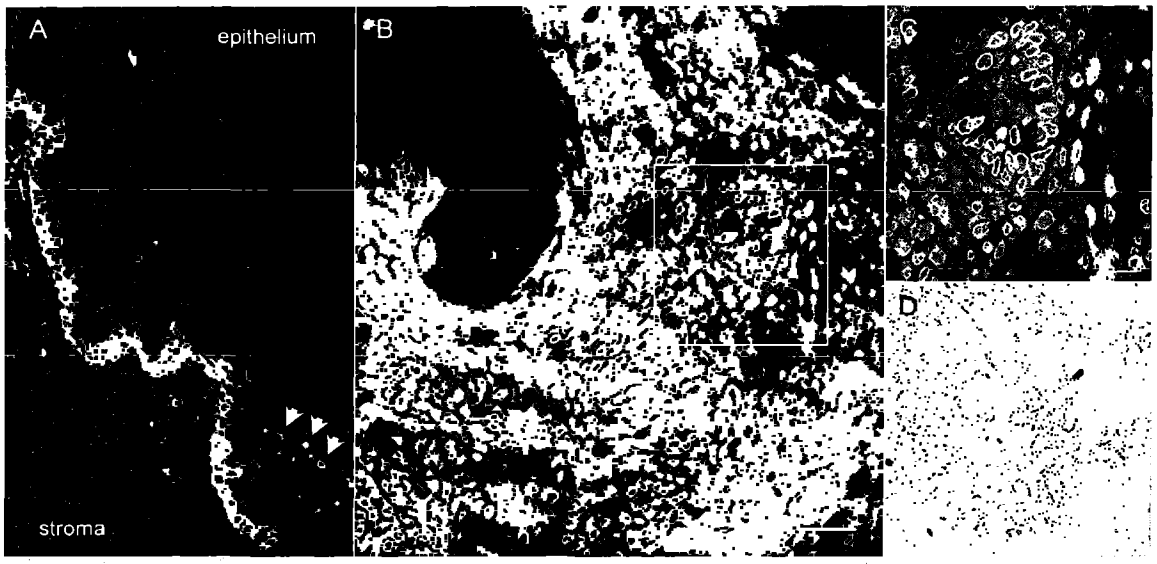

Figure 12. False-colored confocal images of hTERT labeling in transverse slices of oral biopsies. A) In normal tongue tissue, hTERT labeling is limited to basal and parabasal layers of the epithelium. Labeling of the basal epithelium is predominantly cytoplasmic, whereas weak nuclear labeling is observed in some parabasal cells (arrows). B) In well-differentiated squamous cell carcinoma, distinctive nuclear labeling is observed throughout the width of the lesion. C) At higher magnification, the labeled nuclei predominantly appear as ring-like structures. D) H&E image of the region of interest. The scale bars represent 50 μm, 20 μm, and 100 μm respectively

The PC563 antibody used in these studies appears to be specific for hTERT and reliable for the detection of differences in hTERT expression. The positive labeling observed *in vitro* is limited to cell lines that express hTERT. Competitive binding studies with the immunizing peptide demonstrate that the antibody affinity for hTERT is reduced in the presence of excess peptide, confirming the specificity of the antibody for the central hTERT amino acid sequence. Using confocal microscopy, it was determined that the mean labeling intensity within any given population is highly reproducible. Greater than 10-fold differences in labeling intensity could be detected by varying the amount of serum provided in culture. Interestingly, the PC563-hTERT antibody proved most sensitive to detecting rapidly proliferating cells, suggesting that cell-to-cell differences in labeling intensity may represent differences in the rate of cell doubling.

My finding that the PC563-hTERT primarily labels targets in the nucleus of cancer cell lines agrees with the current literature. To date, hTERT expression has been observed in many different cell compartments. Studies utilizing transient *hTERT* transfection have begun to improve our understanding of hTERT localization. It appears that primary cells and cell lines which do not express the telomerase RNA subunit present hTERT primarily in the nucleoli following transfection [115-117]. SV40 transformation of these cells causes hTERT to preferentially localize in the nucleoplasm [117]. In cells derived from human cancers, hTERT is found primarily in the nucleoplasm [117, 118], but also in mitochondria [118], nucleoli [115, 119], and cajal bodies [119]. Mutation of central hTERT sequences [115, 116] or deletion of the hTERT C-terminus [120] redistributes hTERT out of the nucleoplasm,

suggesting that hTERT preferentially localizes to the nucleoplasm under normal conditions.

I investigated the feasibility of using Triton-X100 as a chemical permeation enhancer to deliver the PC563-hTERT antibody to the nucleus of live cells. It was found that Triton-X100, topically applied at the appropriate concentration and duration, can permeabilize cell monolayers rapidly and safely. A ten-minute treatment with 0.55pmol/cell Triton-X100 is sufficient to permeabilize the cytoplasm and nucleus of cells for antibody labeling. Cells are permeable for several hours, facilitating multi-step labeling protocols. Using the MTT assay, it was verified that permeabilized cells recover their full metabolic activity within 24 hours of treatment. The results of these studies are in good agreement with the work described in chapter 3.

The detection of hTERT protein in human tissues has to date been limited to fluorescence in situ hybridization and immunohistochemistry of fixed tissue sections. I found that hTERT can be successfully labeled in freshly excised human tissues. Consistent with published data [51, 96, 106, 121], we observed some labeling in the basal and parabasal layers of normal epithelium. This labeling is generally weak in intensity and more likely to be found in the cytoplasm. In oral squamous cell carcinoma tissue, positive labeling is observed across the width of the lesion. As noted by others [106, 122, 123], this labeling is more intense compared to normal epithelial cells, despite the increase in cell-to-cell variability. Cytoplasmic labeling is found in some populations of cancer cells, and is generally associated with strong nuclear labeling. Thus, in a side-by-side comparison of

paired oral mucosa biopsies, we observe differences in the number of cells expressing hTERT, the amount of hTERT expressed per cell, the intracellular localization of hTERT, and the spatial distribution of cells expressing hTERT. These differential labeling trends suggest it may be possible to distinguish between normal and cancer tissue based on hTERT labeling.

hTERT appears to be a promising molecular target for *in vivo* optical contrast agents; however, several important considerations need to be met before an hTERT-specific agent is clinically feasible. A successful contrast agent must: 1) be appropriately sized to penetrate through tissue, 2) be optically active at tissue penetrating wavelengths, 3) retain its bioactivity as it moves through different cell compartments, and 4) have molecular-specific detection capabilities. Here it is demonstrated that antibodies can be successfully targeted in live cell monolayers and the surface of fresh tissues following treatment with the use of a topical permeation enhancer. One drawback of Triton-X100 treatment is that antibody-mediated nuclear labeling of tissues is limited to the superficial cell layers. Higher concentrations of Triton-X100 were evaluated but did not yield deeper nuclear labeling (data not shown). For the data presented here, the Triton-X100 treatment conditions were selected to yield a final concentration of 0.55pmol/cell based on the tissue dimensions and depth of labeling. The engineering of smaller hTERT-specific probes with nuclear penetration capabilities will likely circumvent this problem.

To evaluate the clinical implications and diagnostic potential of hTERT imaging, it will important to quantitatively assess multiple labeling parameters. Wide-field imaging or

spectroscopy could be used to evaluate the mean labeling intensity over a region of interest. High resolution imaging could facilitate the measurement of additional parameters such as the spatial distribution of hTERT labeling, the fraction of cells expressing hTERT, and the relative labeling intensity per cell. There is increasing evidence that all these parameters can be useful for detecting cancer [50, 51], measuring disease progression [106-108], and predicting patient outcome [99-105].

In conclusion, hTERT appears to be a promising molecular target for *in vivo* contrast agents. Provided here the first evidence that hTERT is available for labeling in live cells and tissues. Specific, reproducible labeling can be achieved by combining molecular-specific antibodies with a topical permeation enhancer. Triton-X100, applied topically at the appropriate concentration and duration, permits live cells to be permeabilized rapidly and safely. Labeling with PC563-hTERT and AlexaFluor 647 IgG antibodies generates a distinctive labeling pattern consistent across multiple cell lines. In tissues, individual cells can be distinguished by the intensity and localization of hTERT labeling. Labeling in normal oral mucosa is limited to the basal and parabasal layers of the epithelium, whereas labeling in squamous cell carcinoma appears across the entire lesion. The number of cells expressing hTERT, as well as the amount of hTERT expression per cell is increased relative to normal tissue. Further work is needed to establish the clinical feasibility of hTERT-specific agents for optical detection and monitoring of cancer *in vivo*.

CHAPTER 5

ENHANCED MUCOSAL DELIVERY OF TOPICAL CONTRAST AGENTS FOR CANCER BIOMARKER DETECTION

Uniform delivery of optical contrast agents through mucosal tissue has proven a significant challenge. Topical permeation enhancers which have proven useful for skin, demonstrate limited success in mucosal tissue. I sought to develop a topical permeation strategy capable of delivering tissue-impermeant molecular-specific contrast agents through mucosal epithelium in a uniform, controlled manner. In this chapter I demonstrate that Triton-X100 can be utilized to deliver targeted and untargeted optical contrast agents through freshly excised normal mucosal epithelium and epithelial cancer. Macromolecules up to 150kDa in size were successfully delivered via transcellular and paracellular routes. The depth of Triton-mediated permeation was modulated by varying the treatment time and concentration. Uniform epithelial penetration to a depth of 500 μm was achieved in approximately 1.5 hours for molecules of 40kDa or less. Larger optical probes required longer treatment times. Co-administration of molecular-specific contrast agents with Triton-X100 treatment facilitated simultaneous labeling of biomarkers on the cell membrane, in the cytoplasm, and in the nucleus with high specificity. Together, these data suggest that Triton-X100 is a promising topical permeation enhancer for mucosal delivery of tissue-impermeant molecular-specific optical contrast agents.

5.1 INTRODUCTION

Advances in molecular-specific optical contrast agents have recently shown promise for the detection of cancer and its precursors. Targeting agents which have been successfully used for optical detection of cancer biomarkers in preclinical models include antibodies [20-25], growth factors [26-30], peptide analogs of extracellular ligands [31-34], and enzymatically activatable polymers [35-39]. The coupling of optical tags to these targeting agents allows molecular events to be monitored non-invasively *in vivo* [40]. These molecular-specific optical contrast agents have the potential to provide dynamic, real-time information without the need for biopsy and associated patient discomfort.

The use of optical contrast agents as topical probes for the screening of epithelial precancer has been hindered by the difficulty of delivering macromolecules through mucosal tissue. The molecular changes preceding cancer generally begin in the basal layers of epithelium [124], thus early detection strategies require contrast agents be delivered at least several hundred microns deep. Studies of small molecule optical probes with tissue-permeant properties, such as fluorescent sugar derivatives [125-127] and acriflavine [128-130], have highlighted the promise of using optical imaging to distinguish molecular changes in small populations of cells. The penetration of larger molecules through mucosal tissue, however, is substantially reduced for molecular weights above 300Da [131]. Chemical modification strategies, including increasing lipophilicity [132, 133], conjugation with polymers [134, 135], and encapsulation in liposomes [136-138], have improved the penetration of molecules up to 6kDa in size.

Topical permeation enhancers, substances that temporarily reduce the impermeability of tissues, have been investigated for the delivery of larger molecules. Dimethyl sulfoxide (DMSO), for example, enhances the transdermal permeation of a variety of drugs by modifying the keratin structure and lipid composition of skin [139]. Combinations of topical permeation enhancers have been shown to facilitate the transdermal penetration of proteins as large as 140kDa [140, 141]. Permeation enhancers shown to be effective in skin, however, have met little success in mucosal tissue [142]. Studies utilizing various surfactant, lipid, and bile salt formulations have demonstrated enhanced mucosal penetration of only small molecules like insulin (6kDa) and calcitonin (3.5kDa) [143].

In Chapter 3, it was demonstrated that Triton-X100 can be used to permeabilize live cells in a sufficiently reproducible manner to facilitate intracellular labeling of cancer biomarkers. I hypothesized that the permeabilization properties of Triton-X100 would render it useful for the delivery of cell- and tissue-impermeant optical contrasts agents though mucosal tissue. To evaluate Triton-X100 as a topical permeation enhancer for contrast agent delivery, several key criteria were identified, including 1) uniform delivery of molecules up to 150kDa in size, 2) a controlled depth of permeation, and 3) the capability to wash out unbound probes for high optical contrast. Because of the need for controlled local delivery rather than systemic delivery, new methodologies for the assessment of contrast agent delivery were developed.

This chapter describes the use of Triton-X100 to deliver targeted and untargeted optical contrast agents in three different tissues. To translate Triton-X100 for tissue use, biopsies

of reproducible dimensions are topically treated with a fixed volume of 0.5% to 2.5% Triton-X100. The concentration and duration of treatment, adjusted relative to the epithelial thickness and cell density, is selected to expose the cells to a final dose of 1.1 pmol/cell or less. Using this approach, transverse sections of bladder and oral mucosa specimens are probed with optically active contrast agents following Triton-X100 treatment to determine the extent of tissue permeation. Using confocal microscopy, the depth and rate of macromolecule penetration are evaluated as a function of optical probe size to determine under what conditions Triton-X100 treatment meets the design criteria. The delivery of molecular-specific optical contrast agents is tested in xenograft tumor specimens co-treated with Triton-X100 and compared to tissues treated with DMSO or saline solution. I demonstrate that Triton-X100 can facilitate simultaneous labeling of clinically relevant extracellular and intracellular biomarkers in a controlled, uniform manner.

5.2 MATERIALS AND METHODS

Cell Lines. The targeting of EGFR- and CyclinD1-specific optical contrast agents was evaluated using 1483 cells and xenograft tumors. This EGFR-positive cell line, derived from a patient with head and neck squamous cell carcinoma [75], was obtained from Dr. Reuben Lotan at the M.D. Anderson Cancer Center (Houston, TX). 1483 cells were cultured in Dulbecco's Modified Eagle Medium: Nutrient Mix F-12® medium supplemented with L-glutamine (Invitrogen, Carlsbad, CA) and 10% fetal bovine serum (Hyclone, Logan, UT).

Tissue Models. Three different tissue models were evaluated for permeability in the presence and absence of topical permeation enhancers. Porcine oral mucosa was selected as a model of stratified squamous epithelium. Heads of American Yorkshire pigs, aged 6 months, were obtained from a local slaughterhouse at the time of sacrifice. The buccal mucosa of the oral cavity and approximately 1 mm of underlying tissue was separated from the surrounding muscle layers via dissection. Guinea pig bladder mucosa was selected as a model of transitional epithelium. Whole bladders were excised from 2-3 week old female Hartley guinea pigs (Charles River Laboratories, Wilmington, MA) directly following animal sacrifice. Xenograft tumors, generated subcutaneously in mice, were selected as model of squamous cell carcinoma for the study of cancer biomarker targeting. Briefly, 1483 cells (2×10^6 viable cells in 100 µl PBS) were implanted subcutaneously in the left and right posterior mammary fat pads of 6–8 week old female Nu/Nu mice (Charles River Laboratories). When tumors reached 4-5mm in diameter, the animals were anaesthetized and sacrificed via cervical dislocation. All animals were cared for in accordance with institutional guidelines. The protocols were reviewed and approved by the IACUC at Rice University.

Permeation of Fresh Tissues. To reproducibly permeate tissues for contrast agent delivery, tissue biopsies of uniform surface area were topically treated with permeation enhancers. A 4mm-diameter dermal punch (Miltex Inc., York, PA) was used to produce cylindrical samples of oral and bladder mucosa. Subcutaneously generated tumors, grown as cylinders to the appropriate diameter, were cut in half to expose the tumor surface. The tissue cylinders were embedded vertically into 3% ultrapure agarose

(Invitrogen), leaving the apical surface available for topical labeling. Two topical permeation enhancers, Triton-X100 and DMSO (Sigma- Sigma-Aldrich, St. Louis, MO) diluted in phosphate buffered saline (PBS; Sigma-Aldrich), were evaluated for their ability to permeate fresh tissue. PBS alone was used as a negative control. One ml of permeation enhancing solution was topically applied to the apical surface each tissue biopsy for 0 to 4 hours at 4°C.

Permeabilization Detection Using Macromolecules. To determine whether Triton-X100 treated tissues are selectively permeable to macromolecules of a specific size, bladder biopsies were probed with fluorescent macromolecules of three sizes. The tissues were topically treated for 1 hour with 0.5% Triton-X100 (to yield a treatment dose of 0.55pmol/cell assuming full-thickness permeation) or PBS, washed once in PBS, and covered with a 1:1:1 mixture of rhodamine-dextran (3kDa, Invitrogen), fluorescein-dextran (40kDa, Invitrogen), and AlexaFluor647 IgG (150kDa, Invitrogen), each diluted to a concentration of 1μM in PBS. Tissues were immersed with this solution for 15 minutes at 4°C and then imaged using fluorescence confocal microscopy at three different excitation wavelengths (described below). Images were collected in 5 μm steps from the surface into the tissue. Following imaging, the tissues were washed 3 times in cold PBS (15 minutes total) and re-imaged to assess the removal of unbound macromolecules. A total of 10 bladders were evaluated in independent experiments.

Tracking the Time Course of Tissue Permeation. To monitor Triton-mediated permeation of bladder epithelium as a function of time, fresh biopsies were treated for

different time intervals. Agarose-embedded punch biopsies were topically treated with 0.5% Triton-X100 for 0, 5, 10, 15, 30, or 60 minutes. Following the permeation treatment, the tissues were washed once in cold PBS and probed with the 1:1:1 mixture of fluorescent macromolecules described above. Confocal microscopy images were collected 40μm below the tissue surface to allow for optical sectioning of both the epithelium and underlying tissues. Each time-point was evaluated in 5 independent experiments.

Determination of the Depth of Penetration. The depth of Triton-mediated macromolecule penetration as a function of time and concentration was evaluated in cross-sections of fresh oral mucosa. Agarose-embedded punch biopsies were topically treated for 0 to 4 hours with Triton-X100 concentrations ranging from 0% to 2.5%. These concentrations were selected to treat cells with up to 1.1pmol/cell of Triton-X100. The permeabilized tissues were cross-sectioned using a Krumdieck tissue slicer (Alabama Research & Development, Munford, AL) and immersed for 15 minutes in the 1:1:1 mixture of fluorescent macromolecules. Confocal fluorescence images of the transverse sections were collected 40μm below the cut surface to avoid confounding effects due to damage at cut surface. The penetration depth for each size of macromolecule was evaluated by measuring the distance between the apical surface of the tissue and the leading edge of the fluorescent macromolecules using ImageJ v1.34 software (http://rsbweb.nih.gov/ij). Measurements were collected at 20 μm intervals across 4 representative images in 4 independent experiments (16 images total per treatment

condition). The rate of tissue permeation as a function of Triton-X100 concentration was determined from a linear least squares fit to this data.

Comparison of Macromolecule Penetration in Normal and Cancer Tissue. To determine whether the depth and rate of permeation varies between tissues, macromolecule penetration was assessed in fresh normal oral mucosa and squamous cell carcinoma. Agarose-embedded oral biopsies and 1483 tumors were treated for 1 hour with 1% Triton-X100, 10% DMSO, or PBS only. Following the permeation treatment, the tissues were cross-sectioned with a Krumdieck tissue slicer and probed with the 1:1:1 mixture of fluorescent macromolecules for 15 minutes. Confocal fluorescence images of the transverse sections were collected 40μm below the cut surface. The depth of penetration from the apical surface was assessed for each macromolecule at 20 μm intervals across 4 representative images from 4 independent experiments (16 images total per treatment condition). The rate of tissue permeation was determined from a linear least squares fit to this data.

Synthesis and Validation of Molecular-Specific Contrast Agents. Mouse anti-human antibodies targeted to epidermal growth factor receptor (EGFR; clone 108; custom synthesized by the Baylor College of Medicine, Houston, TX) and Cyclin D1 (clone 72-13G; Santa Cruz Biotechnology Inc, Santa Cruz, CA) were reacted with AlexaFluor® 647 and AlexaFluor® 488 carboxylic acid succinimidyl esters using commercially available labeling kits (Invitrogen). The purified conjugates were suspended in PBS at a concentration of 1.0 mg/ml and 0.2mg/ml respectively. Dye-labeled isotype controls

were synthesized at the same concentrations. Prior to tissue labeling, the bioactivity and specificity of the conjugates was confirmed in live 1483 cells as described in [144] in the presence and absence of Triton-X100.

Comparison of anti-EGFR Delivery Strategies in Tumors. To assess the ability of permeation enhancers to deliver molecular-specific optical contrast agents through tissue, subcutaneously generated 1483 xenograft tumors were for labeled for EGFR in the presence of 1% Triton-X100, 10% DMSO, or PBS. AntiEGFR-647 (1:50) was diluted in permeation enhancers and topically applied to the cut surface of agarose-embedded tumors for 1 hour at 4°C. The labeled tissues were washed 3 times in cold PBS, sliced perpendicular to the surface using a Krumdieck tissue slicer, and counter-stained for 30 seconds with 0.05% acriflavine-HCL (Sigma-Aldrich), a cell permeant nucleic acid dye. The depth and localization of EGFR labeling was assessed from confocal fluorescence images acquired 40μm below the cross-section surface. A total of 10 tumors (5 mice) were evaluated.

Demonstration of Multi-Target Labeling in Tumors. To demonstrate the feasibility of simultaneously targeting multiple cancer biomarkers in different cell compartments, 1483 xenograft tumors were simultaneously labeled with 3 tissue and/or cell impermeant probes. AntiEGFR-647 (1:50), antiCyclinD1-488 (1:10), and propidium iodide (15μM, Sigma Aldrich) were used to label cell membrane, cytoplasmic, and nuclear targets respectively. The contrast agents and isotype controls were diluted in 1% Triton-X100 and topically applied for 1 hour. The labeled tissues were washed 3 times in cold PBS

and sliced perpendicular to the surface using a Krumdieck tissue slicer. The localization of labeling was assessed from confocal fluorescence images acquired 40μm below the cross-section surface. A total of 10 tumors (5 mice) were evaluated.

Confocal Image Acquisition and Analysis. All images were obtained using a Carl Zeiss LSM 510 confocal microscope (Thornwood, New York) equipped with 488 nm (30mW), 543 nm (1mW), and 633 nm (5mW) lasers. Images were collected using PMT detectors and Zeiss LSM 5 image examiner software. Samples were sequentially excited with each laser line, with power settings of 50%, 100%, 100% respectively. Fluorescence emission was collected using 500-530 nm, 565-615 nm, and 650-710 nm band-pass filters respectively. Tissue reflectance at 633 nm was collected using a 635 nm dichroic beam splitter. Images were acquired at 0.5 frames per second using a 63X oil, 20X, or 10X objectives with a pinhole of 2.56 Airy units. For the non-specific macromolecule permeation studies, the gain was held constant just below saturation level of the extracellular solution. In the molecular-specific targeting studies, the gain was held constant at 440 for antiEGFR-647 (633 nm excitation), 650 for antiCyclin D1-488 (488 excitation), 400 for propidium iodide (543 excitation), and 535 for acriflavine-HCL (488 nm excitation).

5.3 RESULTS

Permeabilization of Fresh Guinea Pig Bladder. The ability of Triton-X100 to permeabilize guinea pig bladder mucosa was assessed using untargeted fluorescent macromolecules of three different sizes. Figure 13 shows representative confocal images of tissue biopsies topically treated for 1 hour with 0.5% Triton-X100 or PBS, and then probed with a 1:1:1 mixture 3kDa rhodamine-dextran, 40kDa fluorescein-dextran, and 150kDa Alexa647-IgG. The tissue reflectance images are shown on the left and the corresponding fluorescence images are shown to the right. The yellow/white lines indicate the basal boundaries of the epithelium. Due to the three-dimensional folding of the deflated bladder, it was possible to image the transitional epithelium in cross-section using confocal microscopy at a depth of 40 μm. In the reflectance images, the epithelium was distinguished from the underlying, more highly scattering tissues by its darker appearance. Triton-X100 treatment facilitated trans-epithelial penetration of all three sizes of molecules. The 3kDa and 40kDa molecules successfully penetrated both the cytoplasm and nucleus of epithelial cells, whereas the 150kDa molecules only penetrated the cytoplasm of epithelial cells. With several brief washes, a significant portion of the macromolecules were removed. In the PBS treated controls, the macromolecule penetration was limited to 1-2 layers of superficial cells. Videos of confocal optical sectioning through Triton-X100 and PBS-treated bladder tissue can be found in the supplementary materials.

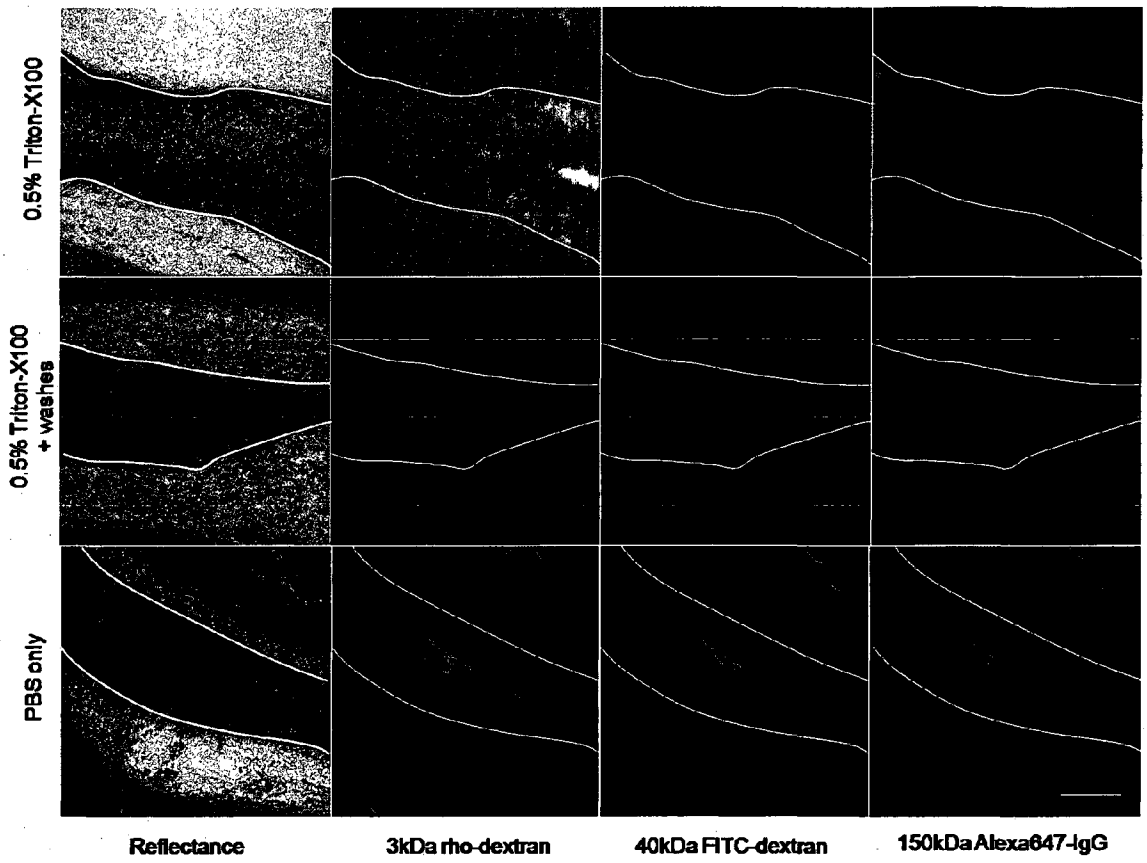

Figure 13. Macromolecule penetration of guinea pig bladder epithelium following permeation treatment. Tissues were topically treated for 1 hour with 0.5% Triton-X100 or PBS and then probed with a 1:1:1 mixture of 3kDa rhodamine-dextran, 40kDa fluorescein-dextran, and Alexa647-IgG. The yellow/white lines indicate the basal surface of the epithelium. In reflectance images, the epithelium was distinguished from the underlying tissues by its darker appearance. Following treatment with Triton-X100, trans-epithelial penetration was observed for all three sizes of molecules. After washing with PBS, the fluorescence intensity of the labeled tissue was significantly reduced. In PBS-treated controls, macromolecule penetration was limited to a few cells in the superficial layers. The scale bar represents 100 μm.

The time-course of tissue permeation with Triton-X100 treatment was tracked using confocal microscopy. Figure 14 shows representative images of biopsies treated with 0.5% Triton-X100 for 5, 10, and 15 minutes and then probed with fluorescent macromolecules of 3 sizes. At 5 minutes, the leading edge of permeabilized epithelium featured irregular borders. At 10 minutes, full-thickness epithelial permeation was observed in some epithelial regions. Individual, non-permeabilized cells were easily distinguished by their dark appearance. At 15 minutes, trans-epithelial penetration was observed for all three sizes of molecules. With time, the overall fluorescence intensity of the epithelium increased to approach that of the exogenous solution; however, the nuclei of cells probed with 150kDa molecules remained dark. Fluorescence in the underlying tissues was observed as early as five minutes and increased steadily with time.

Depth of Mucosal Permeation. The depth of Triton-mediated permeation was assessed in a model of porcine oral mucosa ranging in thickness from 600 to 1000 μm. Epithelial punch biopsies were topically treated with different concentrations of Triton-X100 (ranging from 0% to 2.5%) for different time intervals (ranging from 0 to 4 hours), sliced in cross-section, and probed with fluorescent macromolecules. Figure 15 demonstrates the relationship of treatment time and Triton-X100 concentration to the depth of tissue permeation. Triton-X100 treatment was found to produce very uniform, reproducible tissue permeation with well defined borders. When leading edge of macromolecule labeling was assessed at regular time intervals, the depth of penetration was found to increase at a steady, linear rate (Fig. 15a). The smaller probe molecules consistently showed deeper penetration than the 150kDa molecules.

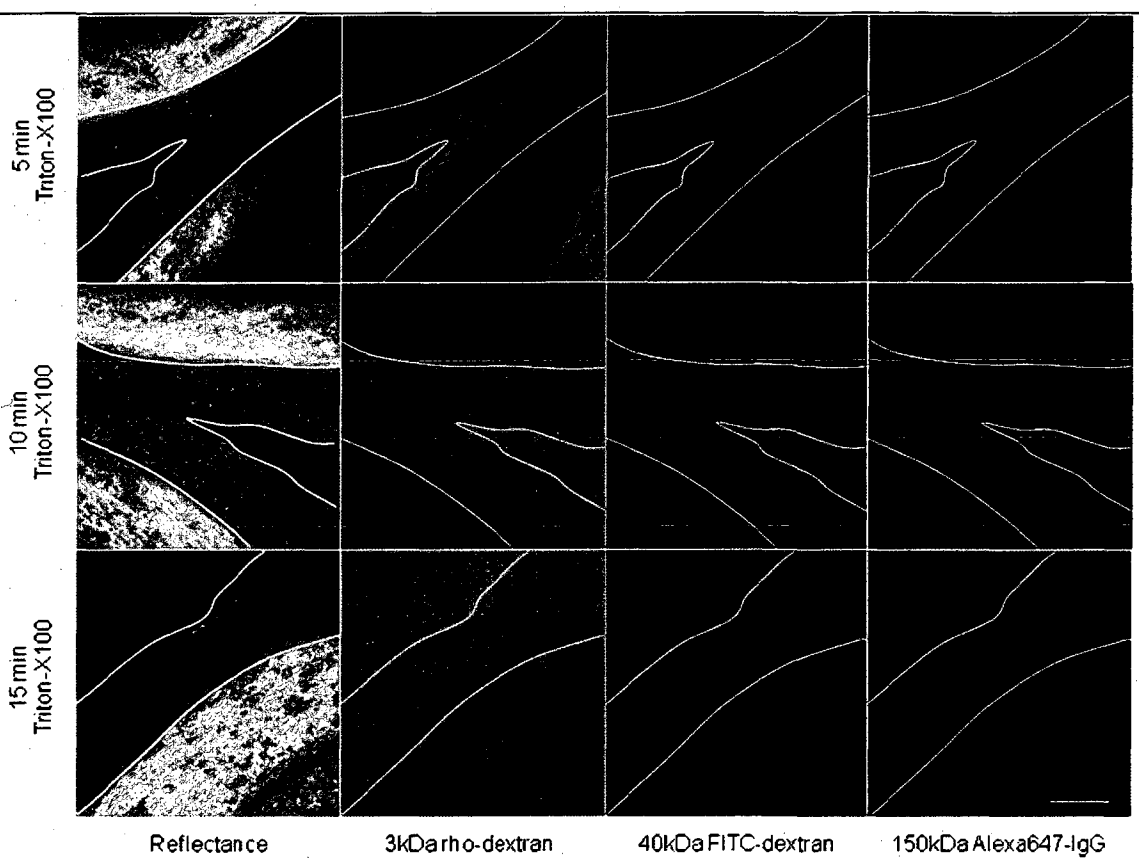

Figure 14. The time course of tissue permeation following treatment with 0.5% Triton-X100. Fresh guinea pig bladder biopsies were topically treated with 0.5% Triton-X100 for 0 to 60 minutes and then probed fluorescent molecules of three sizes. Representative confocal images, acquired 40μm below the tissue surface, are shown for the 5, 10, and 15 minute time-points. The yellow/white lines indicate the apical and basal surfaces of the epithelium. The depth and uniformity of permeation increased with treatment time. Differences were observed between the cell and tissue penetration of different size probe molecules. Fluorescence signal in stroma was observed as early as 5 minutes following Triton-X100 treatment. The scale bar represents 100 μm.

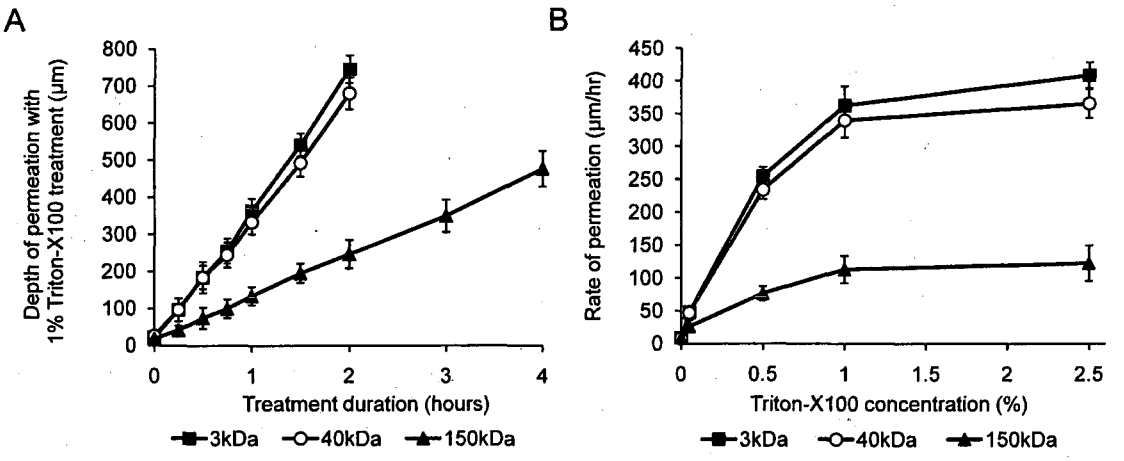

Figure 15. Permeation of normal oral mucosa as a function of time and Triton-X100 concentration. Normal porcine oral mucosa was topically treated with different concentrations of Triton-X100 for regular time intervals, sliced, and probed with fluorescent macromolecules of 3 sizes: 3kDa (■), 40kDa (○), and 150kDa (▲). The depth and rate of macromolecule penetration was determined from confocal fluorescence images of transverse tissue sections. A) The relationship between the depth of permeation and duration of treatment with 1% Triton-X100. A steady, linear increase in permeation depth is observed with time. B) Rate of tissue permeation as a function of Triton-X100 concentration. Increasing the Triton-X100 concentration increased the depth of tissue permeabilization; however, the extent of macromolecule penetration was limited by size

Using a linear least squares fit, the rate of tissue permeation was evaluated for a range of Triton-X100 concentrations (Fig. 15b). Increasing the Triton-X100 concentration was found to increase the rate of tissue permeation; however, at concentrations above 1% Triton-X100, little improvement in the rate of permeation was observed. Size dependent differences in macromolecule penetration were observed for all concentrations of Triton-X100, although there was generally no significant difference between the penetration depth of 3kDa and 40kDa macromolecules. Longer probe times were evaluated to confirm that the differences in penetration depth were not due to inadequate labeling time (data not shown).

Comparison of Macromolecule Penetration in Normal and Cancer Tissue. To determine whether the depth and rate of topical permeation varies between normal and abnormal tissue, macromolecule penetration following of topical permeation was evaluated in normal oral mucosa and tumor models. Figure 16 compares the depth and rate of macromolecule penetration in two tissue models using three different labeling solutions. The maximal penetration depth following 1 hour of treatment with 1% Triton-X100 was found to be approximately 25% greater in squamous carcinoma tissue than normal epithelium (Fig. 16a). Little permeation, less than 100 μm deep, was observed in DMSO- and PBS-treated tissues. When the rate of macromolecule penetration following Triton-X100 treatment of was evaluated as a function size, all sizes of macromolecules consistently penetrated more rapidly in carcinoma tissue than normal epithelium (Fig. 15b). The largest difference in rate was observed for the 150kDa molecules, although this size of molecule consistently penetrated more slowly than smaller molecules.

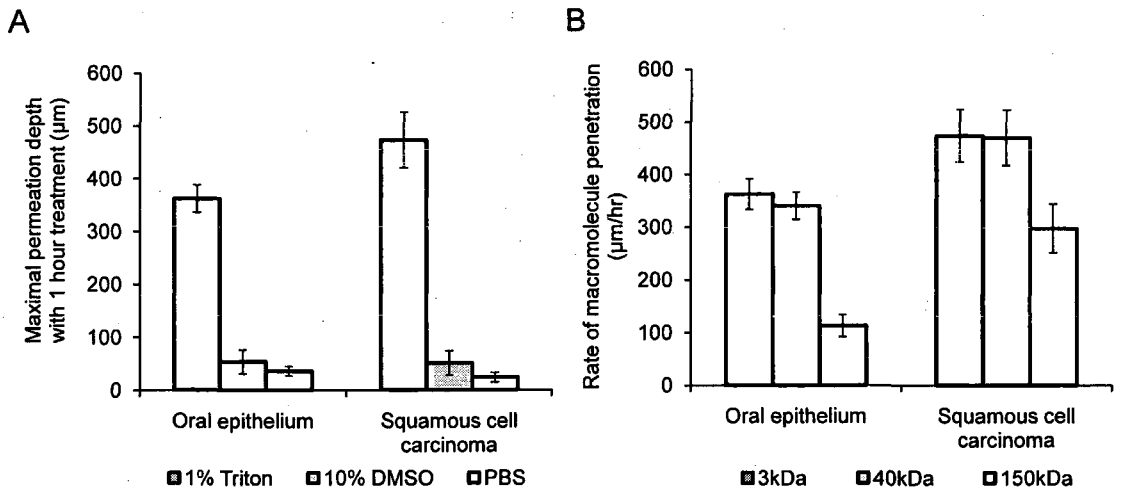

Figure 16. Comparison of macromolecule penetration in normal oral mucosa and squamous cell carcinoma. Tissues were treated with 1% Triton-X100, 10% DMSO, or PBS, sliced, and probed with fluorescent macromolecules of three sizes. The depth and rate of macromolecule penetration was determined from confocal fluorescence images of transverse tissue sections. A) The maximal penetration depth following a 1 hour treatment with permeation enhancers, measured using 3kDa rhodamine-dextran. The maximal depth with Triton-X100 treatment was found to be greater for cancer tissue than normal epithelium. Little permeation was observed with DMSO- and PBS-treated controls. B) The rate of macromolecule penetration by size with 1% Triton-X100 treatment. The rate of penetration was consistently more rapid in carcinoma tissue for all sizes of macromolecules evaluated.

EGFR Targeting in Cancer. To determine whether Triton-X100 is useful for the delivery of molecular-specific optical contrast agents, subcutaneous tumors were labeled for EGFR in the presence of topical permeation enhancers. Freshly excised tumors were topically treated for 2 hours with antiEGFR-647 diluted in 1% Triton-X100, 10% DMSO, or PBS. The labeled tissues were sliced in cross-section, counter-stained with acriflavine-HCL, and imaged perpendicular to the labeling surface. Figure 17 shows representative confocal fluorescence images of EGFR labeling in the presence of different topical permeation enhancers. The surface of the tissue where the contrast agent was applied appears at the top of each panel. EGFR labeling is denoted in red and acriflavine-HCL labeling in green. Treatment with 1% Triton-X100 yielded uniform EGFR labeling around all squamous cells to a depth of 500-600μm. The honeycomb pattern of labeling was consistent with that observed *in vitro.* In contrast, EGFR labeling in DMSO- and PBS-treated tissues was limited to the superficial layers of cells (~ 20-60 μm deep).

Multi-Target Labeling in Tumors. To demonstrate the feasibility of delivering multiple optical contrast agents to different cell compartments, three different targeting moieties were topically applied to tumors in the presence of Triton-X100. The specificity and bioactivity of each targeting moiety was established *in vitro* prior to tissue labeling. No differences in targeting were observed with Triton-X100 co-treatment of live and fixed cells (data not shown).

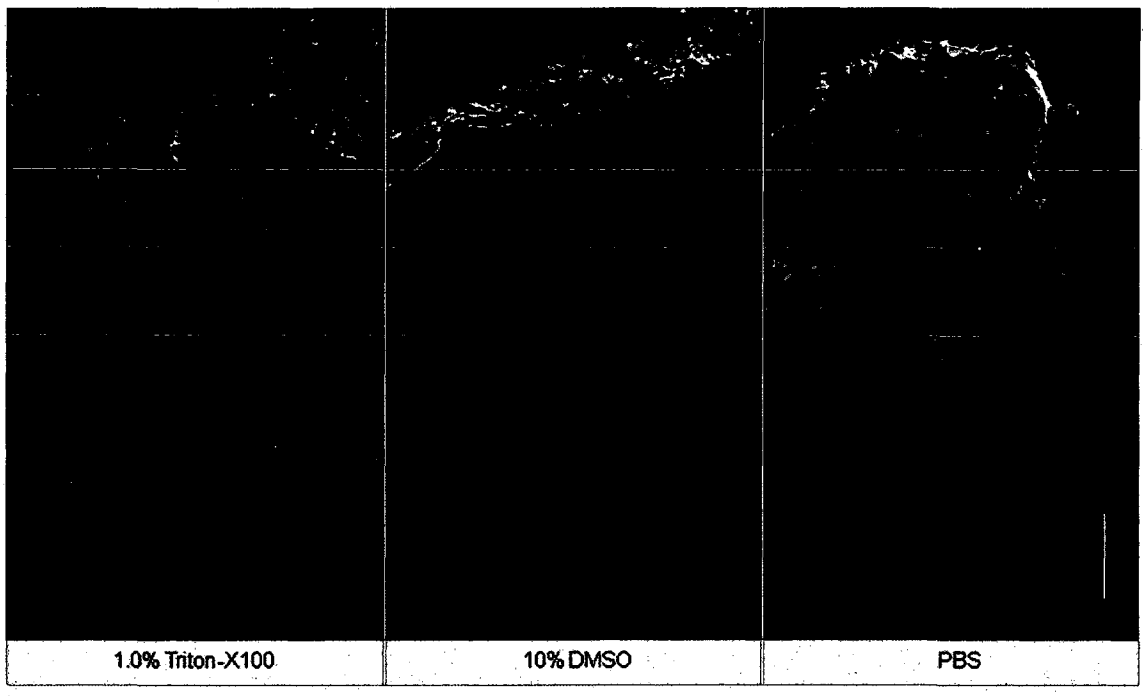

Figure 17. EGFR targeting in the presence of topical permeation enhancers. Subcutaneously generated 1483 tumors were topically labeled for 2 hours with antiEGFR-647 (red) diluted in 1% Triton-X100, 10% DMSO, or PBS. The tissues were sliced and imaged perpendicular to the labeling surface, shown at the top. Tissues were counterstained with acriflavine-HCL (green) to highlight the tissue morphology. In Triton-X100 treated tissues, uniform EGFR labeling was observed around all squamous cells to a depth of 500-600 μm. EGFR labeling in the DMSO- and PBS- treated controls was limited to the superficial cell layers. The scale bar represents 100 μm.

Figure 18 shows representative images of freshly excised tumor tissue labeled for EGFR, Cyclin D1, and nucleic acid content in the presence of 1% Triton-X100. The tissues were topically labeled, sliced, and imaged perpendicular to the labeling surface. AntiEGFR-647 labeling (red) appeared in a characteristic honeycomb pattern. AntiCyclin D1-488 labeling (green) was diffusely spread through the cytoplasm of cancer cells. Propidium iodide labeling (orange) was limited to cells permeabilized by the Triton-X100 treatment. No EGFR or Cyclin D1 labeling was observed in or around cells lacking propidium iodide labeling (data not shown). Little to no antibody labeling was observed when isotype controls and propidium iodide were administered in the presence of Triton-X100. No propidium iodide labeling was present in PBS-treated controls (data not shown).

5.4 DISCUSSION

Optical contrast agents developed for cancer biomarker detection have demonstrated high specificity in cell and tissue models. Generally ranging in size from 6kDa (peptides and affibodies) to 150kDa (antibodies), most molecular-specific contrast agents have a limited ability to penetrate mucosal tissue. Chemical modification and encapsulation strategies to improve tissue penetration have only proven useful for molecules at the small end of the size spectrum [143]. The topical delivery of tissue-impermeant contrast agents presents an interesting challenge, since the success of tissue labeling is dependent on the efficiency and uniformity of contrast agent delivery. Furthermore, unbound contrast agents generally need to be washed out prior to imaging for high optical contrast. Here I evaluate ability of Triton-X100 to deliver optical contrast agents that lack the appropriate physiochemical properties for unaided tissue permeation.

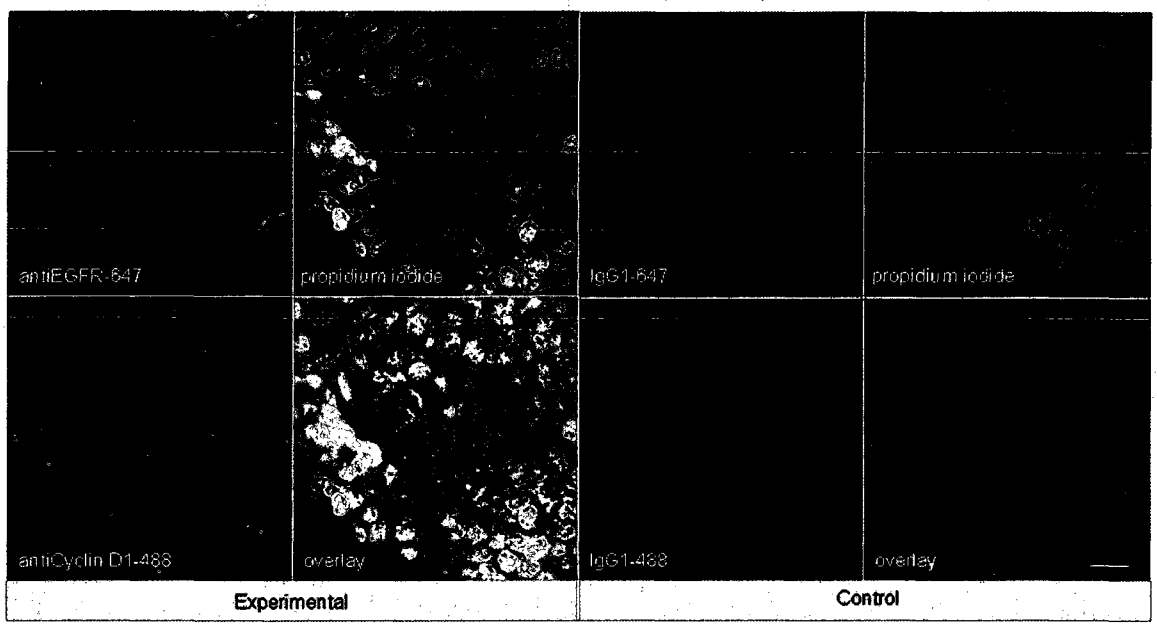

Figure 18. Simultaneous labeling of clinically relevant cancer biomarkers with 1.0% Triton-X100 co-treatment. Three different cell and tissue-impermeant targeting moieties, antiEGFR-647 (red), antiCyclinD1 (green), and propidium iodide (orange), were targeted to membrane, cytoplasmic, and nuclear biomarkers respectively. The tissue was imaged perpendicular to the topical labeling surface. The molecular-specific labeling was observed to be highly uniform and reproducible in permeabilized tissues. Little to no antibody labeling was observed using isotype controls with Triton-X100 co-treatment. The scale bar represents 20 μm.

Confocal microscopy studies of macromolecule penetration in the bladder mucosa were used to examine the uniformity of tissue permeabilization. The bladder mucosa is a particularly interesting model because the natural folding of the deflated bladder allows the epithelium to be imaged in cross-section without the need for tissue slicing. In this model, it was observed that a fixed volume of 0.5% Triton-X100 can deliver molecules up to 150kDa in size across treated epithelium. By my estimate, the cells of the epithelium are receiving a treatment dose of 0.5 to 0.6 pmol/cell. Tissue permeation appears to primarily follow a transcellular route, appearing as a strong fluorescent signal within cells. In tissues probed with 3kDa and 40kDa macromolecules, the fluorescence is uniform across the entire epithelium. In tissues probed with 150kDa molecules, only the cell nuclei appear as dark spots. Extracellular fluorescence is evident between cells at the leading edge of the treatment, suggesting that Triton-X100 also facilitates paracellular delivery. Washing of the epithelium removes both intracellular and extracellular probes, yielding a uniformly dark tissue. Together, these observations indicate that Triton-X100 may be useful for the delivery of contrast agents targeted to both intracellular and extracellular biomarkers.

Studies of Triton-X100 treatment in fresh oral mucosa specimens indicate that the depth of permeation can be controlled. The leading edge of permeation treatment was well-defined at all concentrations examined, allowing measurement of penetration depth as a function time and concentration. The penetration depth increased linearly with treatment time for all sizes of probe macromolecules over a 4 hour observation period. The maximal rate of epithelial permeation increased with increasing Triton-X100

concentration. These trends were highly reproducible, varying less than 10% from sample to sample. This data demonstrates that it is possible to regulate the depth of Triton-X100 treatment by adjusting the Triton-X100 concentration and treatment duration. The depth of labeling following treatment will be determined by contrast agent size, with larger probes demonstrating shallower penetration at the same treatment concentration as smaller molecules. Interestingly, it does not appear advantageous to use Triton-X100 concentrations much above 1%, since little improvement in the rate of permeation is observed between tissues treated with 1% and 2.5% Triton-X100.

Differences were apparent in the permeation of tissues when compared to cell monolayers. In Chapter 3, it was demonstrated that cells can be permeabilized with 0.27 pmol/cell Triton-X100 and that nuclear penetration of 40kDa and 150kDa molecules can be achieved with 0.55 to 1.1 pmol/cell Triton-X100. In tissue, nuclear penetration is limited to molecules of 40kDa or less. Occasional nuclear penetration of 150kDa molecules is observed at the surface of treated tissue and is generally limited to 1-2 cell layers. If one considers an oral biopsy treated with 1% Triton-X100 for 1 hour, the mean concentration of Triton-X100 is close to 0.55pmol/cell. Enhanced nuclear permeation is not observed with higher Triton-X100 concentrations or changes in treatment time. Thus it appears likely that Triton-X100 preferentially permeabilizes cell membranes in its movement through tissue and is not sufficiently concentrated locally for the generation of large nuclear pores.

Depth control will be advantageous for the use of topical contrast agents in humans. By limiting the penetration of optical contrast agents to a finite depth, the systemic delivery of contrast agents with undefined toxicity can be avoided. Since the mucosal epithelium is a renewable tissue, contrast agents adhering to epithelial cells will likely be shed with tissue turnover. For the optical detection of disease biomarkers, some compensation may be required for differences in permeation rate of normal and abnormal tissue. In the tissues studied here, however, less than a 25% difference was observed between normal squamous epithelium and undifferentiated cancer tissue. Depth-sensitive optical imaging or spectroscopy devices could potentially be used to monitor the depth of permeation and determine when to halt the reaction by washing.

The use of Triton-X100 as a topical permeation enhancer allows the delivery of optical contrast agents that lack the appropriate size and chemical properties for tissue penetration. Molecular-specific contrast agents as large as antibodies can be successfully delivered to both intracellular and extracellular targets using Triton-X100. Here it is demonstrated that three clinically relevant biomarkers of cancer can be simultaneously labeled with the topical co-administration with Triton-X100. The EGF receptor, located on the surface of cells, is thought to be a promising target because its expression is elevated in a variety of dysplastic and cancerous tissues [41-43]. The over-expression of Cyclin D1, detected here in the cytoplasm, is associated with a poor prognosis in patients with head and neck tumors [145-148]. Measures of nuclear morphology, delineated here with propidium iodide, have been proposed as an objective measure of the transition from pre-neoplastic to neoplastic tissue [149]. The topical labeling of these markers was uniform and

reproducible in all transverse sections examined by confocal microscopy. In contrast, treatment with DMSO or PBS failed to enhance the penetration tissue-impermeant optical probes.

The feasibility of translating Triton-X100 for *in vivo* use remains to be determined. In Chapter 3, it was demonstrated that Triton-X100 mediated permeabilization of cells is reversible, and that cells retain their metabolic and proliferative capacities while recovering membrane integrity. Others have demonstrated that only concentrations above 10% produce visible side effects in patch tests of human skin, consisting of transdermal water loss and erythema [150]. It has been reported that two or more permeation enhancers applied together can act synergistically [151], suggesting that it may be possible to further reduce the effective Triton-X100 concentration by combining it with other topical agents. Tissue damage reported with the use of other surfactant-based permeation enhancers has generally been limited and reversible [152-154]. The next step will be to characterize the safety, toxicity, biological activity, and reversibility of Triton-X100 mediated permeation at clinically useful doses in animal models.

In conclusion, this paper demonstrates that Triton-X100 is a promising topical permeation enhancer for the mucosal delivery of tissue-impermeant optical contrast agents. Compared to other topical permeation enhancers, Triton-X100 can deliver a much broader size range of molecules. No chemical modifications of optical contrast agents are needed, both targeted and untargeted molecules as large as 150kDa can be delivered uniformly through normal and cancer tissue. The depth of tissue permeation

can be modulated, allowing for epithelial containment of topical contrast agents. The co-administration of Triton-X100 with molecular-specific contrast agents facilitates the simultaneous labeling of cell membrane, cytoplasmic, and nuclear targets. Further work is needed to establish the safety of this approach for *in vivo* use.

CHAPTER 6

DISCUSSION AND FUTURE DIRECTIONS

Although many surfactants have been evaluated as topical permeation enhancers, none have proven to be ideal. Both anionic and cationic surfactants have been shown to swell the stratum corneum of skin and interact with intracellular keratin. Non-ionic surfactants are generally regarded as safer because they lack the protein denaturation properties associated with charged surfactants. The ideal topical permeation enhancer has been given [155] as one which:

- Is non-toxic, non-irritating, and non-allergenic
- Works rapidly in a predictable and reproducible manner
- Has no pharmacological activity within the body
- Works uni-directionally to prevent the loss of endogenous material
- Allows the reversal of tissue permeability when removed
- Is appropriate for formulation into diverse topical preparations

In the remaining portion of this chapter, I will discuss how Triton-X100 meets these criteria and what additional studies are required to determine the clinical utility of Triton-X100.

The body of work contained in this thesis demonstrates that Triton-mediated permeation of cells is fast, efficient, and reproducible. In tissues, Triton-X100 advances at a constant rate in a uniform, reproducible manner. The flux of macromolecules through tissue can be modulated by controlling the Triton-X100 concentration and treatment duration. When topically applied at the appropriate concentration, damage to the cell membrane is reversible. Treated cells retain metabolic and proliferative capacities, suggesting that Triton-X100 is non-toxic at specific concentrations.

The next important step in this research will be to establish the safety of Triton-X100 use. Concerns over surfactant toxicity have limited their widespread acceptance as topical permeation enhancers. There exists a large body of evidence suggesting a correlation between permeation enhancer efficacy and toxicity. However, a recent survey of permeation enhancers in cell monolayers has demonstrated that surfactants can have high permeation efficacy with minimal toxicity when applied at specific concentrations [156]. This survey was the first to introduce the concept of a therapeutic concentration window and emphasize the importance of considering concentration when analyzing the permeation efficiency-to-toxicity relationship of chemical permeation enhancers. My studies agree with this observation, demonstrating that Triton-X100 can be non-toxic when applied at or near the minimum effective permeation concentration.

Establishing acceptable values of toxicity for safe use *in vivo* remains a challenge. Surfactant toxicity will depend on many factors including the test model and conditions,

as well as the frequency and duration of treatment. Light microscopy studies of animal intestines infused with Triton-X100 have demonstrated superficial desquamation, shortening of the microvilli, and intermittent necrosis [157-159]. This damage was associated with increased mucus production [159], release of cytoplasmic lactate dehydrogenase [159], and loss of water from the epithelium [160]. In all cases, the damage was reversed within hours. It is interesting to note that the reversibility studies were performed using continuous perfusion of 1% to 5% Triton-X100 for up to 3 hours, which would lead to much higher concentration of Triton-X100 per cell than our studies. These studies suggest that it will be important to monitor the transient loss of water, proteins, and metabolites when establishing the safety profile of Triton-X100 treatment.

The pharmacological activity of Triton-X100 *in vivo* remains to be determined. Although no studies have specifically evaluated the long-term effects of Triton-X100, dogs and rats receiving a one-time treatment of 1% Triton-X100 were followed for over 30 days and shown to have no difference in survival compared to controls [161, 162]. Triton-X100 is known to interact primarily with proteins bound to membrane lipids. Solubilization of these proteins using Triton-X100 generally does not result in major conformational changes or loss of activity [57]. Furthermore, Triton-X100 appears to be very inefficient at breaking protein-protein interactions. Thus the tertiary and quaternary structure of most proteins is conserved in the presence of Triton-X100 [163-165]. My studies of cell recovery following Triton-X100 treatment suggest that proteins affected by low amounts of surfactant are not critical to cell survival. Together, this data suggests that Triton-X100 will have minimal pharmacological activity. Further studies are needed to determine the

long-term local and systemic activity of Triton-X100 delivered at clinically relevant doses.

In thinking about potential animal models for further studies, it is useful to consider the dimensions, accessibility, and clinical relevance of potential Triton-X100 application sites. I have demonstrated that controlling the Triton-X100 concentration relative to the number of cells being treated is important for maintaining cell viability, thus the concentration will need to be adjusted based on the volume of tissue to be treated. Ideally, the labeling site should have dimensions similar to that of clinically relevant sites. Alternatively, smaller volumes of tissue could be treated in a scalable manner. Due to differences in epithelial thickness, organization, and function between organs, it will be important to test Triton-X100 treatment in clinically relevant organs. To facilitate clinical translation, the site chosen for Triton-X100 application should be easily accessible for both labeling and non-invasive imaging.

The bladder mucosa presents an interesting first model for studying the epithelial delivery of cancer-specific contrast agents. Comprised of only a few cell layers, the bladder epithelium can be optically sectioned though its full thickness. Squamous cell carcinoma of the bladder is associated with a poor prognosis in humans and its recurrence is difficult to detect using existing technologies [166]. Bladder carcinogenesis is readily induced in rodent models using chemical carcinogens and its progression monitored with ultrasound [167]. Triton-X100 can be delivered in a highly controlled manner by catheterization and

flushing of the bladder prior to Triton-X100 infusion. The rodent bladder architecture is similar to that of humans and I anticipate that the minimum effective Triton-X100 concentration will be scalable for human use. It will also be possible to collect back the bladder infusion and analyze it for water, protein, and metabolite content.

Establishment of the optimum volume and concentration of Triton-X100 treatment should be performed in normal animals. Bladder permeability can be assessed by excising the bladder following treatment and monitoring the influx of fluorescent macromolecule probes using confocal microscopy. Once the optimum dose is determined, the local and systemic toxicity should be monitored at regular intervals following a one-time infusion of Triton-X100. Using light microscopy and electron microscopy of excised tissue sections, it will be possible to identify structural changes to the epithelium and stroma. At early time-points, it will be important to look for desquamation, necrosis, cellular atypisms, and loss of epithelial continuity. At later time-points, tissues should be examined for inflammation, ulceration, denervation, and continued epithelial abnormalities. To monitor for systemic changes, animals should be examined daily for urinary retention, hematuria, abdominal tenderness, and other signs of distress. Routine blood chemistry analysis and urinalysis may also be useful.

Triton-mediated delivery of contrast agents for *in vivo* cancer biomarker detection can be evaluated in model of bladder carcinogenesis. Using a catheter, a fixed volume of molecular-specific optical contrast agents can be co-administered with Triton-X100. I

have already established that the specificity of contrast agents and the tertiary structure of their targets can be conserved in the presence of Triton-X100. To facilitate the rapid assessment of labeling, we propose that the bladder of sedated animals be labeled for 15 or 30 minutes, flushed once with saline solution, and examined *ex vivo* immediately following animal sacrifice. The localization and intensity of labeling, as well as the integrity of the epithelium, should be compared to that of saline-infused controls. A semi-quantitative assessment of labeling in groups of animals receiving different durations of carcinogen treatment can be used to determine whether Triton-mediated labeling can distinguish between normal, low grade dysplasia, high grade dysplasia, and cancer tissue. The selection of appropriate biomarkers will be dependent on the carcinogen model; however, it may be advantageous to use a multiplexed approach to target multiple cell compartments.

If these studies are successful, it will be useful to pursue models of increased complexity. For example, Triton-mediated delivery of EGFR-targeted contrast agents to the oral mucosa could have a positive impact on the early detection of oral neoplasia. I propose evaluating the topical application of Triton-X100 in porcine buccal mucosa due to its similarities to human buccal mucosa. My preliminary studies of Triton-X100 in freshly excised buccal tissue suggest that a 1.5 hour treatment of 1% Triton-X100 will provide a sufficient dose for antibody penetration. Again, it will be important to establish the local and systemic toxicity of this Triton-X100 dose using normal animals. Groups of carcinogen-treated pigs will be useful for determining the sensitivity of the labeling strategy. To facilitate clinical translation, contrast agent imaging should be performed

non-invasively *in vivo* using live, anesthetized pigs. Biopsies of the treated tissues can be collected to assess tissue pathology and monitor the tissue recovery at regular time intervals.

Studies of Triton-X100 in the rodent bladder and porcine buccal mucosa will provide important information about the toxicity, bioactivity, and irritation capacity of clinically relevant doses of Triton-X100. The data collected in cells and tissues suggest that Triton-X100 is likely to meet many of the criteria of an ideal topical permeation enhancer. While we recognize that the use of Triton-X100 will not prevent the loss of some endogenous material from the body, it is hoped that Triton-mediated membrane damage *in vivo* will be sufficiently mild and reversible to warrant further study.

CHAPTER 7

CONCLUSIONS

The research presented in this dissertation lays the groundwork for a novel strategy to detect cancer biomarkers in live cells and tissues using existing molecular-specific optical contrast agents. I have demonstrated that Triton-X100 can permeabilize a variety of live cells in an efficient, reproducible, and scalable manner. Both targeted and untargeted optical contrast agents, ranging in size from 3kDa to 150kDa, were reproducibly delivered by controlling the moles of Triton-X100 relative to the number of cells being treated. When Triton-X100 was delivered at or near the minimum effective concentration, the cells recovered after treatment. The intracellular labeling of live cells following Triton-X100 treatment was both specific and sensitive. Differences in hTERT protein expression could be distinguished based on the intensity and localization of protein labeling. The translation of this approach for tissue labeling proved feasible, with Triton-X100 facilitating controlled contrast agent distribution. The co-administration of Triton-X100 with molecular-specific contrast agents allowed the simultaneous labeling of cell membrane, cytoplasmic, and nuclear targets. Together, these findings provide the first evidence that cell- and tissue-impermeant contrast agents can be delivered into mucosal tissue in a sufficiently controlled and uniform manner to allow for cancer biomarker detection. Further studied are needed to establish the safety of Triton-X100 for topical use *in vivo* at clinical relevant doses.

REFERENCES

1. R. S. Cotran, V. Kumar and T. Collins, "Pathological basis of disease, 6th Ed.," (1999)

2. G. J. Kelloff, E. T. Hawk, J. A. Crowell, C. W. Boone, S. G. Nayfield, M. Perloff, V. E. Steele and R. A. Lubet, "Strategies for identification and clinical evaluation of promising chemopreventive agents," *Oncology (Williston Park)* **10**(10), 1471-1484; discussion 1484-1478 (1996)

3. G. J. Kelloff, C. C. Sigman, K. M. Johnson, C. W. Boone, P. Greenwald, J. A. Crowell, E. T. Hawk and L. A. Doody, "Perspectives on surrogate end points in the development of drugs that reduce the risk of cancer," *Cancer epidemiology, biomarkers & prevention : a publication of the American Association for Cancer Research, cosponsored by the American Society of Preventive Oncology* **9**(2), 127-137 (2000)

4. N. Ramanujam, M. F. Mitchell, A. Mahadevan, S. Warren, S. Thomsen, E. Silva and R. Richards-Kortum, "In vivo diagnosis of cervical intraepithelial neoplasia using 337-nm-excited laser-induced fluorescence," *Proc Natl Acad Sci U S A* **91**(21), 10193-10197 (1994)

5. R. Richards-Kortum, M. F. Mitchell, N. Ramanujam, A. Mahadevan and S. Thomsen, "In vivo fluorescence spectroscopy: potential for non-invasive, automated diagnosis of cervical intraepithelial neoplasia and use as a surrogate endpoint biomarker," *J Cell Biochem Suppl* **19**(111-119 (1994)

6. G. A. Wagnieres, W. M. Star and B. C. Wilson, "In vivo fluorescence spectroscopy and imaging for oncological applications," *Photochem Photobiol* **68**(5), 603-632 (1998)

7. J. G. Fujimoto, C. Pitris, S. A. Boppart and M. E. Brezinski, "Optical coherence tomography: an emerging technology for biomedical imaging and optical biopsy," *Neoplasia (New York, N.Y* **2**(1-2), 9-25 (2000)

8. S. K. Chang, Y. N. Mirabal, E. N. Atkinson, D. Cox, A. Malpica, M. Follen and R. Richards-Kortum, "Combined reflectance and fluorescence spectroscopy for in vivo detection of cervical pre-cancer," *Journal of biomedical optics* **10**(2), 024031 (2005)

9. N. Ramanujam, M. F. Mitchell, A. Mahadevan, S. Thomsen, A. Malpica, T. Wright, N. Atkinson and R. Richards-Kortum, "Spectroscopic diagnosis of cervical intraepithelial neoplasia (CIN) in vivo using laser-induced fluorescence spectra at multiple excitation wavelengths," *Lasers Surg Med* **19**(1), 63-74 (1996)

10. R. Richards-Kortum, R. P. Rava, M. Fitzmaurice, J. R. Kramer and M. S. Feld, "476 nm excited laser-induced fluorescence spectroscopy of human coronary arteries: applications in cardiology," *Am Heart J* **122**(4 Pt 1), 1141-1150 (1991)

11. N. M. Marin, A. Milbourne, H. Rhodes, T. Ehlen, D. Miller, L. Benedet, R. Richards-Kortum and M. Follen, "Diffuse reflectance patterns in cervical spectroscopy," *Gynecologic Oncology* **99**(3, Supplement 1), S116 (2005)

12. K. Carlson, I. Pavlova, T. Collier, M. Descour, M. Follen and R. Richards-Kortum, "Confocal microscopy: imaging cervical precancerous lesions," *Gynecol Oncol* **99**(3 Suppl 1), S84-88 (2005)

13. A. Nath, K. Rivoire, S. Chang, L. West, S. B. Cantor, K. Basen-Engquist, K. Adler-Storthz, D. D. Cox, E. N. Atkinson, G. Staerkel, C. MacAulay, R. Richards-Kortum and M. Follen, "A pilot study for a screening trial of cervical fluorescence spectroscopy," *Int J Gynecol Cancer* **14**(6), 1097-1107 (2004)

14. Y. N. Mirabal, S. K. Chang, E. N. Atkinson, A. Malpica, M. Follen and R. Richards-Kortum, "Reflectance spectroscopy for in vivo detection of cervical precancer," *Journal of biomedical optics* 7(4), 587-594 (2002)

15. A. C. Society, "Cancer Facts and Figures," *Publication No. 93-400M, No. 5008-03* (2003)

16. W. H. Crawford, Mucosa: Cancer and Premalignant Diseases, Health-Soft-Edu, Los Angeles (2002).

17. J. Sexton, "Surgical Pathology of the Oral Cavity," *Clin. Dermatol.* **18**(601-611 (2000)

18. B. B. Yeole, A. V. Ramananakumar and R. Sankaranayanan, "Survival from Oral Cancer in Mumbai (bombay), India," *Cancer Causes Control* **14**(945-952 (2003)

19. J. J. Sciubba, "Oral Cancer: The Importance of Early Diagnosis and Treatment," *American Journal of Clinical Dermatology* **2**(4), 239-251 (2001)

20. S. Folli, P. Westermann, D. Braichotte, A. Pelegrin, G. Wagnieres, H. van den Bergh and J. P. Mach, "Antibody-indocyanin conjugates for immunophotodetection of human squamous cell carcinoma in nude mice," *Cancer Res* **54**(10), 2643-2649 (1994)

21. B. Ballou, G. W. Fisher, J. S. Deng, T. R. Hakala, M. Srivastava and D. L. Farkas, "Cyanine fluorochrome-labeled antibodies in vivo: assessment of tumor imaging using Cy3, Cy5, Cy5.5, and Cy7," *Cancer detection and prevention* **22**(3), 251-257 (1998)

22. N. S. Soukos, M. R. Hamblin, T. F. Deutsch and T. Hasan, "Monoclonal antibody-tagged receptor-targeted contrast agents for detection of cancers," in Proceedings of SPIE: Biomarkers and Biological Spectra Imaging, pp. 115-128, San Jose, CA (2001).

23. N. S. Soukos, M. R. Hamblin, S. Keel, R. L. Fabian, T. F. Deutsch and T. Hasan, "Epidermal growth factor receptor-targeted immunophotodiagnosis and photoimmunotherapy of oral precancer in vivo," *Cancer Res* **61**(11), 4490-4496 (2001)

24. Y. Koyama, T. Barrett, Y. Hama, G. Ravizzini, P. L. Choyke and H. Kobayashi, "In vivo molecular imaging to diagnose and subtype tumors through receptor-targeted optically labeled monoclonal antibodies," *Neoplasia (New York, N.Y* **9**(12), 1021-1029 (2007)

25. Y. Koyama, Y. Hama, Y. Urano, D. M. Nguyen, P. L. Choyke and H. Kobayashi, "Spectral fluorescence molecular imaging of lung metastases targeting HER2/neu," *Clin Cancer Res* **13**(10), 2936-2945 (2007)

26. K. E. Adams, S. Ke, S. Kwon, F. Liang, Z. Fan, Y. Lu, K. Hirschi, M. E. Mawad, M. A. Barry and E. M. Sevick-Muraca, "Comparison of visible and near-infrared wavelength-excitable fluorescent dyes for molecular imaging of cancer," *Journal of biomedical optics* **12**(2), 024017 (2007)

27. J. L. Kovar, W. M. Volcheck, J. Chen and M. A. Simpson, "Purification method directly influences effectiveness of an epidermal growth factor-coupled targeting agent for noninvasive tumor detection in mice," *Analytical biochemistry* **361**(1), 47-54 (2007)

28. J. L. Kovar, M. A. Johnson, W. M. Volcheck, J. Chen and M. A. Simpson, "Hyaluronidase expression induces prostate tumor metastasis in an orthotopic mouse model," *Am J Pathol* **169**(4), 1415-1426 (2006)

29. S. Ke, X. Wen, M. Gurfinkel, C. Charnsangavej, S. Wallace, E. M. Sevick-Muraca and C. Li, "Near-infrared optical imaging of epidermal growth factor receptor in breast cancer xenografts," *Cancer Res* **63**(22), 7870-7875 (2003)

30. K. L. Carraway, 3rd and R. A. Cerione, "Fluorescent-labeled growth factor molecules serve as probes for receptor binding and endocytosis," *Biochemistry* **32**(45), 12039-12045 (1993)

31. C. H. Tung, Y. Lin, W. K. Moon and R. Weissleder, "A receptor-targeted near-infrared fluorescence probe for in vivo tumor imaging," *Chembiochem* **3**(8), 784-786 (2002)

32. S. Achilefu, R. B. Dorshow, J. E. Bugaj and R. Rajagopalan, "Novel receptor-targeted fluorescent contrast agents for in vivo tumor imaging," *Investigative radiology* **35**(8), 479-485 (2000)

33. A. Becker, C. Hessenius, K. Licha, B. Ebert, U. Sukowski, W. Semmler, B. Wiedenmann and C. Grotzinger, "Receptor-targeted optical imaging of tumors with near-infrared fluorescent ligands," *Nature biotechnology* **19**(4), 327-331 (2001)

34. D. Citrin, T. Scott, M. Sproull, C. Menard, P. J. Tofilon and K. Camphausen, "In vivo tumor imaging using a near-infrared-labeled endostatin molecule," *International journal of radiation oncology, biology, physics* **58**(2), 536-541 (2004)

35. R. Weissleder, C. H. Tung, U. Mahmood and A. Bogdanov, Jr., "In vivo imaging of tumors with protease-activated near-infrared fluorescent probes," *Nature biotechnology* **17**(4), 375-378 (1999)

36. C. H. Tung, U. Mahmood, S. Bredow and R. Weissleder, "In vivo imaging of proteolytic enzyme activity using a novel molecular reporter," *Cancer research* **60**(17), 4953-4958 (2000)

37. K. Marten, C. Bremer, K. Khazaie, M. Sameni, B. Sloane, C. H. Tung and R. Weissleder, "Detection of dysplastic intestinal adenomas using enzyme-sensing molecular beacons in mice," *Gastroenterology* **122**(2), 406-414 (2002)

38. C. Bremer, C. H. Tung, A. Bogdanov, Jr. and R. Weissleder, "Imaging of differential protease expression in breast cancers for detection of aggressive tumor phenotypes," *Radiology* **222**(3), 814-818 (2002)

39. M. Kamiya, H. Kobayashi, Y. Hama, Y. Koyama, M. Bernardo, T. Nagano, P. L. Choyke and Y. Urano, "An enzymatically activated fluorescence probe for targeted tumor imaging," *Journal of the American Chemical Society* **129**(13), 3918-3929 (2007)

40. J. V. Frangioni, "In vivo near-infrared fluorescence imaging," *Current opinion in chemical biology* **7**(5), 626-634 (2003)

41. H. Modjtahedi and C. J. Dean, "The receptor for EGF and its ligands: expression, prognostic value, and target for therapy in cancer," *Int J Oncol* **4**(277-296 (1994)

42. W. Yasui, H. Sumiyoshi, J. Hata, T. Kameda, A. Ochiai, H. Ito and E. Tahara, "Expression of epidermal growth factor receptor in human gastric and colonic carcinomas," *Cancer Res* **48**(1), 137-141 (1988)

43. J. A. Vet, F. M. Debruyne and J. A. Schalken, "Molecular prognostic factors in bladder cancer," *World journal of urology* **12**(2), 84-88 (1994)

44. N. Normanno, A. De Luca, C. Bianco, L. Strizzi, M. Mancino, M. R. Maiello, A. Carotenuto, G. De Feo, F. Caponigro and D. S. Salomon, "Epidermal growth factor receptor (EGFR) signaling in cancer," *Gene* **366**(1), 2-16 (2006)

45. S. Costa, H. Stamm, A. Almendral, H. Ludwig, R. Wyss, D. Fabbro, A. Ernst, A. Takahashi and U. Eppenberger, "Predictive value of EGF receptor in breast cancer," *Lancet* **2**(8622), 1258 (1988)

46. K. Laimer, G. Spizzo, G. Gastl, P. Obrist, T. Brunhuber, D. Fong, V. Barbieri, S. Jank, W. Doppler, M. Rasse and B. Norer, "High EGFR expression predicts poor prognosis in patients with squamous cell carcinoma of the oral cavity and oropharynx: a TMA-based immunohistochemical analysis," *Oral Oncol* **43**(2), 193-198 (2007)

47. K. K. Ang, B. A. Berkey, X. Tu, H. Z. Zhang, R. Katz, E. H. Hammond, K. K. Fu and L. Milas, "Impact of epidermal growth factor receptor expression on survival and pattern of relapse in patients with advanced head and neck carcinoma," *Cancer Res* **62**(24), 7350-7356 (2002)

48. F. Ciardiello and G. Tortora, "EGFR Antagonists in Cancer Treatment," *N Engl J Med* **358**(11), 1160-1174 (2008)

49. J. Mendelsohn and J. Baselga, "Status of Epidermal Growth Factor Receptor Antagonists in the Biology and Treatment of Cancer," *J Clin Oncol* **21**(14), 2787-2799 (2003)

50. J. W. Shay and S. Bacchetti, "A Survey of Telomerase Activity in Human Cancer," *European Journal of Cancer* **33**(5), 787-791 (1997)

51. E. Hiyama, K. Hiyama, T. Yokoyama and J. W. Shay, "Immunohistochemical detection of telomerase (hTERT) protein in human cancer tissues and a subset of cells in normal tissues," *Neoplasia (New York, N.Y* **3**(1), 17-26 (2001)

52. M. Belting, S. Sandgren and A. Wittrup, "Nuclear delivery of macromolecules: barriers and carriers," *Advanced drug delivery reviews* **57**(4), 505-527 (2005)

53. E. M. De Robertis, R. F. Longthorne and J. B. Gurdon, "Intracellular migration of nuclear proteins in Xenopus oocytes," *Nature* **272**(5650), 254-256 (1978)

54. C. Dingwall, S. V. Sharnick and R. A. Laskey, "A polypeptide domain that specifies migration of nucleoplasmin into the nucleus," *Cell* **30**(2), 449-458 (1982)

55. Z. W. Yu and P. J. Quinn, "Dimethyl sulphoxide: a review of its applications in cell biology," *Bioscience reports* **14**(6), 259-281 (1994)

56. Z. W. Yu and P. J. Quinn, "The modulation of membrane structure and stability by dimethyl sulphoxide (review)," *Molecular membrane biology* **15**(2), 59-68 (1998)

57. A. Helenius and K. Simons, "Solubilization of membranes by detergents," *Biochimica et biophysica acta* **415**(1), 29-79 (1975)

58. G. Trejo-Tapia, J. Cuevas-Celis, G. Salcedo-Morales, J. L. Trejo-Espino, M. L. Arenas-Ocampo and A. Jimenez-Aparicio, "Beta vulgaris L. suspension cultures permeabilized with triton X-100 retain cell viability and betacyanines production ability: a digital image analysis study," *Biotechnology progress* **23**(2), 359-363 (2007)

59. P. Brodelius, "Permeabilization of plant cells for release of intracellularly stored products: viability studies," *Applied Microbiology and Biotechnology* **27**(5), 561-566 (1988)

60. R. Thimmaraju, N. Bhagyalakshmi, M. S. Narayan and G. A. Ravishankar, "Kinetics of pigment release from hairy root cultures of Beta vulgaris under the influence of pH, sonication, temperature and oxygen stress," *Process Biochemistry* **38**(7), 1069-1076 (2003)

61. R. Serrano, J. M. Gancedo and C. Gancedo, "Assay of Yeast Enzymes in situ. A Potential Tool in Regulation Studies," *European Journal of Biochemistry* **34**(3), 479-482 (1973)

62. H. W. David Hettwer, "Protein release from <I>Escherichia coli</I> cells permeabilized with guanidine-HCl and Triton X100," *Biotechnology and Bioengineering* **33**(7), 886-895 (1989)

63. U. Kragh-Hansen, M. le Maire, J. P. Noel, T. Gulik-Krzywicki and J. V. Moller, "Transitional steps in the solubilization of protein-containing membranes and liposomes by nonionic detergent," *Biochemistry* **32**(6), 1648-1656 (1993)

64. N. P. Franks and W. R. Lieb, "The structure of lipid bilayers and the effects of general anaesthetics. An x-ray and neutron diffraction study," *Journal of molecular biology* **133**(4), 469-500 (1979)

65. C. D. Richards, K. Martin, S. Gregory, C. A. Keightley, T. R. Hesketh, G. A. Smith, G. B. Warren and J. C. Metcalfe, "Degenerate perturbations of protein structure as the mechanism of anaesthetic action," *Nature* **276**(5690), 775-779 (1978)

66. P. Seeman, "The membrane actions of anesthetics and tranquilizers," *Pharmacological reviews* **24**(4), 583-655 (1972)

67. H. Heerklotz, H. Szadkowska, T. Anderson and J. Seelig, "The sensitivity of lipid domains to small perturbations demonstrated by the effect of Triton," *Journal of molecular biology* **329**(4), 793-799 (2003)

68. H. Heerklotz, "Triton promotes domain formation in lipid raft mixtures," *Biophysical journal* **83**(5), 2693-2701 (2002)

69. A. E. Garner, A. Smith and N. M. Hooper, "Visualisation of detergent solubilisation of membranes: Implications for the isolation of rafts," *Biophys. J.* biophysj.107.114108 (2007)

70. H. Shogomori and D. A. Brown, "Use of detergents to study membrane rafts: the good, the bad, and the ugly," *Biological chemistry* **384**(9), 1259-1263 (2003)

71. J. P. Andersen, M. Le Maire, U. Kragh-Hansen, P. Champeil and J. V. Moller, "Perturbation of the structure and function of a membranous Ca2+-ATPase by non-solubilizing concentrations of a non-ionic detergent," *European journal of biochemistry / FEBS* **134**(2), 205-214 (1983)

72. B. De Foresta, F. Henao and P. Champeil, "Cancellation of the cooperativity of Ca2+ binding to sarcoplasmic reticulum Ca(2+)-ATPase by the non-ionic detergent dodecylmaltoside," *European journal of biochemistry / FEBS* **223**(2), 359-369 (1994)

73. B. de Foresta, F. Henao and P. Champeil, "Kinetic characterization of the perturbation by dodecylmaltoside of sarcoplasmic reticulum Ca(2+)-ATPase," *European journal of biochemistry / FEBS* **209**(3), 1023-1034 (1992)

74. D. B. McIntosh and G. A. Davidson, "Effects of nonsolubilizing and solubilizing concentrations of Triton X-100 on Ca2+ binding and Ca2+-ATPase activity of sarcoplasmic reticulum," *Biochemistry* **23**(9), 1959-1965 (1984)

75. P. G. Sacks, S. M. Parnes, G. E. Gallick, Z. Mansouri, R. Lichtner, K. L. Satya-Prakash, S. Pathak and D. F. Parsons, "Establishment and characterization of two new squamous cell carcinoma cell lines derived from tumors of the head and neck," *Cancer Res* **48**(10), 2858-2866 (1988)

76. F. M. Yakes and B. Van Houten, "Mitochondrial DNA damage is more extensive and persists longer than nuclear DNA damage in human cells following oxidative stress," *PNAS* **94**(2), 514-519 (1997)

77. A. G. Ostermeyer, B. T. Beckrich, K. A. Ivarson, K. E. Grove and D. A. Brown, "Glycosphingolipids are not essential for formation of detergent-resistant membrane rafts in melanoma cells. methyl-beta-cyclodextrin does not affect cell surface transport of a GPI-anchored protein," *The Journal of biological chemistry* **274**(48), 34459-34466 (1999)

78. T. J. Naglak and H. Y. Wang, "Recovery of a foreign protein from the periplasm of Escherichia coli by chemical permeabilization," *Enzyme and Microbial Technology* **12**(8), 603-611 (1990)

79. E. H. Blackburn, "Structure and function of telomeres," *Nature* **350**(6319), 569-573 (1991)

80. E. H. Blackburn, "Telomeres: no end in sight," *Cell* **77**(5), 621-623 (1994)

81. S. E. Holt, W. E. Wright and J. W. Shay, "Regulation of telomerase activity in immortal cell lines," *Mol Cell Biol* **16**(6), 2932-2939 (1996)

82. E. Hiyama and K. Hiyama, "Clinical utility of telomerase in cancer," *Oncogene* **21**(4), 643-649 (2002)

83. D. Broccoli, J. W. Young and T. de Lange, "Telomerase activity in normal and malignant hematopoietic cells," *Proc Natl Acad Sci U S A* **92**(20), 9082-9086 (1995)

84. R. B. Effros and A. Globerson, "Hematopoietic cells and replicative senescence," *Exp Gerontol* **37**(2-3), 191-196 (2002)

85. J. Y. Chang, "Telomerase: a potential molecular marker and therapeutic target for cancer," *J Surg Oncol* **87**(1), 1-3 (2004)

86. N. W. Kim, "Clinical implications of telomerase in cancer," *Eur J Cancer* **33**(5), 781-786 (1997)

87. J. W. Shay and W. E. Wright, "Telomerase activity in human cancer," *Curr Opin Oncol* **8**(1), 66-71 (1996)

88. M. J. Ahn, Y. H. Noh, Y. S. Lee, J. H. Lee, T. J. Chung, I. S. Kim, I. Y. Choi, S. H. Kim, J. S. Lee and K. H. Lee, "Telomerase activity and its clinicopathological significance in gastric cancer," *Eur J Cancer* **33**(8), 1309-1313 (1997)

89. E. Hiyama, T. Yokoyama, N. Tatsumoto, K. Hiyama, Y. Imamura, Y. Murakami, T. Kodama, M. A. Piatyszek, J. W. Shay and Y. Matsuura, "Telomerase activity in gastric cancer," *Cancer Res* **55**(15), 3258-3262 (1995)

90. N. Tatsumoto, E. Hiyama, Y. Murakami, Y. Imamura, J. W. Shay, Y. Matsuura and T. Yokoyama, "High telomerase activity is an independent prognostic indicator of poor outcome in colorectal cancer," *Clin Cancer Res* **6**(7), 2696-2701 (2000)

91. G. M. Clark, C. K. Osborne, D. Levitt, F. Wu and N. W. Kim, "Telomerase activity and survival of patients with node-positive breast cancer," *J Natl Cancer Inst* **89**(24), 1874-1881 (1997)

92. L. A. Carey, N. W. Kim, S. Goodman, J. Marks, G. Henderson, C. B. Umbricht, J. S. Dome, W. Dooley, S. R. Amshey and S. Sukumar, "Telomerase activity and prognosis in primary breast cancers," *J Clin Oncol* **17**(10), 3075-3081 (1999)

93. A. Marchetti, G. Bertacca, F. Buttitta, A. Chella, G. Quattrocolo, C. A. Angeletti and G. Bevilacqua, "Telomerase activity as a prognostic indicator in stage I non-small cell lung cancer," *Clin Cancer Res* **5**(8), 2077-2081 (1999)

94. T. Komiya, I. Kawase, T. Nitta, T. Yasumitsu, M. Kikui, M. Fukuoka, K. Nakagawa and T. Hirashima, "Prognostic significance of hTERT expression in non-small cell lung cancer," *Int J Oncol* **16**(6), 1173-1177 (2000)

95. M. M. Patel, L. J. Parekh, F. P. Jha, R. N. Sainger, J. B. Patel, D. D. Patel, P. M. Shah and P. S. Patel, "Clinical usefulness of telomerase activation and telomere length in head and neck cancer," *Head Neck* **24**(12), 1060-1067 (2002)

96. H. Tahara, H. Kuniyasu, H. Yokozaki, W. Yasui, J. W. Shay, T. Ide and E. Tahara, "Telomerase activity in preneoplastic and neoplastic gastric and colorectal lesions," *Clin Cancer Res* **1**(11), 1245-1251 (1995)

97. C. Chadeneau, K. Hay, H. W. Hirte, S. Gallinger and S. Bacchetti, "Telomerase activity associated with acquisition of malignancy in human colorectal cancer," *Cancer Res* **55**(12), 2533-2536 (1995)

98. E. Hiyama, K. Hiyama, T. Yokoyama, Y. Matsuura, M. A. Piatyszek and J. W. Shay, "Correlating telomerase activity levels with human neuroblastoma outcomes," *Nat Med* **1**(3), 249-255 (1995)

99. E. Hiyama, K. Hiyama, K. Ohtsu, H. Yamaoka, T. Ichikawa, J. W. Shay and T. Yokoyama, "Telomerase activity in neuroblastoma: is it a prognostic indicator of clinical behaviour?," *Eur J Cancer* **33**(12), 1932-1936 (1997)

100. S. Lantuejoul, J. C. Soria, D. Moro-Sibilot, L. Morat, S. Veyrenc, P. Lorimier, P. Y. Brichon, L. Sabatier, C. Brambilla and E. Brambilla, "Differential expression of telomerase reverse transcriptase (hTERT) in lung tumours," *Br J Cancer* **90**(6), 1222-1229 (2004)

101. J. Domont, T. M. Pawlik, V. Boige, M. Rose, J.-C. Weber, P. M. Hoff, T. D. Brown, D. Zorzi, L. Morat, J.-P. Pignon, A. Rashid, D. Jaeck, L. Sabatier, D. Elias, T. Tursz, J.-C. Soria and J.-N. Vauthey, "Catalytic Subunit of Human Telomerase Reverse Transcriptase Is an Independent Predictor of Survival in Patients Undergoing Curative Resection of Hepatic Colorectal Metastases: A Multicenter Analysis," *J Clin Oncol* **23**(13), 3086-3093 (2005)

102. D. L. Smith, J.-C. Soria, L. Morat, Q. Yang, L. Sabatier, D. D. Liu, R. A. Nemr, A. Rashid and J.-N. Vauthey, "Human Telomerase Reverse Transcriptase (hTERT) and Ki-67 are Better Predictors of Survival than Established Clinical Indicators in Patients Undergoing Curative Hepatic Resection for Colorectal Metastases," *Ann Surg Oncol* **11**(1), 45-51 (2004)

103. H. Brustmann, "Immunohistochemical detection of human telomerase reverse transcriptase (hTERT) and c-kit in serous ovarian carcinoma: A clinicopathologic study," *Gynecologic Oncology* **98**(3), 396 (2005)

104. B. Luzar, M. Poljak, A. Cor, U. Klopcic and V. Ferlan-Marolt, "Expression of human telomerase catalytic protein in gallbladder carcinogenesis," *J Clin Pathol* **58**(8), 820-825 (2005)

105. B. Luzar, M. Poljak and N. Gale, "Telomerase catalytic subunit in laryngeal carcinogenesis--an immunohistochemical study," *Mod Pathol* **18**(3), 406-411 (2005)

106. M. Branca, C. Giorgi, M. Ciotti, D. Santini, L. Di Bonito, S. Costa, A. Benedetto, D. Bonifacio, P. Di Bonito, P. Paba, L. Accardi, L. Mariani, M. Ruutu, S. Syrjanen, C. Favalli and K. Syrjanen, "Upregulation of telomerase (hTERT) is related to the grade of

cervical intraepithelial neoplasia, but is not an independent predictor of high-risk human papillomavirus, virus persistence, or disease outcome in cervical cancer," *Diagn Cytopathol* **34**(11), 739-748 (2006)

107. S. Bravaccini, M. A. Sanchini, A. Amadori, L. Medri, L. Saragoni, D. Calistri, F. Monti, A. Volpi and D. Amadori, "Potential of telomerase expression and activity in cervical specimens as a diagnostic tool," *J Clin Pathol* **58**(9), 911-914 (2005)

108. R. V. Lord, D. Salonga, K. D. Danenberg, J. H. Peters, T. R. DeMeester, J. M. Park, J. Johansson, K. A. Skinner, P. Chandrasoma, S. R. DeMeester, C. G. Bremner, P. I. Tsai and P. V. Danenberg, "Telomerase reverse transcriptase expression is increased early in the Barrett's metaplasia, dysplasia, adenocarcinoma sequence," *J Gastrointest Surg* **4**(2), 135-142 (2000)

109. S. K. Kumar, R. B. Zain, S. M. Ismail and S. C. Cheong, "Human telomerase reverse transcriptase expression in oral carcinogenesis--a preliminary report," *J Exp Clin Cancer Res* **24**(4), 639-646 (2005)

110. C. Gulmann, S. Lantuejoul, A. Grace, M. Leader, S. Patchett and E. Kay, "Telomerase activity in proximal and distal gastric neoplastic and preneoplastic lesions using immunohistochemical detection of hTERT," *Digestive and Liver Disease* **37**(6), 439 (2005)

111. S. Lantuejoul, J. C. Soria, L. Morat, P. Lorimier, D. Moro-Sibilot, L. Sabatier, C. Brambilla and E. Brambilla, "Telomere Shortening and Telomerase Reverse Transcriptase Expression in Preinvasive Bronchial Lesions," *Clin Cancer Res* **11**(5), 2074-2082 (2005)

112. B. Schnabl, C. A. Purbeck, Y. H. Choi, C. H. Hagedorn and D. Brenner, "Replicative senescence of activated human hepatic stellate cells is accompanied by a pronounced inflammatory but less fibrogenic phenotype," *Hepatology* **37**(3), 653-664 (2003)

113. M. M. Patel, D. D. Patel, L. J. Parekh, G. N. Raval, R. M. Rawal, J. M. Bhatavdekar, B. P. Patel and P. S. Patel, "Evaluation of telomerase activation in head and neck cancer," *Oral Oncol* **35**(5), 510-515 (1999)

114. S. E. Holt, D. L. Aisner, J. W. Shay and W. E. Wright, "Lack of cell cycle regulation of telomerase activity in human cells," *PNAS* **94**(20), 10687-10692 (1997)

115. K. T. Etheridge, S. S. R. Banik, B. N. Armbruster, Y. Zhu, R. M. Terns, M. P. Terns and C. M. Counter, "The Nucleolar Localization Domain of the Catalytic Subunit of Human Telomerase," *J. Biol. Chem.* **277**(27), 24764-24770 (2002)

116. S. Khurts, K. Masutomi, L. Delgermaa, K. Arai, N. Oishi, H. Mizuno, N. Hayashi, W. C. Hahn and S. Murakami, "Nucleolin Interacts with Telomerase," *J. Biol. Chem.* **279**(49), 51508-51515 (2004)

117. J. M. Y. Wong, L. Kusdra and K. Collins, "Subnuclear shuttling of human telomerase induced by transformation and DNA damage," *Nat Cell Biol* **4**(9), 731 (2002)

118. J. H. Santos, J. N. Meyer, M. Skorvaga, L. A. Annab and B. Van Houten, "Mitochondrial hTERT exacerbates free-radical-mediated mtDNA damage," *Aging Cell* **3**(6), 399-411 (2004)

119. Y. Zhu, R. L. Tomlinson, A. A. Lukowiak, R. M. Terns and M. P. Terns, "Telomerase RNA accumulates in Cajal bodies in human cancer cells," *Mol Biol Cell* **15**(1), 81-90 (2004)

120. H. Seimiya, H. Sawada, Y. Muramatsu, M. Shimizu, K. Ohko, K. Yamane and T. Tsuruo, "Involvement of 14-3-3 proteins in nuclear localization of telomerase," *Embo J* **19**(11), 2652-2661 (2000)

121. A. Volpi, S. Bravaccini, L. Medri, S. Cerasoli, M. Gaudio and D. Amadori, "Usefulness of immunological detection of the human telomerase reverse transcriptase," *Cell Oncol* **27**(5-6), 347-353 (2005)

122. E. A. Jarboe, K. L. Liaw, L. C. Thompson, D. E. Heinz, P. L. Baker, J. A. McGregor, T. Dunn, J. E. Woods and K. R. Shroyer, "Analysis of telomerase as a diagnostic biomarker of cervical dysplasia and carcinoma," *Oncogene* **21**(4), 664-673 (2002)

123. Z. Chen, Y. Zhao, S. M. Srinivas, J. S. Nelson, N. Prakash and R. D. Frostig, "Optical Doppler Tomography," *IEEE Journal of Selected Topics in Quantum Electronics* **5**(4), 1134-1142 (1999)

124. R. Cotran, V. Kumar and T. Collins, Robbins Pathologic Basis of Disease, W. B. Saunders, Philadelphia (1999).

125. J. Levi, Z. Cheng, O. Gheysens, M. Patel, C. T. Chan, Y. Wang, M. Namavari and S. S. Gambhir, "Fluorescent Fructose Derivatives for Imaging Breast Cancer Cells," *Bioconjugate Chem.* **18**(3), 628-634 (2007)

126. R. O'Neil, L. Wu and N. Mullani, "Uptake of a Fluorescent Deoxyglucose Analog (2-NBDG) in Tumor Cells," *Molecular Imaging and Biology* **7**(6), 388-392 (2005)

127. Z. Cheng, J. Levi, Z. Xiong, O. Gheysens, S. Keren, X. Chen and S. S. Gambhir, "Near-Infrared Fluorescent Deoxyglucose Analogue for Tumor Optical Imaging in Cell Culture and Living Mice," *Bioconjugate Chem.* **17**(3), 662-669 (2006)

128. T. J. Muldoon, M. C. Pierce, D. L. Nida, M. D. Williams, A. Gillenwater and R. Richards-Kortum, "Subcellular-resolution molecular imaging within living tissue by fiber microendoscopy," *Opt. Express* **15**(25), 16413-16423 (2007)

129. Y. Kakeji, S. Yamaguchi, D. Yoshida, K. Tanoue, M. Ueda, A. Masunari, T. Utsunomiya, M. Imamura, H. Honda, Y. Maehara and M. Hashizume, "Development and assessment of morphologic criteria for diagnosing gastric cancer using confocal endomicroscopy: an ex vivo and in vivo study," *Endoscopy* **38**(9), 886-890 (2006)

130. A. L. Polglase, W. J. McLaren, S. A. Skinner, R. Kiesslich, M. F. Neurath and P. M. Delaney, "A fluorescence confocal endomicroscope for in vivo microscopy of the upper- and the lower-GI tract," *Gastrointestinal endoscopy* **62**(5), 686-695 (2005)

131. I. A. Siegel, K. T. Izutsu and E. Watson, "Mechanisms of non-electrolyte penetration across dog and rabbit oral mucosa in vitro," *Archives of oral biology* **26**(5), 357-361 (1981)

132. V. H. Lee, "Enzymatic barriers to peptide and protein absorption," *Critical reviews in therapeutic drug carrier systems* **5**(2), 69-97 (1988)

133. R. A. Hughes, I. Toth, P. Ward, S. J. Ireland and W. A. Gibbons, "Lipidic peptides. III: Lipidic amino acid and oligomer conjugates of morphine," *Journal of pharmaceutical sciences* **80**(12), 1103-1105 (1991)

134. H. A. Benson, "Transdermal drug delivery: penetration enhancement techniques," *Current drug delivery* **2**(1), 23-33 (2005)

135. M. Thanou, J. C. Verhoef and H. E. Junginger, "Oral drug absorption enhancement by chitosan and its derivatives," *Advanced drug delivery reviews* **52**(2), 117-126 (2001)

136. V. Erjavec, Z. Pavlica, M. Sentjurc and M. Petelin, "In vivo study of liposomes as drug carriers to oral mucosa using EPR oximetry," *International journal of pharmaceutics* **307**(1), 1-8 (2006)

137. H. Li, J. H. An, J. S. Park and K. Han, "Multivesicular liposomes for oral delivery of recombinant human epidermal growth factor," *Archives of pharmacal research* **28**(8), 988-994 (2005)

138. F. S. Farshi, A. Y. Ozer, M. T. Ercan and A. A. Hincal, "In-vivo studies in the treatment of oral ulcers with liposomal dexamethasone sodium phosphate," *Journal of microencapsulation* **13**(5), 537-544 (1996)

139. A. N. C. Anigbogu, A. C. Williams, B. W. Barry and H. G. M. Edwards, "Fourier transform raman spectroscopy of interactions between the penetration enhancer dimethyl sulfoxide and human stratum corneum," *International journal of pharmaceutics* **125**(2), 265-282 (1995)

140. H. A. E. Benson, "Transfersomes for transdermal drug delivery," *Expert Opinion on Drug Delivery* **3**(6), 727-737 (2006)

141. P. N. Gupta, V. Mishra, P. Singh, A. Rawat, P. Dubey, S. Mahor and S. P. Vyas, "Tetanus toxoid-loaded transfersomes for topical immunization," *The Journal of pharmacy and pharmacology* **57**(3), 295-301 (2005)

142. J. Hao and P. W. Heng, "Buccal delivery systems," *Drug development and industrial pharmacy* **29**(8), 821-832 (2003)

143. F. Veuillez, Y. N. Kalia, Y. Jacques, J. Deshusses and P. Buri, "Factors and strategies for improving buccal absorption of peptides," *Eur J Pharm Biopharm* **51**(2), 93-109 (2001)

144. E. R. Hsu, E. V. Anslyn, S. Dharmawardhane, R. Alizadeh-Naderi, J. S. Aaron, K. V. Sokolov, A. K. El-Naggar, A. M. Gillenwater and R. R. Richards-Kortum, "A far-red fluorescent contrast agent to image epidermal growth factor receptor expression," *Photochem Photobiol* **79**(3), 272-279 (2004)

145. A. Namazie, S. Alavi, O. I. Olopade, G. Pauletti, N. Aghamohammadi, M. Aghamohammadi, J. A. Gornbein, T. C. Calcaterra, D. J. Slamon, M. B. Wang and E. S. Srivatsan, "Cyclin D1 amplification and p16(MTS1/CDK4I) deletion correlate with poor prognosis in head and neck tumors," *The Laryngoscope* **112**(3), 472-481 (2002)

146. J. A. Akervall, R. J. Michalides, H. Mineta, A. Balm, A. Borg, M. R. Dictor, Y. Jin, B. Loftus, F. Mertens and J. P. Wennerberg, "Amplification of cyclin D1 in squamous cell carcinoma of the head and neck and the prognostic value of chromosomal abnormalities and cyclin D1 overexpression," *Cancer* **79**(2), 380-389 (1997)

147. R. J. Michalides, N. M. van Veelen, P. M. Kristel, A. A. Hart, B. M. Loftus, F. J. Hilgers and A. J. Balm, "Overexpression of cyclin D1 indicates a poor prognosis in squamous cell carcinoma of the head and neck," *Archives of otolaryngology--head & neck surgery* **123**(5), 497-502 (1997)

148. R. Michalides, N. van Veelen, A. Hart, B. Loftus, E. Wientjens and A. Balm, "Overexpression of cyclin D1 correlates with recurrence in a group of forty-seven operable squamous cell carcinomas of the head and neck," *Cancer Res* **55**(5), 975-978 (1995)

149. M. F. Mitchell, W. N. Hittelman, W. K. Hong, R. Lotan and D. Schottenfeld, "The natural history of cervical intraepithelial neoplasia: an argument for intermediate endpoint biomarkers," *Cancer epidemiology, biomarkers & prevention : a publication of the American Association for Cancer Research, cosponsored by the American Society of Preventive Oncology* **3**(7), 619-626 (1994)

150. F. van Ruissen, M. Le, J. M. Carroll, P. G. M. van der Valk and J. Schalkwijk, "Differential Effects of Detergents on Keratinocyte Gene Expression," **110**(4), 358 (1998)

151. B. Mollgaard, "Synergistic effects in percutaneous enhancement," *in Pharmaceutical skin penetration enhancement* K. A. Walters and J. Hadgraft, Eds., pp. 220-242, Marcel Dekker, New York (1993).

152. E. S. Swenson, W. B. Milisen and W. Curatolo, "Intestinal permeability enhancement: efficacy, acute local toxicity, and reversibility," *Pharmaceutical research* **11**(8), 1132-1142 (1994)

153. E. K. Anderberg and P. Artursson, "Epithelial transport of drugs in cell culture. VIII: Effects of sodium dodecyl sulfate on cell membrane and tight junction permeability in human intestinal epithelial (Caco-2) cells," *Journal of pharmaceutical sciences* **82**(4), 392-398 (1993)

154. E. K. Anderberg, C. Nystrom and P. Artursson, "Epithelial transport of drugs in cell culture. VII: Effects of pharmaceutical surfactant excipients and bile acids on transepithelial permeability in monolayers of human intestinal epithelial (Caco-2) cells," *Journal of pharmaceutical sciences* **81**(9), 879-887 (1992)

155. B. W. Barry, Dermatological Formulations: Percutaneous Absorption, Marcel Dekker, New York (1983).

156. K. Whitehead, N. Karr and S. Mitragotri, "Safe and Effective Permeation Enhancers for Oral Drug Delivery," *Pharmaceutical research*

157. S. Takatsuka, T. Morita, Y. Horikiri, H. Yamahara and H. Saji, "Influence of various combinations of mucolytic agent and non-ionic surfactant on intestinal absorption of poorly absorbed hydrophilic compounds," *International journal of pharmaceutics* **349**(1-2), 94-100 (2008)

158. S. Takatsuka, T. Morita, A. Koguchi, Y. Horikiri, H. Yamahara and H. Yoshino, "Synergistic absorption enhancement of salmon calcitonin and reversible mucosal injury by applying a mucolytic agent and a non-ionic surfactant," *International journal of pharmaceutics* **316**(1-2), 124-130 (2006)

159. R. L. Oberle, T. J. Moore and D. A. Krummel, "Evaluation of mucosal damage of surfactants in rat jejunum and colon," *Journal of pharmacological and toxicological methods* **33**(2), 75-81 (1995)

160. J. W. Robinson, B. Winistorfer and V. Mirkovitch, "Source of net water and electrolyte loss following intestinal ischaemia," *Research in experimental medicine* **176**(3), 263-275 (1980)

161. W. J. Harmon, D. M. Barrett, J. Qian, R. W. Lauvetz, D. G. Bostwick and M. Gocken, "Transurethral enzymatic ablation of the prostate: canine model," *Urology* **48**(2), 229-233 (1996)

162. D. A. Fox, M. L. Epstein and P. Bass, "Surfactants selectively ablate enteric neurons of the rat jejunum," *The Journal of pharmacology and experimental therapeutics* **227**(2), 538-544 (1983)

163. A. Helenius and K. Simons, "The binding of detergents to lipophilic and hydrophilic proteins," *The Journal of biological chemistry* **247**(11), 3656-3661 (1972)

164. P. Cuatrecasas, "Properties of the insulin receptor isolated from liver and fat cell membranes," *The Journal of biological chemistry* **247**(7), 1980-1991 (1972)

165. D. Snary, P. Goodfellow, M. J. Hayman, W. F. Bodmer and M. J. Crumpton, "Subcellular separation and molecular nature of human histocompatibility antigens (HL-A)," *Nature* **247**(441), 457-461 (1974)

166. A. A. Shokeir, "Squamous cell carcinoma of the bladder: pathology, diagnosis and treatment," *BJU international* **93**(2), 216-220 (2004)

167. O. N. Gofrit, T. Birman, A. Dinaburg, S. Ayesh, P. Ohana and A. Hochberg, "Chemically induced bladder cancer--a sonographic and morphologic description," *Urology* **68**(1), 231-235 (2006)